T.C.
MANISA CELAL BAYAR UNIVERSITY
GRADUATE EDUCATION INSTITUTE

M.Sc. THESIS
DEPARTMENT OF BIOENGINEERING
SCIENCE OF BIOENGINEERING

EVALUATION OF NEW DRUG INGREDIENTS AFFECTING PROSTATE SPECIFIC ANTIGEN (PSA) PROTEIN CONCENTRATION IN PROSTATE CANCER TREATMENT USING MOLECULAR MODELING METHODS STUDY

Begüm KARALAR

Supervisor
Asst. Prof. Dr. Deniz KARATAŞ

MANISA–2025

LETTER OF COMMITMENT

This thesis was written in Manisa Celal Bayar University Graduate Education Institute, Department of Bioengineering, in accordance with the academic and ethical rules, and all the literature information used is included in the thesis by reference. It is entirely my own work. I declare that I do not use artificial intelligence or programs.

Begüm KARALAR

ÖZET

Yüksek Lisans Tezi

Prostat Kanseri Tedavisinde Prostat Spesifik Antijen (PSA) Protein Konsantrasyonuna Etki Eden Yeni İlaç Bileşenlerinin Moleküler Modelleme Yöntemleri Kullanılarak Değerlendirilmesi

Begüm KARALAR

Manisa Celal Bayar Üniversitesi
Lisansüstü Eğitim Enstitüsü
Biyomühendislik Anabilim Dalı

Danışman: Dr. Öğretim Üyesi Deniz KARATAŞ

Moleküler modelleme alanında, moleküler docking yöntemi, bir hedef molekülün ikinci hedef moleküle bağlanarak stabil bir kompleks oluşturmasın kapsamaktadır. Yapılan moleküler docking yöntemi, protein-ligand veya enzim-ligand ilişkisini açıklamak için önemli bir yere sahiptir. Ayrıca enzim inhibisyonu süreçlerinin çalışmalarında da rol oynamaktadır. Moleküler docking çalışmalarında elde edilen milyonlarca bileşiklerin etkili ve verimli olası ilaç etken maddeleri olup olmadığının belirlenmesi araştırılırken kullanılan reseptörler ve kompleks yapılar yardımıyla da görüntüleme sağlanır. Bu yüksek lisans bitirme projesi çalışması kapsamında, prostat kanserine çözüm olarak üretilen FDA onaylı yeni ilaçların bileşenleri üzerine odaklanılmıştır. Spesifik olarak, Abiraterone, Olaparib, Pylarify, Rucaparib ve Locametz ilaçlarının, androjen reseptörünün ligand bağlanma domainlerine ait olan 1E3G, 8E1A, 2ZCH ve 2ZCL kristal yapıların üzerindeki etkileşimleri değerlendirilmiş ve bunlar Autodock programında gözlemlenmiştir. Yapılan 180 moleküler docking analizin sonuçları ile ADMET sonuçlarının en iyilerini Olaparib ve Rucaparib ilaçları vermiştir. Ek olarak, 50 nslik 25 tane moleküler dinamik simülasyonları gerçekleştirildi. Open Babel GUI, Discovery Studio ve Avogadro programlarıyla bu çalışma desteklenerek sonuçlar kaydedilmiştir. Bu çalışmada ilacın gerçekten inhibisyon yapıp yapmadığı ve ilaçların moleküler etkileşimlere destek olup olmadığı sonuçlarına da ulaşılabilinir.

Anahtar Kelimeler: prostate cancer, Abiraterone, Olaparib, Pylarify, Rucaparib and Locametz, protein-drug interaction, molecular docking, molecular dynamics simulation, Autodock

2025, 151 pages

ABSTRACT

M.Sc. THESIS

Evaluation of New Drug Components Affecting Prostate Specific Antigen (PSA) Protein Concentration in Prostate Cancer Treatment Using Molecular Modeling Methods

Begüm KARALAR

Manisa Celal Bayar University

Graduate Education Institute

Bioengineering Department

Supervisor: Asst. Prof. Dr. Deniz KARATAŞ

In the field of molecular modeling, the molecular docking method involves the binding of a target molecule to a second target molecule to form a stable complex. The molecular docking method has an important place in explaining the protein-ligand or enzyme-ligand relationship. It also plays a role in the studies of enzyme inhibition processes. While determining whether the millions of compounds obtained in molecular docking studies are effective and efficient possible drug active ingredients, imaging is also provided with the help of the receptors and complex structures used. Within the scope of this master's degree graduation project study, the components of new FDA-approved drugs produced as a solution to prostate cancer were focused on. The interactions of Abiraterone, Olaparib, Pylarify, Rucaparib and Locametz drugs on the crystal structures of 1E3G, 8E1A, 2ZCH and 2ZCL belonging to the ligand binding domains of the androgen receptor were evaluated and observed in the Autodock program. Based on the results of 180 molecular docking analyses, Olaparib and Rucaparib yielded the best ADMET results. Additionally, 25 molecular dynamics simulations of 50 ns were performed. The results were recorded using Open Babel GUI, Discovery Studio, and Avogadro, supporting this work. This study also provides insights into whether the drugs actually inhibit and whether they facilitate molecular interactions.

Keywords: prostate cancer, Abiraterone, Olaparib, Pylarify, Rucaparib and Locametz, protein-drug interaction, molecular docking, molecular dynamics simulation, Autodock

2025, 151 pages

PREFACE AND ACKNOWLEDGEMENTS

I would like to thank my advisor Asst. Prof. Dr. Deniz KARATAŞ, who patiently supported me throughout the entire process of my M.Sc. thesis, never withheld his knowledge and experience from me, and guided me. I would like to thank our department head, Prof. Dr. Yılmaz Yürekli and my colleagues for their valuable contributions.

I would like to thank my beloved family, Aylin Karalar and Mesut Karalar, who have supported me in all the choices I have made and throughout my life and have always been by my side.

I would like to thank Turgut Ay, a person as bright as the light of science, who never lost his faith in me and who has always been my greatest supporter.

Begüm KARALAR
Manisa, 2025

SYMBOLS AND ABBREVATIONS INDEX

WHO	World Health Organization
AJCC	American Joint Committee on Cancer
UICC	Union International Center Cancer
PCa	Prostate Cancer
mCRPC	Metastatic Castration-Resistant Prostate Cancer
PTEN	Phosphatase and Tensin Homolog
ER	Estrogen Receptor
PR	Progesterone Receptor
MD	Molecular Docking
MDS	Molecular Docking Simulation
OH	Hydroxyl
IR	Infrared Radiation
UV	Ultraviolet
NMR	Nuclear Magnetic Resonance
HF-SCF	Hartree-Fock Self Consistent Field
IR	Molecular Dynamic Simulation
UV	Ultraviolet
ρ	Density
MM	Mechanics Method
pH	Power of Hydrogen
EPR	Electron Paramagnetic Resonance
GPU	Graphics Processing Unit
CPU	Cental Processing Unit
PBC	Periodic Boundary Conditions
PME	Particle Mesh Ewald
USG	Ultrasonography
MRI	Magnetic Resonance Imaging

TNM	Tumor-Node-Metastasis
PET-CT	Positron Emission Tomography
CT	Computed Tomography
DNA	Deoxyribonucleic Acid
RNA	Ribonucleic Acid
FDA	Food and Drug Administration
LHRH	Luteinizing Hormone-Releasing Hormone
LH	Luteinizing Hormone
IC50	Half Maximal Inhibitory Concentration
PDB ID	Protein Data Bank Identification Number
UCSF Chimera	University of California, San Francisco Chimera
ChEMBL	Chemical Database of Bioactive Molecules
UniProtKB	Universal Protein Resource Knowledgebase
UHeM	The National Center for High Performance Computing
PubChem	Public Chemical Database
PDBQT	Protein Data Bank, Partial Charge (Q), Atom Type (T)
RMSD	Root Mean Square Deviation
RMSF	Root Mean Square Fluctuation
Rg	Gyration Radius
SASA	Solvent Accessible Surface Area
MSD	Mean Square Displacement
ADMET	Absorption, Distribution, Metabolism, Excretion, and Toxicity

FIGURES INDEX

Page

Figure 1.1. Timeline of drugs approved by the FDA for the treatment of prostate cancer…… 4
Figure 1.2. Mechanism of PARP inhibitor action……..... 5
Figure 1.3. Pylarify (Piflufolastat F 18 or 18F-DCFPyL) mechanism of action….. 6
Figure 2.1. Interaction between target and ligand and molecular localization image. 11
Figure 2.2. Typical workflow of molecular docking between target molecule and ligand…… 12
Figure 2.3. Tabular display of protein-ligand classification for molecular docking.. 13
Figure 2.4. Steps of the MD simulation process…… 15
Figure 2.5. Prostate anatomy of a normal male individual…… 21
Figure 2.6. Workflow of MRI-TRUS(Ultrasound) Fusion Biopsy method…….. 26
Figure 2.7. T staging for prostate cancer……... 29
Figure 2.8. Whole body magnetic resonance imaging (WB-MRI) and PSMA (Prostate Specific Membrane Antigen) PET/CT images of a 68-year-old man with stage IV prostate cancer……. 30
Figure 2.9. Prostate small cell carcinoma with HE (hematoxylin-eosin) stain….. 31
Figure 2.10. Needle core biopsy of mucinous prostate adenocarcinoma…….. 32
Figure 2.11. Molecular and cellular progression stages of prostate cancer……. 36
Figure 2.12. Images of all grades from Grade1 to Grade5 were scanned at 40x optical magnification…… 37
Figure 2.13. The treatment methods of prostate cancer…… 41
Figure 2.14. Radiotherapy treatment plan applied to a prostate cancer patient with an appropriate dose and post-radiotherapy with Cone Beam Computed Tomography (CBCT) method……... 42
Figure 3.1. 3D image of 1E3G and 8E1A receptors obtained from UCSF Chimera.. 46
Figure 3.2. 3D image of 2ZCH and 2ZCL receptors obtained from UCSF Chimera.. 47
Figure 3.3. Illustration of the identification of hydrogen bonds with donor and acceptor atoms in an MDS process…… 56
Figure 4.1. 2D ligand-protein diagram using Discovery Studio program showing amino acid transfers between 1E3G receptor and Apigenin, Rucaparib, CHEMBL182412, Estrone ligands, respectively……. 61
Figure 4.2. 2D ligand-protein interaction diagram with Discovery Studio program showing amino acid interactions between 8E1A receptor and Baicalin, Olaparib, CHEMBL267270, Mibolerone ligands, respectively…….. 65
Figure 4.3. 2D ligand-protein interaction diagram with Discovery Studio program showing amino acid interactions between EGCG, Olaparib, Fukugetin, Paclitaxel ligands with 2ZCH receptor, respectively…… 68
Figure 4.4. 2D ligand-protein interaction diagram with Discovery Studio program showing amino acid interactions between 2ZCL receptor and Astragaloside, Orgovyx, Fukugetin, Docetaxel ligands, respectively……... 71
Figure 4.5. RMSD analysis results graph of 1E3G, 8E1A, 2ZCH and 2ZCL receptors bound to Abiraterone drug in MD simulation…… 75
Figure 4.6. MD simulation, RMSF analysis results graph of Abiraterone drug bound to 1E3G, 2ZCH, 2ZCL and 8E1A receptors……. 77
Figure 4.7. Graph of Rg analysis results bound to 1E3G, 2ZCH, 2ZCL and 8E1A receptors for Abiraterone drug in MD simulation……. 78
Figure 4.8. Results of SASA bound to 1E3G, 2ZCH, 2ZCL and 8E1A receptors with

Abiraterone drug during MD simulation…… 79
Figure 4.9. RMSD analysis results graph of 1E3G, 8E1A, 2ZCH and 2ZCL receptors bound to Olaparib drug in MD simulation……. 80
Figure 4.10. RMSF analysis results graph of Olaparib drug bound to 1E3G, 2ZCH, 2ZCL and 8E1A receptors in MD simulation…… 81
Figure 4.11. Graph of Rg analysis results for Olaparib drug bound to 1E3G, 2ZCH, 2ZCL and 8E1A receptors in MD simulation……... 82
Figure 4.12. Results of SASA bound to 1E3G , 2ZCH, 2ZCL and 8E1A receptors with Olaparib drug during MD simulation…… 83
Figure 4.13. RMSD analysis results graph of 1E3G, 8E1A, 2ZCH and 2ZCL receptors bound to Pylarify drug in MD simulation……. 85
Figure 4.14. RMSF analysis results graph of Pylarify drug bound to 1E3G, 2ZCH, 2ZCL and 8E1A receptors in MD simulation…… 86
Figure 4.15. Plot of Rg analysis results bound to 1E3G, 2ZCH, 2ZCL and 8E1A receptors for the drug Pylarify in MD simulation……. 87
Figure 4.16. Results of SASA bound to 1E3G, 2ZCH, 2ZCL and 8E1A receptors with Pylarify drug during MD simulation……. 88
Figure 4.17. RMSD analysis results graph of 1E3G, 2ZCH and 2ZCL receptors bound to Rucaparib drug in MD simulation…… 90
Figure 4.18. RMSF analysis results graph of Rucaparib drug bound to 1E3G, 2ZCH and 2ZCL receptors in MD simulation……. 91
Figure 4.19. Rg analysis results graph for Rucaparib drug in MD simulation, bound to 1E3G, 2ZCH and 2ZCL receptors…… 92
Figure 4.20. SASA results for 1E3G, 2ZCH and 2ZCL receptors with Rucaparib during MD simulation…….. 93
Figure 4.21. RMSD analysis results graph of 1E3G, 2ZCH and 2ZCL receptors bound to Locametz drug in MD simulation…… 94
Figure 4.22. RMSF analysis results of Locametz drug bound to 1E3G, 2ZCH and 2ZCL receptors in MD simulation…… 95
Figure 4.23. Rg analysis results graph for Locametz drug bound to 1E3G, 2ZCH and 2ZCL receptors in MD simulation…… 96
Figure 4.24. SASA results for 1E3G, 2ZCH and 2ZCL receptors with Locametz drug during MD simulation…….. 97
Figure 4.25. ADMETLab2.0 results for potential drug candidacy of Abiraterone with the 2ZCH receptor…… 99
Figure 4.26. ADMETLab2.0 results for potential drug candidacy of Olaparib with the 8E1A receptor…….. 101
Figure 4.27. ADMETLab2.0 results for potential drug candidacy of Rucaparib with 1E3G receptor…….. 103
Figure 4.28. ADMETLab2.0 results for potential drug candidacy of Pylarify with the 2ZCL receptor…….. 105
Figure 4.29. ADMETLab2.0 results for Locametz's potential drug candidacy with the 8E1A receptor…….. 107

TABLE INDEX **Page**

Table 2.1. Goals and fields of study of bioinformatics ……..……. 8
Table 2.2. Main topics related to molecular modeling…… 9
Table 2.3. Prostate cancer symptoms……..... 23
Table 2.4. Distribution of PSA levels and risk ratios…… 24
Table 2.5. Advantages of the MR-Ultrasound Fusion Biopsy test…… 26
Table 2.6. Gleason Scoring System and Prostate Cancer Stages…….. 33
Table 2.7. Genes involved in prostate cancer…… 35
Table 2.8. Prostate Cancer Stages and TNM staging…… 39
Table 2.9. Classification of drugs used in prostate cancer hormone therapy… 45
Table 3.1. CHEMBL codes of New Prostate Cancer Drugs, natural agents, traditional drugs and IC50 drugs……. 49
Table 3.2. Centers, dimensions and coordinates of the grid box of receptors and ligands with AutoDock Vina and Autodock Tools…… 51
Table 3.3. Descriptions of ligand files and GitHub GROMACS Protein-Ligand files……. 53
Table 4.1. Receptor-ligand structures with lowest binding energy with AutoDock Vina and AutoDock Tools…….. 59
Table 4.2. Grid box parameter file of 1E3G receptor and ligands with AutoDock Vina…… 61
Table 4.3. Grid box parameter file of 8E1A receptor and ligands with AutoDock Vina…… 64
Table 4.4. Grid box parameter file of 2ZCH receptor and ligands with AutuDock Vina…… 67
Table 4.5. Grid box parameter file of 2ZCL receptor and ligands with AutuDock Vina……..... 70
Table 4.6. MD simulation parameters…… 74

CONTENT

	Page
SUMMARY	I
ABSTRACT	III
FOREWORD AND ACKNOWLEDGMENTS	IV
SYMBOLS AND ABBREVATIONS INDEX	V
FIGURES INDEX	VII
TABLES INDEX	IX
CONTENT	X
INTRODUCTION	1
CHAPTER I	
ORGANIZATION OF THESIS3	
1.1. Overview of Prostate Cancer Drugs	4
1.1.1. Working Mechanisms of New Prostate Cancer Drugs	5
CHAPTER II	
GENERAL INFORMATIONS	
2.1. Molecular Docking and Basic Concepts	11
2.2. Interaction of Protein-Ligand Docking	12
2.3. Molecular Dynamics Simulation Techniques	13
2.3.1. Ewald Summation Techniques	16
2.3.2. Energy-Minimization Methods	16
2.3.3. Solvent Models	16
2.3.4. Thermostats	16
2.3.5. Periodic Boundary Conditions (PBC)	16
2.3.6. Particle Mesh Ewald Method	17
2.4. Prostate Cancer: Epidemiology and Risk Factors	17
2.4.1. Prostate Gland Anatomy, Tissue and Signaling Pathways	20
2.4.2. Clinical Symptoms of Prostate Cancer	22
2.4.3. Early Detection Methods in Prostate Cancer	23
2.4.4. Staging of Prostate Cancer	26
2.4.4.1. TNM Staging Method in Prostate Cancer	27
2.4.4.2. Histological Classification of Prostate Cancer	30
2.4.4.3. Molecular Claassification of Prostate Cancer	34
2.4.4.4. Pathological Classification of Prostate Cancer	36
2.4.4.5. Stage Groups for Prostate Cancer	37
2.5. Prostate Cancer Treatment Methods	40
2.5.1. Surgical Methods	41
2.5.2. Radiotherapy	41
2.5.3. Hormone Therapy	43
2.5.4. Chemotherapy	45
CHAPTER III	
MATERIALS AND METHODS	
3.1. New Prostate Cancer Drugs	47

3.2. Protein Preparation 48
3.3. Ligand Preparation 48
3.4. Protein-Ligand Docking 49
3.5. Molecular Docking Procedure with Autodock Tools & Autodock Vina 49
3.6. Molecular Dynamics Simulatios Procedure with GROMACS Tutorial 52
3.7. Molecular Dynamics Simulation Tutorial-5 Analysis..... 54
3.7.1. Clustering Analysis (Frame Selection) 54
3.7.2. RMSD (Root Mean Square Deviation)..... 55
3.7.3. RMSF (Root Mean Square Fluctuations) 55
3.7.4. Hydrogen Bond Analysis 55
3.7.5. Radius of Gyration (Rg) 56
3.7.6. SASA (Solvent Accessible Surface Area) 57
3.7.7. ADMET (Absorption, Distribution, Metabolism, Excretion and Toxicity)…… 57

CHAPTER IV
RESEARCH FINDINGS AND DISCUSSION

4.1. Molecular Docking Findings…….. 59
4.1.1. Molecular Docking Studies of the 1E3G Receptor with Drugs and Ligands.....
4.1.2. Molecular Docking Studies of 8E1A Receptor with Drugs and Ligands……..... 63
4.1.3. Molecular Docking Studies of 2ZCH Receptor with Drugs and Ligands……..... 67
4.1.4. Molecular Docking Studies of 2ZCL Receptor with Drugs and Ligands……. 70
4.2. Molecular Dynamics Simulations Results (Stability of Ligand Receptor Complexes)……... 73
4.2.1. Molecular Dynamics Simulations of 1E3G, 8E1A, 2ZCH, 2ZCL Receptors with Abiraterone Drug…….. 74
4.2.2. Molecular Dynamics Simulations of 1E3G, 8E1A, 2ZCH,2ZCL Receptors with the Drug Olaparib ……..... 79
4.2.3 Molecular Dynamics Simulations of 1E3G, 8E1A, 2ZCH, 2ZCL Receptors with the Pylarify Drug …… 84
4.2.4. Molecular Dynamics Simulations of 1E3G, 2ZCH, 2ZCL Receptors with the Drug Rucaparib…… 89
4.2.5. Molecular Dynamics Simulations of 1E3G, 2ZCH, and 2ZCL Receptors with the Locametz Drug …… 93
4.3. ADMET Data Results with Abiraterone, Olaparib, Pylarify, Rucaparib,Locametz Drugs……... 98

CHAPTER V
CONCLUSION AND SUGGESTIONS
5.1. Overall Conclusions, Suggestions and Final Thoughts..... 109

REFERENCES **111**

APPENDICES **122**
APPENDIX A. Molecular Docking Results with Autodock Vina **122**
APPENDIX B. GROMACS Tutorial/ Protein-Ligand Complex **132**

1. INTRODUCTION

Cancer is an important public health problem that causes many deaths worldwide. Increasing incidence is a major problem both in the world and in our country. However, cancer and its types have different incidence and mortality rates worldwide (Ribelles et al., 2024).

The meaning of the term cancer is expressed as uncontrollable cell proliferation in various parts of the body, resulting in an increase in abnormal cell numbers and the formation of tumor tissues, invading other tissues and disrupting their functioning structure. There are varieties of cancer such as prostate, lung, breast, leukemia, lymphoma, brain and colon. In general, the causes of cancer can be listed as genetic predisposition, gender, age, race, eating habits, obesity, harmful habits, environmental factors, chemical substances, radiation. Prostate cancer develops due to the same reasons (Jenča et al., 2024), (Gandaglia et al., 2021).

In men worldwide, prostate cancer is the second most prevalent type of cancer. Men worldwide have a 1 in 8 chance of developing this cancer in their lifetime. In 2024, it is estimated that approximately 300,000 men in the United States will be diagnosed with prostate cancer and more than 35,000 will die from prostate cancer (Schaeffer et al., 2024).

According to the 2018 Turkey Unified Database, prostate cancer is among the top five most common cancers in men in Turkey and ranks second after lung cancer. In the percentage distribution of all age groups, the rate of prostate cancer is 15% (Açıkgöz, Çımrın, & Ergör, 2018).

Prostate cancer is a malignant tumor that occurs as a result of the uncontrolled growth and proliferation of cells in the prostate gland, an important section of the male reproductive system. The prostate gland is a walnut-sized gland located between the bladder section and penis sections of the male reproductive system and surrounding the bladder outlet, and weighs approximately 30 grams. The function of the prostate gland is to produce a slightly alkaline white secretion. This secretion is about 30% of semen. Because it is alkaline, it neutralizes the acidic vaginal environment and

prolongs the life of sperm. The prostate gland consists of 5 regions in its internal structure. These regions are peripheral region, central region, transitional region, fibromuscular region and preprostatic sphincteric region. The majority (70-80%) of the starting point of prostate cancer originates in the peripheral region. The malignant tumor that forms in these cells can spread as metastasis to lymph nodes, bones and even other tissues (McNeal, 1988), (Yu, Yan, Liu, & Zhang, 2024).

One of the causes of prostate cancer is genetic predisposition and 60 percent is inherited. It has been proven that some genes can increase the risk of prostate cancer. AR (Androgen Receptor) gene, PSA/ KLK3 (Prostate Specific Antigen) gene, HOXB13 (Homeobox Protein) genes have been associated with prostate cancer (Aurilio et al., 2020). Apart from genetic predisposition, aging (50 years and older), family history of prostate cancer, obesity, hormone imbalances (high testosterone levels), unbalanced and high-fat diet, smoking and alcohol use, lack of physical activity, exposure to environmental toxins are considered among the risk factors for prostate cancer (Gandaglia et al., 2021).

Today, prostate cancer diagnostic methods include prostate specific antigen (PSA) test, insulin-like growth factor (IGF), pressure flow test, urine analysis, symptom score, uroflowmetry, cystoscopy, residual urine measurement, MR ultrasound and biopsy. After the diagnosis of prostate cancer, appropriate treatment methods are examined according to the stage of prostate cancer. These treatment modalities include surgery, radiotherapy, hormone therapy, chemotherapy, drugs, immunotherapy, targeted therapy and radioactive substances (Sekhoacha et al., 2022), (Fu et al., 2021).

Among these treatment methods, medication is clinically the treatment of choice in all cases. Drug treatment has side effects, especially when the drug crosses the blood-brain barrier, which means that it can cause a lot of negative side effects. New drug discoveries continue rapidly to minimize side effects such as nausea, vomiting, weakness, fatigue, diarrhea, bleeding and reduced resistance to infection. In clinical trials, drugs such as Abiraterone (2018), Olaparib (2020), Rucaparib (2020), Pylarify (2021), Locametz (2022) have been used for trials (Książek et al., 2024), (Zhang & Chadha, 2024), (van Brandwijk, Aalbersberg, Hosseini, Huitema, &

Hendrikx, 2024).

Due to the high prevalence of prostate cancer among men, there is a need to go beyond standard treatment to improve the quality of life of patients suffering from prostate cancer, to improve their response to drug therapies, to increase the number of patients who benefit from treatment, to revolutionize cancer treatment and to discover targeted treatment methods. New drugs need to be developed according to the stage of development, type and structure of the cancer, and they need to be better explained at the molecular level and possible target molecules need to be accurately identified.

In this master's thesis study, prostate cancer cell structures and the structures of new prostate cancer drugs approved by the FDA were modeled at the atomistic level with the aim of eliminating some defects in the studies in the literature, adjusting the optimum amount of drug doses to get the best efficiency, and determining the best conformations of receptor and receptor structures. We are looking for alternative solutions to prostate cancer with molecular modeling and molecular dynamics simulation methods with reference to the components of new FDA approved drugs.

One of the unique aspects of this study is the use of Molecular Docking, Molecular Dynamics Simulation (MDS) and Absorption, Distribution, Metabolism, Excretion, and Toxicity (ADMET) methods. Molecular docking was used to create an interaction network between new drugs and important genes associated with prostate cancer and to predict the binding affinities of the compounds to the genes.

CHAPTER I. ORGANIZATION OF THESIS

1.1. Overview of Prostate Cancer Drugs

In the mid-19th century, the tumor cells of prostate cancer were first discovered during surgery and treatment of men suffering from urinary tract obstruction. Although prostatectomy treatment was applied to these individuals as an initial step, with the development of technology, radiation treatments and hormone therapies were applied to cure patients suffering from prostate cancer. Charles B. Huggins received the Nobel Prize for the discovery of the first hormone therapy. In 1941, after Huggins and Hodges developed Androgen Suppression Therapy (ABT) for prostate cancer patients, treatment options continued to increase (Samuel R Denmeade & John T Isaacs, 2002).

In the late 1960s, the androgen receptor was discovered. Since androgen receptors are associated with prostate cancer, in order to find blockers of these receptors, a 'pure' steroid anti-androgen had to be discovered that could somehow inhibit the binding of the dihydrotestosterone (DHT) molecule or the testosterone molecule to this receptor, and this was the drug cyproterone acetate. Because of some of the major side effects of the drug cyproterone acetate (liver hyperplasia, loss of sexual potency, etc.), efforts were continued to find a 'pure' anti-androgen. This drug became flutamide and was approved by the United States Food and Drug Administration (FDA) in 1989 (Samuel R Denmeade & John T Isaacs, 2002).

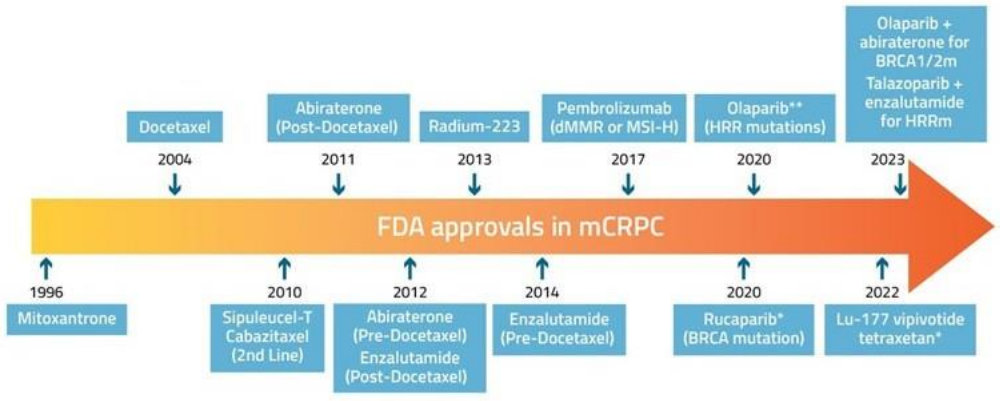

Figure 1.1. Timeline of drugs approved by the FDA for the treatment of prostate cancer (Samuel R Denmeade & John T Isaacs, 2002).

In this thesis, the contents of the components that affect prostate-specific antigen (PSA/KLK3) and Androgen Receptor (AR) of the new drugs recently

approved by the FDA for the treatment of prostate cancer, Abiraterone (2018), Olaparib (2020), Rucaparib (2020), Pylarify (2021) and Locametz (2022), were evaluated using molecular modeling methods.

1.1.1. Mechanisms of New Prostate Cancer Drugs

The mechanism of action of the drug Abiraterone involves the inhibition of CYP17A1 and the suppression of the synthesis of the androgen molecule and the cortisol molecule to a large extent. In humans, the CYP17A1 gene is responsible for the synthesis of testosterone and estrogen molecules. The CYP17A1 gene promotes androgen, on which tumor cells depend. By inhibiting CYP17A1 with the drug Abiraterone, tumor cell growth is prevented. In 2018, the FDA agency approved the drug Abiraterone Acetate as a solution against high-risk metastatic castration-sensitive prostate cancer (Attard et al., 2012).

Olaparib and Rucaparib, also known as a poly (ADP-ribose) polymerase inhibitor, target prostate cancer cells. The PARP protein repairs breaks in the DNA of damaged or mutated cancer cells. PARP protein inhibitors prevent the repair of breaks in the DNA of these cells, allowing the cells to self-destruct. In 2020, the FDA approved Olaparib, a solution for metastatic castration-resistant prostate cancer with the HRR gene mutation (Longoria et al., 2023).

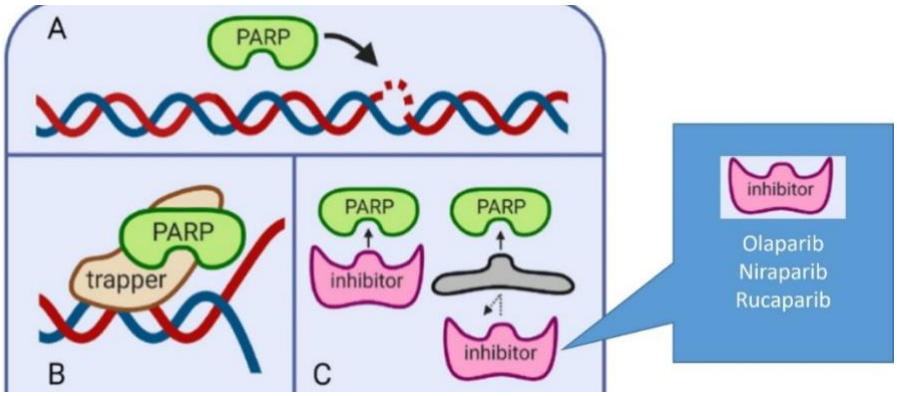

Figure 1.2. Mechanism of PARP inhibitor action (O'Malley et al., 2023).

The synthesis of PARP inhibitors can be produced in laboratory conditions by experts through multistep chemical and biological processes. These inhibitors can be obtained by chemical synthesis methods. These methods can be similar to amidation,

halogenation and alkylation. Primidine derivatives are obtained by synthesis of benzoic acid derivatives. Although PARP inhibitors cannot be obtained from natural sources, curcumin and flavonoid-like molecules can alter the enzyme activity of PARP protein (He, H. et al., 2024).

Malignant prostate cancer cells have prostate-specific membrane antigen (PSMA) located on their surface. Pylarify (Piflufolastat F 18 or 18F-DCFPyL) works by binding to cells expressing PSMA and leading to endocytosis. Fluorine-18 (F 18), a β+ emitting radionuclide molecule, can be used to detect prostate cancer cells by positron emission tomography (Voter, A.F. et al., 2022).

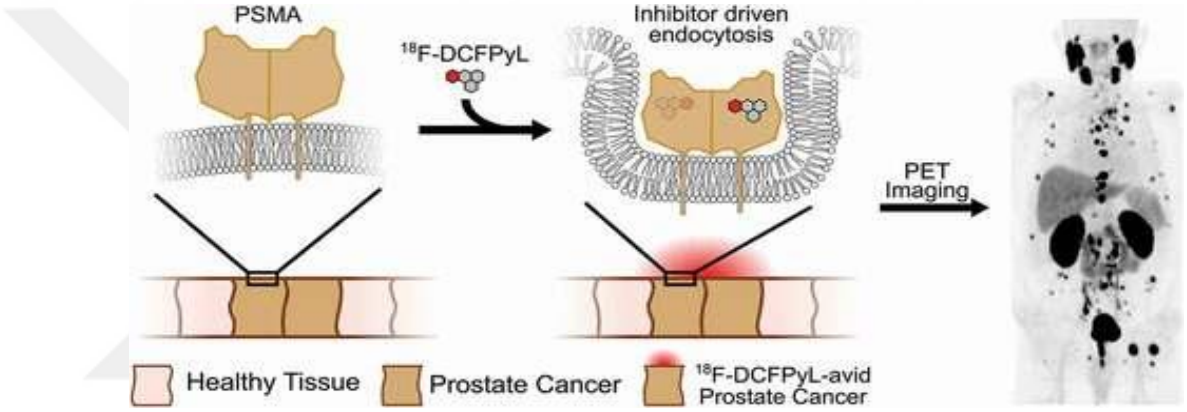

Figure 1.3. Pylarify (Piflufolastat F 18 or 18F-DCFPyL) mechanism of action (Voter, A.F. et al., 2022).

Pylarify (Piflufolastat F 18 or 18F-DCFPyL) can be created in hospital departments of universities or licensed radiopharmaceutical production centers. Due to F 18, the duration of this substance is very short. F18 molecule can be obtained from O-18 enriched water via cyclotron. This molecule is dried with sodium carbonate-like substances, especially to gain nucleophilic activity. 18F and PSMA ligand combine to form the 18F-DCFPyL molecule. The resulting product can be separated into other ingredients by high-performance liquid chromatography (HPLC) (Wang, H. et al., 2024).

Prostate-specific membrane antigen (PSMA) is present on the surface of malignant prostate cancer cells and some cells. The mechanism of action of **Locametz (Gallium (68Ga) gozetotide)** is to bind to cells expressing PSMA and lead to

endocytosis. Gallium (68Ga) is a radionuclide molecule that can be used to visualize prostate cancer cells using positron emission tomography (PET) (Wang, I. E. et al., 2024).

There are steps in the formation of Locametz (Gallium (68Ga) gozetotide). The first one is the conversion of ^{68}Ge into ^{68}Ga using ^{68}Ge/^{68}Ga radionuclide generators. These ions are combined with DOTA gozetotide and form a tight structure. The resulting product can be separated into other ingredients by high-performance liquid chromatography (HPLC) (Wang, I. E. et al., 2024).

CHAPTER II. GENERAL INFORMATIONS

Bioinformatics is an interdisciplinary science that mediates the processing, analysis, storage, organization and reporting of biological and genetic data obtained from many fields in a computer environment, creating large databases, covering many different fields such as medical sciences, biology, biochemistry, mathematics, biostatistics. The fields of bioinformatics include accurate drug development, rational diagnosis and treatment applications, biological and genomic studies. As medicine and technology progressed, scientists' efforts to learn more about the human genome sequence contributed to the birth of the field of bioinformatics. Although the term bioinformatics started to be used in the 1980s, it took off with the National Center for Biotechnology Information (NCBI) in 1988 and the Human Genome Project (HGP) in 1990 (Akın, A. C. et al., 2014).

Table 2.1. Goals and fields of study of bioinformatics (Akın, A. C. et al., 2014).

Protein-Protein relationships and determination of protein structures
Protein-Ligand relationship
Protein and DNA sequence studies
Simulation of molecular structures and interactions
Molecular analyses obtained from Human, Animal, Plant-oriented projects
Big data analysis and creation of three-dimensional molecular databases
Gene expression analysis

Universities and large companies have bioinformatics laboratories for scientists working on gene analysis and for the diagnosis of diseases. Physicians, geneticists and engineers working in laboratories carry out these studies and projects. In addition, many biological databases that support these studies are used by these bioinformatics scientists (Liu, Z. Et al., 2015).

1. National Center for Biotechnology Information (NCBI)
2. Protein Data Bank (PDB)
3. PubChem
4. PubMed
5. ChEMBL

6. BLAST (Basic Local Alignment Search Tool)
7. UniProt
8. GenBank

In addition, one of the important areas of bioinformatics is rational drug design. The aim of rational drug design is to analyze and design drug candidates that have the potential to interact with the information obtained on biological targets. The rational drug design process consists of four steps. These steps include identification of the biological target (protein or enzyme), structural analysis of the biological target, selection and design of ligands that can bind to the targets and molecular docking, and virtual modeling and simulations. Using algorithms, rational drug design can be achieved and can go beyond traditional trial-and-error methods to test and determine an appropriate direction for the target (Thibaut U., 2002).

1. Biological Target Identification; structurally targeting and identifying genes related to the disease to be analyzed
2. Structural Analysis of Biological Target; obtaining 3D crystallography structures of target genes
3. Ligand Selection; selection of drug candidates that can bind to targets
4. Virtual Simulation; Virtual screening of drug candidate molecules

Molecular modeling is a method of mimicking or modeling the behavior of molecules or their interactions with other molecules in silico. Molecular modeling has many advantages. Some of them are; obtaining the three-dimensional structure of molecules, distinguishing the chemical and physical properties of molecules, comparing a molecule with another possible molecular structure, and possible predictions with the visualizations created by the simulation. Molecular modeling system is divided into volumetric and surface. The volumetric modeling method is done by placing a triangle, similar to the mass spring system, in each corner to symbolize an atom (Silakari, O., & Singh, P. K., 2020).

Table 2.2. Main topics related to molecular modeling (Tripathi, M. K. et al., 2022).

Determination of chemical and physical properties of molecules	Knowledge of steric, electronic etc. properties
Enzyme-substrate interaction	Compatibility with the active site of the enzyme and molecule
IR, UV, NMR Spectra	Chemical structure and spectrum of the structure
Chemical Reactivity	Nucleophilic (regions where electrons are concentrated) and electrophilic (regions where electrons can travel)
3D structure and geometry of the molecule	Bond lengths and angles of molecules

Calculated methods for molecular localization and simulation programs are available. The solution of the calculation of the energy of small molecules based on the Schrödinger equation can be approximated by simulation. Two different methods present themselves. The first one is the Ab-initio method, which is the molecular orbital method. Two different mathematical Ab-initio methods are used. These are the Hartree-Fock Self-Consistent Field Theory (HF-SCF) method and the Density Functional Theory (DFT) method. The Ab-initio method, which means from the beginning, is calculated without values such as the speed of light and Planck's constant, unlike the quasi-experimental method. In the HF model, each electron exists in a system with push-pull forces and its own wave function. Based on the equation for the charge distribution of the electron relative to other electrons, it calculates a frequency for electron interactions called the self-consistent field. The Density Functional Theory (DFT) method is based on the Schrödinger equation, unlike the Hartree-Fock Self-Consistent Field Theory (HF-SCF) method. It calculates the electron probability density (ρ) instead of molecular frequency and charge distribution. The electron density is set as a variable. This method gives much more accurate and precise results

for the chemical properties of molecules (Elshakre, M. E. et al., 2020).

The second method of molecular modeling, the Molecular Mechanics Method (MM), is a method that uses classical mechanical methods to calculate the interactions and intra-atomic and extra-atomic energies in the biological system with force fields. This method is based on the Born-Oppenheimer calculation. The method is based on the fact that the electron and nucleus move together as a ball or a bundle, the bonds between atom-like particles are represented as springs, and the potential energy functions are based on empirical methods (Eren, D., & Yalçın, İ., 2020).

2.1. Molecular Docking and Basic Concepts

Molecular docking involves the insertion of the ligand into the binding site of the receptor in a molecule-ligand complex. This process, called locking, involves the interaction of the active site in the target protein structure with another molecule. These interactions include hydrogen bonds, van der waals bonds and hydrophobic interactions. The distribution of atoms, their charges, orbitals, relative positions, energies and the conformation of the molecule to be docked are all involved in binding to the target molecule. In addition, it enables the simulation of protein-ligand conformation using algorithms. Molecular docking studies have a major role in understanding how existing compounds or drug candidates have an effect on target genes (Hernndez-Santoyo, A. et al., 2013).

An image and typical workflow of molecular docking resulting from the interaction between the target molecule and the ligand binding to the binding site is shown in Figure 2.1.

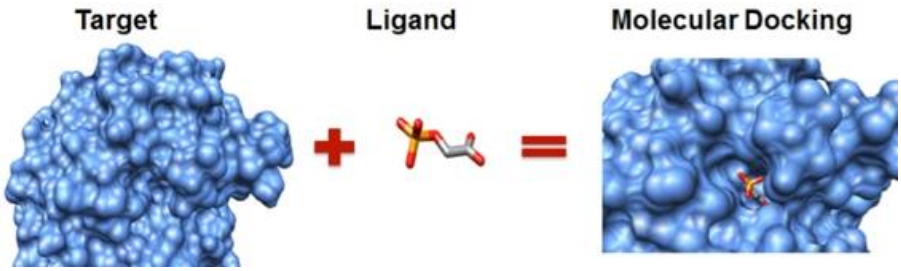

Figure 2.1. Interaction between target and ligand and molecular localization image (Hernndez-Santoyo, A. et al., 2013).

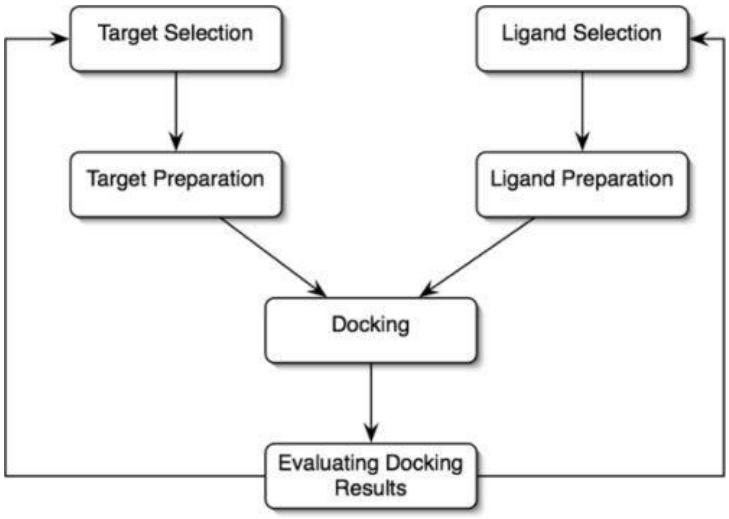

Figure 2.2. Typical workflow of molecular docking between target molecule and ligand (Dnyandev, K. M. et al., 2021).

The appropriate protein-ligand conformation is important for molecular docking to occur, and selecting the appropriate ligand and target molecule from among dozens of compounds is not only impossible to try in vitro, but also has many disadvantages. These in silico experiments do not pose chemical and biological threats. The most important advantage is to identify the right drug components and ensure their optimization. In addition, analysis of molecules that are not suitable to be studied in vitro-in vivo, saving money by creating a simulation environment and easily changing target-ligand structures make molecular docking method attractive (Saikia, S., & Bordoloi, M., 2019).

2.2. Protein-Ligand Docking Interaction

Mimicking protein-ligand molecule docking and interaction is a challenging process because protein-ligand docking has many factors and involves many force fields such as hydrogen bonds, pi alkyl interactions and hydrophobic bonds. This docking is expected to result in the formation of a stable complex. The target molecule must then be prepared for this process, taking into account many factors, including the flexibility of the protein molecule, so that the structure of the protein is suitable for this pairing and gives accurate results. Once the protein structure and data suitable for the molecular match have been established, this structure should be checked. This interaction mimics the positioning of a ligand or drug in the binding site of the target protein in a position that gives the lowest energy to the binding site (Du, X. et al.,

2016).

The most beautiful models of these interactions are the molecular docking used for the treatment of cancer diseases and are used for potential drug candidates. In addition, protein-ligand complex docking (molecular docking) is used in computational chemistry for drug design. The classification of protein ligand docking methods is shown in Figure 2.3. (Hernndez-Santoyo, A. et al., 2013).

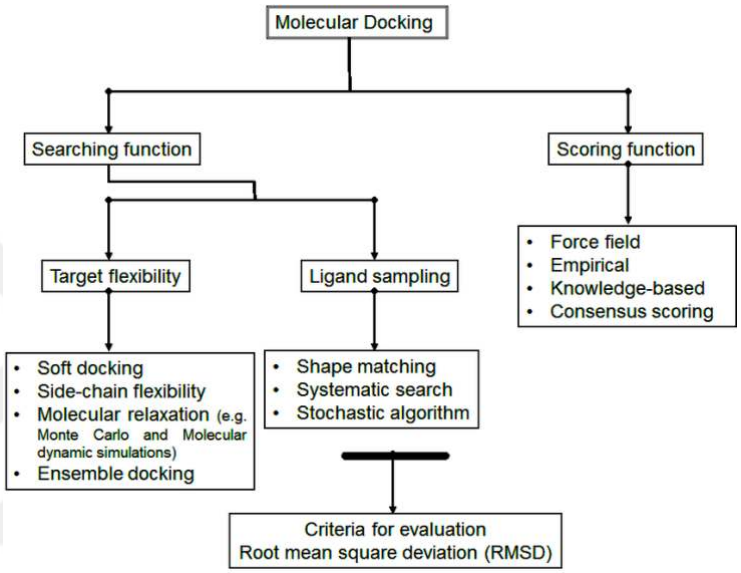

Figure 2.3. Tabular display of protein-ligand classification for molecular docking (Akki, A. J. et al., 2024).

2.3. Molecular Dynamics Simulation Techniques

Molecular dynamics simulations most accurately describe the atoms in an atomic-sized biomolecular system and predict which atom will move how in the system. Likewise, force fields and frequencies of atoms can be calculated. Emerging towards the end of the 20th century, molecular dynamics (MD) simulations and algorithms have become widespread due to their ease and accessibility and the development of technology. Molecular dynamics simulation of simple gases was realized in 1957. MD simulation of protein was performed in the 1970s. MD simulations are used in combination with x-ray crystallography, cryo-electron microscopy (cryo-EM), electron paramagnetic resonance (EPR) methods (Ciccotti, G. et al., 2022).

The MD simulation method uses Newton's second law and makes it possible to determine the force acting on an atom and its spatial position. MD simulation analyzes the physical motion of groups of atoms over time. This method studies the properties of biomolecular processes of molecules such as protein-ligand binding, protein folding, membrane transport and nanomaterials (Ciccotti, G. et al., 2022).

First of all, MD simulations are powerful tools. This is because it can capture the position, conformation and movement of each atom within a desired time frame, which is very difficult in experimental laboratory conditions. Secondly, the initial conformation of the protein and ligand, each molecule in the environment, the mutations or modifications of molecules or genes, the temperature of the environment, the voltage across the membrane are precisely known in this process (Oselusi, S. O. et al., 2024).

In addition, the forces in the MD simulation are calculated by means of force models based on quantum mechanics calculations and mechanical force fields. These are the CHARMM, OPLS, AMBER forces. These force fields capture electrostatic (Coulombic) bonds between atoms, spring-like forces representing the length of bonds, chemical bonds and interatomic interactions. In the MD simulation process, these simulations should be a few femtoseconds (10-15s) to ensure stability. Furthermore, by using the femtosecond time scale, MD simulations reveal the positions of all atoms or groups of atoms involved, which can capture important processes in the protein, such as conformational changes, localization and binding of selected ligands, folding of protein molecules, etc (Wang, L., & O'Mara, M. L., 2021), (Mu Y. et al., 2003).

Biochemical events, structural changes in proteins or ligands occur in nanoseconds, microseconds and longer. Each molecular simulation covers almost billions of time processes. The interactions between atoms and molecules evaluated over these long periods of time increase the demand for these simulations (Yan, X., & Chaudhuri, S., 2022).

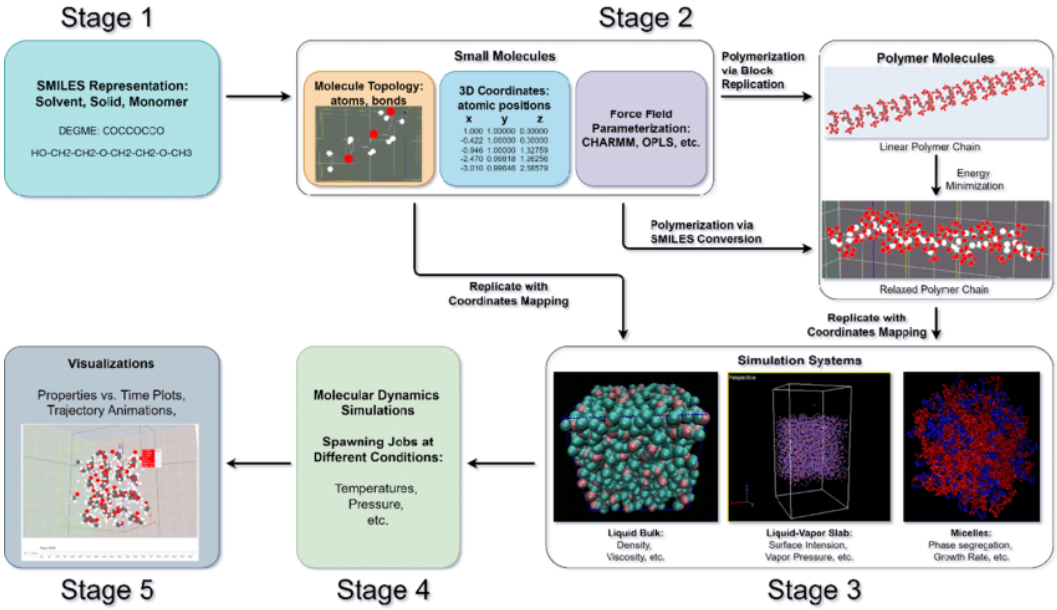

Figure 2.4. Steps of the MD simulation process (Yan, X., & Chaudhuri, S., 2022).

In this process, MD simulation, which illuminates processes such as the detachment and binding of the ligand molecule and the folding of the target protein with high resolution, is also used to analyze the behavior of water molecules, salt ions and solvents that play critical roles in protein-ligand docking. If MD simulation is used in combination with methods such as X-ray crystallography and cryo-EM, structural fluctuations in other regions of the molecule can be measured (Hollingsworth, S. A., & Dror, R. O., 2018).

Molecular dynamics simulations observe the behavior of the biomolecules used at specific temperatures, pressures and salt concentrations and describe the function of the molecules within cells. There are multiple simulation software programs available. These include GROMACS, NAMD, AMBER, CHARMM, Desmond and OpenMM. The computing hardware used is GPU (Graphics Processing Unit) and CPU (Central Processing Unit). GPU is able to run faster simulations at more affordable costs. However, traditional central processing units (CPUs) provide faster results. Although their efficiency is different, the GPU has access to longer time frames and performs high-performance tasks (Tanner, D. E. et al., 2012).

2.3.1. Ewald Summation Techniques

Named after Paul Peter Ewald, the Ewald Summation Technique, a 1984 MD

simulation technique, is a method for calculating long distances and short distances in real space by analyzing interactions for varying electrostatic forces (Toukmaji, A. Y., & Board Jr, J. A. ,1996).

2.3.2. Energy Minimization Techniques

The energy minimization process, which is important for MD simulation to bring the simulation system to equilibrium, determines an orientation towards the protein for minimum energy points and geometries by trying to bring the energy of the system to the lowest point. Energy minimization is done for the stability of the system. Geometry minimization is performed for the equilibrium of the molecules and is based on obtaining the geometry with the lowest energy by gradually decreasing the total energy (Lindahl E. R., 2008).

2.3.3. Solvent Models

Solvent models, one of the MD simulation methods, are important to simulate the appropriate system. Water molecules in the MD simulation environment are needed because they are important for the interactions between the protein-drug complex. Based on properties such as the function, diffusion, radial distribution of water molecules, various water models such as SPC, TIP3P, TIP4P are used (Das, S. et al., 2023).

2.3.4. Thermostats

MD simulations have very large energy fluctuations. In the MD system, advanced thermostat algorithms such as Berendsen, Andersen, Nose-Hoover and Langevin are used to control the system temperature and pressure to keep them at more constant values and to keep the kinetic energy constant (Hünenberger, P. H., 2005).

2.3.5. Periodic Boundary Conditions (PBC)

The definition of periodic boundary conditions is the boundary conditions that are set to approximate a larger system in space using smaller and smaller parts (unit cells). PBCs are used in MD simulations, but can also be used in computer simulations and molecular models in general with specified box sizes (Barclay, P. L., & Zhang, D. Z. ,2021).

2.3.6. Particle Mesh Ewald Method

One of the popular MD Simulation methods is the Particle Mesh Ewald (PME) method. This method is used to calculate long-range Coulomb interactions in 3D systems. The efficiency and accuracy of the Particle Mesh Ewald Method is quite high. These calculations are done with Fourier Space (Mesh) (Duan, Y. et al., 1997).

2.4. Prostate Cancer Epidemiology and Risk Factors

Body tissue cells have their own control mechanism and renew themselves. With this mechanism, damaged tissue is repaired and renewed. Cells that remain out of control and constantly multiply are cell groups called tumors.

Prostate cancer is usually a malignant tumor that starts in the outer shell of the prostate and spreads. If prostate tumors do not stay in the area where they are located and do not spread, they are called benign tumors. The majority of prostate cancers are adenocarcinoma and cancer cells located in the prostate gland can sometimes metastasize by growing and growing in tissues and bones. A classical classification system is used to define whether the cancer is regional or spread, continuing from Stage 1 to Stage 4. In prostate cancer, the cancer cell is quite small in Stage 1. In Stage 2, the cancer cells continue to grow and have not yet spread. In Stage 3, the cancer spreads to tissues outside the prostate gland. Finally, in Stage 4, the cancer has spread to bladder-like tissues and bones (Ashrafizadeh et al., 2024), (Feng et al., 2024).

Prostate cancer was first described in the world by J. Adams in 1853, who examined it histologically. At first, this disease could not be distinguished from urinary tract obstruction, but it continued with the increase in the number of cases. This increase rate showed that new treatment and diagnosis methods should be emphasized. Androgen ablation, which is still the most useful treatment for prostate cancer today, was discovered by Charles Huggins in the 1940s. This treatment involves suppressing or blocking androgen production. Approximately 200 years after this process, prostate cancer has become a very well-known and important disease. It is the most frequently diagnosed disease in men in the United States, Turkey and all over the world. It is one of every 14 cancers diagnosed in the world. It also constitutes 15% of all diseases

diagnosed in men. The mortality rate is quite high. Although the incidence varies all over the world, it is higher in countries such as Northern and Western Europe, the Caribbean, New Zealand and South Africa. The differences in incidence between countries can even vary by region. One of the reasons for this is the advantage of being diagnosed and the health system. However, general risk factors have been determined (James et al., 2024), (S. R. Denmeade & J. T. Isaacs, 2002).

There are risk factors that may affect the development of prostate cancer. Identified risk factors include age, family history, genetic predisposition, race, obesity, and environmental factors. The probability of prostate cancer increases with increasing age. Prostate cancer, which is rare in a 40-year-old man, appears to increase in men after the age of 50. Microscopic prostate cancer is detected in 50% of men over the age of 70 and in most men over the age of 90. Cancer screening is recommended for men over the age of 40 for early diagnosis. 6 individuals in every 10 prostate cancer cases are over the age of 65. The prostate gland grows as it ages and begins to compress the urinary tracts passing through it. As the male individual ages, the Testosterone/Estrogen balance changes towards estrogen. The most important factor in prostate growth after the age of 50 is this hormonal testosterone/estrogen change. While hormones change during the growth process of the prostate, growth factors also play a primary role. The amount and volume of some structures of the prostate increase within the prostate. Race/ethnicity is one of the risk factors for prostate cancer. African-American men are more likely to develop it at an earlier age. In fact, it is 1.6 times more likely to be seen and 2.5 times more likely to die than Caucasians. This rate is lower in Asia. People of Asian descent living in the United States have a higher risk of developing prostate cancer than their Asian relatives (44.1 deaths per 100,000 men vs. 19.1). These rates also highlight dietary and environmental factors. Eating habits can also affect the development of prostate cancer. Diet is very effective in the onset and progression of prostate cancer. Optimal and adequate nutrition plays an important role in prostate cancer. Prostate cancer is slightly more common in people who consume high amounts of red meat and carbohydrates, as well as those who consume low amounts of vegetables and fruits. It has been reported that some natural and lycopene-rich foods such as tomatoes, watermelon, red grapefruit, and even phytochemicals reduce the risk of developing prostate cancer. It is known that the Mediterranean diet reduces the risk of developing cancer. Different bioactive

components in the Mediterranean diet model (resveratrol, curcumin, lycopene, ellagic acid, quercetin, fisetin, epigallocatechin-3-gallate, polyphenols of olive oil) have a positive effect against prostate cancer (Koçak & Tek, 2022),(Sunay, 2010), (Rawla, 2019).

Studies have shown that the risk of developing the disease increases as the number of people with prostate cancer in the family and close relatives and the degree of closeness to the individual increases. For example, the risk of a person whose father/brother has prostate cancer doubles the normal risk of having this disease. Even if the person is young, if more than one person in the family has prostate cancer, this risk increases at the same rate. Approximately 10% of prostate cancer cases are caused by genetic risk. Some genes are also associated with the development of prostate cancer. One of these is hereditary prostate cancer gene 1 (HPCG). Hereditary prostate cancer occurs when more than 2 people in the family have prostate cancer, if there is a prostate cancer death in the family under the age of 60, and if there is a prostate cancer diagnosis in the family under the age of 55 (Tuffaha et al., 2024).

Obesity and weight gain may increase the risk of prostate cancer. As hormonal factors, testosterone hormone promotes the growth of prostate cancer cells. Smoking, alcohol consumption or exposure to certain chemicals are among the risk factors as they may increase the risk of prostate cancer. Studies have shown that smoking can reduce testosterone levels and this may increase the risk of cancer (Palshof et al., 2024). Vitamin D, which is known to be related to bone health, is increasingly known to strengthen human immune function, regulate cellular signaling and processes and prevent cancer cell growth. Epidemiological studies have clearly shown the relationship between prostate cancer and areas exposed to less sunlight and vitamin D deficiency (Cassell & Konneh, 2024).

The following have been identified as general risk factors for prostate cancer: Age, Genetic Factors, Ethnicity/Race, Family History, Hormones, Obesity, Smoking/Alcohol Consumption, Metabolic Syndrome, Eating Habits and Vitamin D (Trock, B. J. et al., 2008).

2.4.1. Prostate Gland Anatomy, Tissue and Signal Pathway

The most important function of the prostate gland is twofold. The first is the production of sperm cells and seminal fluid from the gland. The second is to provide the urinary control mechanism by contracting and relaxing. In addition, prostatic fluid contains antimicrobial components and affects the body's immune system. The anatomical location of the prostate gland is; under the inferior arms of the symphysis pubis, with a narrowed apex at the bottom and a wide ovoid base that continues with the bladder at the top, with the ampulla recti behind it and a tissue that surrounds the urethra by passing through the prostatic urethra. In addition, the ejaculatory duct (seminal duct) passes through it. The function of the prostate gland is to produce a slightly alkaline white secretion, and the secretion is approximately 30% of the semen. Due to the acidic vaginal environment, a slightly alkaline secretion prolongs the life of the sperm. It weighs approximately 30 grams, is 3 cm long, 4 cm wide and 2 cm thick. It consists of smooth and striated muscles. Structurally, it consists of 70% tubuloalveolar glands and 30% fibromuscular stroma. The prostate gland has 5 regions in its internal structure. These are; peripheral region (75%), central region (25%), transitional region (5%), fibromuscular region and preprostatic sphincteric region. Transitional region (5%) is seen as the development region of benign prostatic hyperplasia (BPH), the frequency of which increases with age. 20% of prostate cancers can also develop from this region. Peripheral region (75%) is the region where prostate cancer develops most frequently due to the secretory glands. Since the secretory glands are next to the rectal ampulla, they can be detected during rectal examination. Central region (25%) ejaculatory duct (seminal duct) is located in this region. Prostate cancer originating from here is less common but more aggressive and rapidly progressing. Fibromuscular region contains muscle and connective tissue structure. The preprostatic sphincteric region allows the semen to be expelled forward (Mahadevan et al., 2024), (Xu et al., 2024).

The urinary tract (urethra) surrounded by the prostate, the semen channels coming from both sides (ejaculator channels) open into the part anatomically called "Veru montanum". The prostate muscle tissue consists of sympathetic nerves and the stimulation of these muscles provides the mechanism for closing the bladder part of the seminal fluid during ejaculation (Menezes et al., 2021).

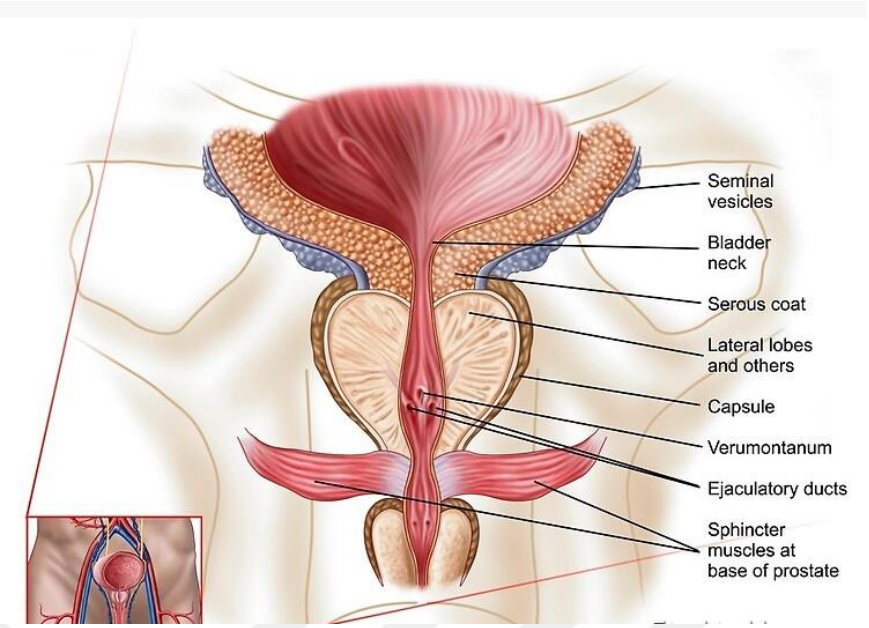

Figure 2.5. Prostate anatomy of a normal male individual (Geavlete, P. A. (Ed.)., 2016).

The prostate gland is surrounded by neurovascular bundles that form nerves and blood vessels. These neurovascular bundles play an important role in normal erection. The peripheral region, due to its proximity to the neurovascular bundles surrounding the prostate, can facilitate the spread of the disease along the perineural and lymphatic pathways and increase the potential for cancer cells to metastasize. The main arterial flow of the prostate is provided by the inferior vesical artery, which is formed from the internal iliac artery. The arteria pudentalis internala and the arteria rectalis media also play a role in the prostate. The smooth muscles in the prostate gland are innervated by sympathetic fibers that are activated at the time of ejaculation (Düzgün, D. (2024).

The main androgens in our body are the testosterone (T) molecule and dihydrotestosterone (DHT) molecules. The testosterone (T) hormone, which is effective in the prostate gland, interacts with the 5-alpha reductase enzyme and NADPH and is converted to dihydrotestosterone (DHT). This DHT molecule binds to the Androgen Receptor (AR). Dihydrotestosterone (DHT) has a higher binding affinity to AR and allows proteins to be separated from AR by binding. This binding causes AR and DHT to translocate into the cell nucleus and activate the target gene. It binds to androgen response elements (ARE) molecules in the promoter region of target genes

(Prostate specific antigen (PSA) and TMPRSS2 etc.). The existence of the AR signaling mechanism is important for the prostate. If there is a fault in this signal, it triggers prostate cancer. Androgen molecules are produced by the testicles and, to a lesser extent, by the adrenal glands. These molecules cause prostate cancer cells to grow and spread. Hormone therapy; androgen deprivation therapy (ADT) or androgen suppression therapy is used to reduce androgen levels and prevent them from being used by cancer cells. In addition, the presence of DHT is necessary for the full development and survival of the prostate. However, excessive DHT plays a role in the pathogenesis of benign prostatic hyperplasia (BPH) and even prostate cancer (Tan, M. H., et al., 2015).

2.4.2. Clinical Symptoms of Prostate Cancer

Most prostate cancers start outside the prostate gland. In order for prostate cancer to show symptoms, tumor cells must grow enough to press on the urethra (urinary canal) and occupy a large volume. For this reason, prostate cancer usually does not show symptoms in the early stages. Since prostate cancer is often asymptomatic and slowly progressing, it does not have any specific symptoms in the early stages. Although prostate cancer does not show any symptoms or signs in the early stages, it can have some important symptoms in the advanced stages. Early diagnosis and diagnosis have an important place in prostate cancer, which can be treated. Late diagnosis reduces the chance of recovery from prostate cancer and reduces the chance of treatment for prostate cancer, bringing it to a critical level. The success rate of the disease also increases with early diagnosis. Screening tests for early diagnosis are used to detect cancer in earlier stages. Considering that the prostate will grow due to reasons such as aging, it is recommended that all men over the age of 40 participate in cancer screenings through a doctor (Demirbaş & Onmaz, 2021), (Gürkan, Ç., et al., 2024).

Table 2.3. Prostate cancer symptoms (Küçükulu, M., 2012).

Symptom	Definition
Difficulty urinating	Abnormal growth of prostate gland cells puts pressure on the urethra, causing the person to have difficulty urinating

Weak urine flow/Interrupted urination	As a result of the enlarged prostate pressing on the urethra, there is a decrease and difficulty in urinating
Frequent urination	Because the prostate gland is located under the bladder and surrounds the urethra, cancerous cells put pressure on the bladder and urethra, causing frequent urination, especially at night.
Blood in the urine	The enlarged prostate presses on the urethra, causing irritation of the bladder and hematuria, which is blood in the urine.
Blood in the semen	Benign polyps or malignant tumor cells can cause blood in the semen.
Bone pain	Uncontrolled growing cells spread from the prostate gland often metastasize to the bone, causing severe pain in the waist, hips and legs.
Appetite and Weight Loss	As prostate cancer progresses, weight and appetite loss may occur because the body's energy consumption increases.

It is known that the frequency of PSA (Prostate Specific Antigen) measurement and rectal examination, which are recommended as screening tests, are performed at very low rates. It has been determined that the reasons for the low test rates are fear, shame and lack of information. According to a study conducted in Turkey, it was stated that 1/4 of men have had prostate cancer screening, but only 1/3 of people think about having these screening tests in the future. If there are signs or symptoms of prostate cancer, it is important to have the tests that will be needed for a diagnosis or treatment (Demirbaş & Onmaz, 2021), (Gürkan, Ç., et al., 2024).

2.4.3. Early Detection and Diagnostic Methods of Prostate Cancer

Prostate cancer is a tumor of epithelial origin of hormone-dependent cells, resulting from the uncontrolled proliferation and proliferation of genetically unstable, transformed and transformed cells. The structure of the prostate gland can be defined as epithelial cells, which are hidden in a fibromuscular stroma and consist of three types of differentiated cell sections: luminal, basal and neuroendocrine cells. Although prostate cancer (PCa) is thought to have a basal phenotype, androgen-dependent luminal cells are thought to be the origin of prostate cancer. PSA (Protein-specific antigen) is located on chromosome 19 and is a member of the kallikrein gene family. The expression of PSA cells is dependent on androgens. PSA cells are produced by luminal cells, a section of the prostate, and are a serine protease (Henttu, P. et al.,

1992).

In the diagnosis of prostate cancer; PSA (prostate specific antigen) test, Multiparametric Prostate MRI (mpMRI), Prostate Biopsy, Rectal Examination (Prostate-Directed), MR-Ultrasound Fusion Biopsy are performed.

1. PSA (Prostate Specific Antigen) Test

Prostate cancer is diagnosed early with the PSA (prostate specific antigen) test, which is produced by the cells in the prostate gland and is performed by looking at a blood sample. It is a suitable test for the initial diagnosis and is applied to a person with prostate cancer symptoms. The PSA value in a person may vary depending on their general health status, age and the size of the prostate. The values sought for the PSA value should be as follows. If the PSA value is below 3 ng/mL, this is considered normal. If the PSA value is between 3 - 4 ng/ml, approximately 30% of the patients have prostate cancer. If the PSA levels are above 10 ng/mL, the risk of prostate cancer will be higher. Since other factors can also affect the level of PSA in the blood, PSA elevation alone is not a definitive diagnosis (Adhyam & Gupta, 2012).

Table 2.4. Distribution of PSA levels and risk ratios (David & Leslie, 2024).

PSA (ng/ml)	Risk Ratios
<3 ng/mL	Normal Range
3 - 4 ng/ml	Limit Level
>10 ng/mL	High Risk

2. Multiparametric Prostate MR Test (mpMRI)

A detailed magnetic resonance imaging method that takes the imaging of the prostate gland to an advanced level and is used to detect abnormal cells in this gland. It is a diagnostic method that supports the diagnosis that can be made in patients with suspected cancer. In addition, the Multiparametric Prostate MR method can determine whether tumor cells have passed through the special capsule of the prostate tissue, whether they can detect the density of the tissue and cells, and whether they have spread to important lymph nodes where they can spread. With its more sensitive and precise technology, it prevents abnormal tissues from being missed (Donati et al., 2013).

3. Prostate Biopsy

The prostate biopsy method is the process of taking samples and pieces from different parts of the prostate with the help of a special needle. Tissues are taken with a device that is inserted into the rectum under local anesthesia and taken to the pathology laboratory to determine if there are cancer cells. This method checks how fast the prostate cancer tumor is developing. With advancing technology, prostate biopsy continues to be popular among the diagnostic methods for prostate cancer (Karalar, M. et al., 2024).

4. Rectal Examination (Prostate-Oriented)

Rectal examination is a method used to understand whether there is an abnormality in the condition of the organs located in the lower abdomen, such as the bladder, urinary tract, large and small intestines, and anus. In particular, prostate rectal examination, this method, which is performed by fingering the anus to understand the condition of the prostate, can help to understand whether the prostate contains hardness and abnormality. A hard tissue or area is suspected of prostate cancer (Gençhellaç, H., & Yılmaz, E., 2015).

5. MR-Ultrasound Fusion Biopsy

It is a smart biopsy method developed in recent years, trying to overcome disadvantages, and instead of taking samples from random tissues of the prostate as in the standard prostate biopsy method, it is a method that is performed in accordance with the target tissues and used to diagnose the stage of cancer. This method has transformed taking a large number of random samples from the person into taking samples for the tissue suspected of being a tumor. The most important privilege of the test is that the Multiparamedic Prostate MR images are transferred to the images on the TRUS (Ultrasound) device and the full determination process is performed. It can perform the process called fusion by moving the 3D dimensional images taken from the Multiparamedic MR from the anus and overlapping the images on the TRUS (Ultrasound) device. This method is called transrectal (Siddiqui et al., 2015), (Lang, J. et al., 2024).

Table 2.5. Advantages of the MR-Ultrasound Fusion Biopsy test (Lang, J. et al., 2024).

Getting results with minimal error and deviation from tumor risk areas
Reduced need for repeat biopsy procedures
30% increase in the detection of aggressive and rapidly spreading cancer cells compared to standard biopsy
In the active observation method in the treatment protocol, the areas taken in the fusion biopsy are precisely determined, which provides a great advantage to the patient.
Avoiding major surgeries for tissues that do not harm the patient

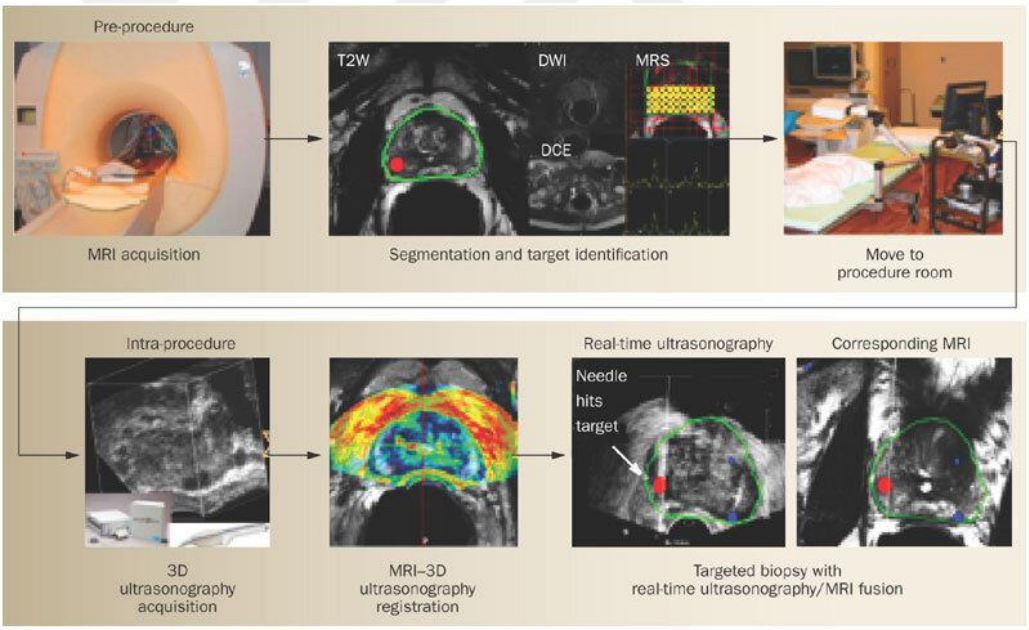

Figure 2.6. Workflow of MRI-TRUS(Ultrasound) Fusion Biopsy method (Turkbey, B., et al., 2009).

2.4.4. Staging of Prostate Cancer

The staging system of cancer is performed to understand the region/regions where the cancer is located, how much the tumor covers which regions, whether it

metastasizes to other tissues, and how much it affects the body's system. The stage of the cancer also shows the patient's chance of survival. Cancers such as lymphoma can respond positively to the treatment process even in the last stage (Stage IV). However, since some types of cancer can be more aggressive and resistant, treatment processes are difficult even in lower stages. The staging system for prostate cancer is a system performed to describe to which regions and to what extent the cancer has spread in the prostate region. Tests such as TNM Staging, PSA (Prostate Specific Antigen) test and Gleason Score are applied for the prostate cancer staging system. The staging system is of vital importance for the most probable treatment method and drugs in cancer (Cosma, G., et al., 2016).

2.4.4.1. TNM Staging Method in Prostate Cancer

The behavioral model of the tumor, the process of treatment and whether a positive response is obtained or not, are very important for a uniform staging system for an accurate exchange of information between institutions internationally. In 1992, the American Joint Committee on Cancer (AJCC) and the International Union for the Control of Cancer (UICC) determined a unified TNM staging system for prostate cancer. The American Joint Committee on Cancer (AJCC) made some changes to the TNM staging system. These are extraprostatic extension and microscopic bladder neck invasion (spread of the tumor), which are included in the category of stage T3a prostate carcinoma (Buyyounouski, M. K. et al., 2017).

The TNM system classification of Prostate Adenocarcinoma is based on 3 categories. These categories are;

• T (Tumor): Primary tumors.

• N (Lymph Node): Describes whether cancerous cells have spread to lymph nodes.

• M (Metastasis): Describes whether cancerous cells have spread to other tissues.

For the T category, it can be said that the cancer is limited to the prostate and has not metastasized to other tissues. In addition, for the T stage, rectal examination, PSA (prostate specific antigen) test, TRUS (Ultrasound) and Multiparametric Prostate MR Test (mpMRI) are used. For the N category, it can be said whether the cancer has

spread to the lymph nodes outside the prostate. For the N stage, clinical examination and imaging methods are used. For the M category, it can be said whether the tumor has spread to other tissues outside the prostate and throughout the body. For the M stage, bone scintigraphy, skeletal studies, biochemical tests and thoracoabdominal CT are used (Borley & Feneley, 2008).

In addition, numbers or letters given within the TNM system are used for data and degrees.

Primary tumor (T):

TX: Primary tumor cannot be evaluated
T0: Primary tumor is not present
T1: Tumor is present but not visible

• T1a: The tumor may have been detected during the treatment of benign prostatic hyperplasia (BPH) and is found in less than 5% of the tissue taken from the prostate.

• T1b: It may have been detected during the treatment of benign prostatic hyperplasia (BPH) and is found in more than 5% of the tissue taken from the prostate.

• T1c: Cells were detected as a result of biopsy in response to a high result in the PSA (Protein Specific Antigen) test.

T2: Tumor is present, visible and palpable, but only present in the prostate

• T2a: Cancer cells located inside the prostate gland are dense only in one part of the prostate.

• T2b: Cancer cells located inside the prostate gland cover half of the dense part of the prostate.

• T2c: Cancer cells located inside the prostate gland are spread to both sides of the gland.

T3: The tumor of prostate cancer is growing outside the prostate gland. Cancerous cells may have spread to the seminal vesicles.

• T3a: Although cancer cells located inside the prostate gland have spread outside the prostate, they are not distributed to the seminal vesicles.

• T3b: Cancer cells located within the prostate gland have also spread to the seminal vesicles.

T4: The tumor of the prostate cancer has spread to both the seminal vesicles and outside the prostate gland. The tumor has not spread to more distant tissues. The areas where the tumor has spread can also be the rectum, bladder, urethral sphincter and pelvic wall.

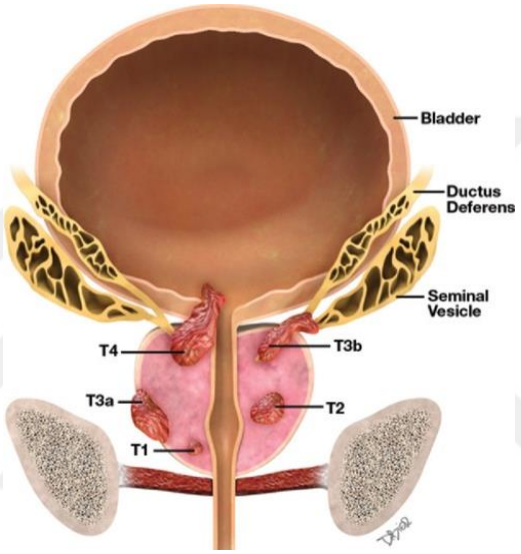

Figure 2.7. T staging for prostate cancer. T1: tumors are present but not of a palpable size and are not clinically apparent. T2: tumors are confined to the prostate gland, T3a: tumors extend beyond the prostate capsule, T3b: tumors invade the seminal vesicles, T4: tumors may spread to the seminal vesicles and invade structures such as the bladder, rectum, pelvis (Boonsirikamchai, P. et al., 2013).

Lymph Node (N):

NX: Tumor in the lymph node cannot be assessed

N0: No tumor in the lymph nodes near the cancerous cell

N1: Tumor in the lymph nodes near the cancerous prostate cell

Metastasis (M):

M0: Prostate cancer tumor has not spread to other parts of the body

M1: Prostate cancer tumor has spread to other parts of the body outside of the

pelvic area. It is divided into two groups: M1a, M1b and M1c.

• M1a: Cancer cells located inside the prostate gland are present in other lymph nodes away from the pelvic area

• M1b: Cancer cells located inside the prostate gland have spread to the bone

• M1c: Prostate cancer has spread to other parts of the body and cancer cells are present in other organs.

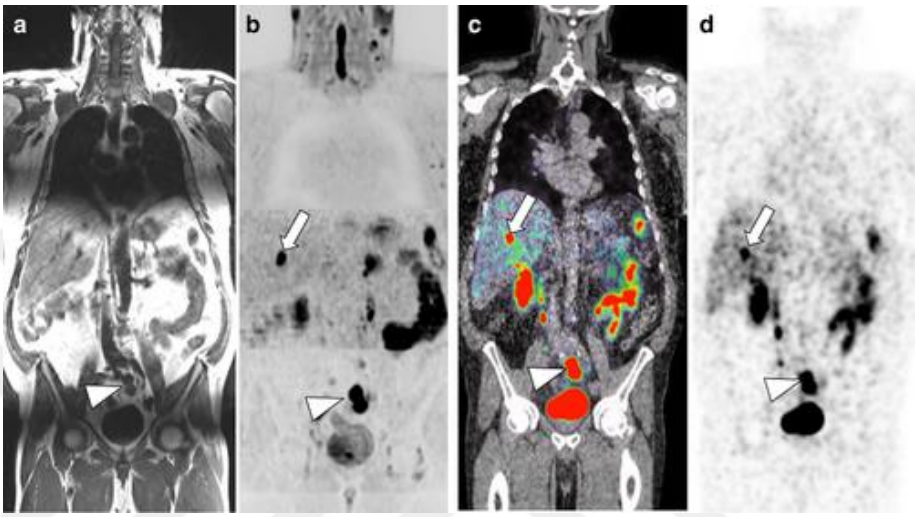

Figure 2.8. Whole body magnetic resonance imaging (WB-MRI) and PSMA (Prostate Specific Membrane Antigen) PET/CT images of a 68-year-old man with stage IV prostate cancer. (a,b) Coronal WB-MRI (Whole Body MRI), (a) T1 TSE (Turbo Spin-Echo), (b) Coronal reformatted inverse grayscale DWIBS images show liver metastasis (arrow) lymph node metastasis (arrow). (c,d) 68 Ga-PSMA-PET/CT (68 Ga labeled Prostate Specific Membrane Antigen Positron Emission Tomography) images show liver metastasis (arrow) lymph node metastasis (arrow) (Van Nieuwenhove, S., et al., 2022).

2.4.4.2. Histological Classification of Prostate Cancer

In order to diagnose prostate carcinoma, it is usually necessary to take a tissue sample and identify it. In the pathology laboratory, routine HE (hematoxylin-eosin) stained sections are often sufficient for microscopy, but immunohistochemical labeling is also used when there is minimal tumor. The vast majority of prostate cancer cells originate from adenocarcinomas of the epithelial tissue of the prostate gland. Prostate adenocarcinomas are used clinically to identify this type of cancer (Humphrey

P. A., 2017).

According to Stanford Medicine Surgical Pathology; prostate cancer is divided into subcategories such as Adenocarcinoma (the most common type), Primary Squamous Cell Carcinomas, Small Cell Carcinomas, Urothelial/Transitional Cell Carcinomas, Soft Tissue Sarcoma Carcinoma, Neuroendocrine Carcinomas, Mucinous Adenocarcinoma (Kabasakal, L., et al., 2017).

Squamous cell carcinomas of the prostate are usually diagnosed at an advanced stage and have a poor prognosis. Squamous cell carcinomas are a rare subtype that originates from squamous cells that surround the organs and are made up of flat cells. It is a fairly aggressive type of prostate cancer. Squamous cell carcinomas constitute less than 1% of prostate cancer and have a invasive character (Kilinç, M. F. 2016).

Small cell carcinoma constitutes 0.55%-2% of prostate cancer. Small cell carcinomas of the prostate usually show clinical findings in advanced stages. Their treatments are chemotherapy-based like other cell cancers. This type causes bowel and bladder symptoms (Tatlı, A., et al., 2016).

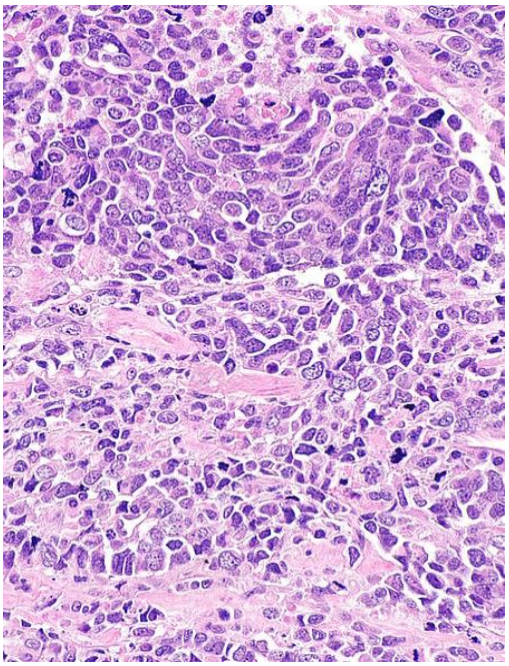

Figure 2.9. Prostate small cell carcinoma with HE (hematoxylin-eosin) stain (Furtado, P. Et al., 2011).

Urothelial/Transitional (Transitional Cell) carcinomas are an aggressive type that tends to spread to the bladder tissue, urethra and ureters due to proximity. These cells constitute 1% to 5% of prostate cancer (Sanguedolce, F., et al., 2019).

Soft Tissue Sarcoma Carcinomas are a type of cancer that affects the stromal or soft tissue cells that make up the body's connective tissues. 20% of sarcomas arise in the abdomen or retroperitoneum. This type of carcinoma is rare and can often be overlooked in diagnosis (Musser, J. E., et al., 2014).

Neuroendocrine Carcinomas are large cells and have poor differentiation capacity, so it is very difficult to identify their cell type. They respond poorly to hormone therapy compared to other types of carcinomas and adenocarcinomas. Additionally, neuroendocrine tumors lack androgen receptors and therefore cannot secrete PSA (Parimi, V., et al., 2014).

Mucinous prostate adenocarcinoma is a primary prostate acinar tumor characterized by at least 25% of the tumor consisting of extraluminal mucinous cells. Mucinous prostate adenocarcinoma is a rarer type of prostate cancer, and this type of adenocarcinoma is more aggressive and has a poor prognosis than the acinar type (Tosun Yildirim, H., et al., 2012).

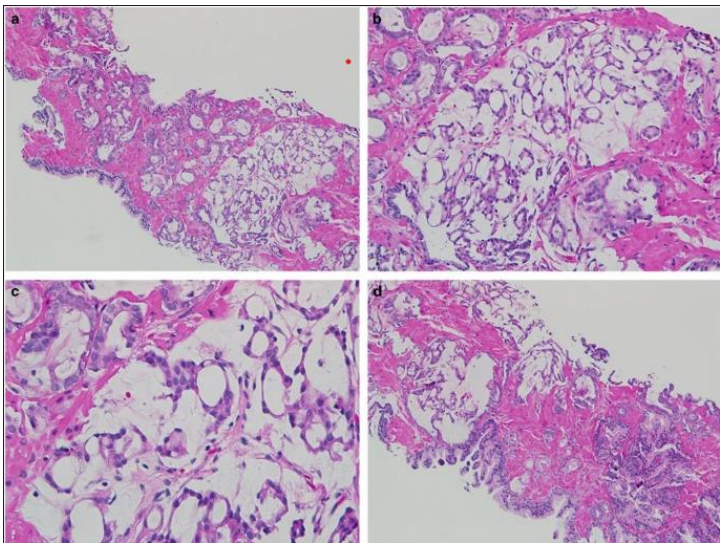

Figure 2.10. Needle core biopsy of mucinous prostate adenocarcinoma (Osunkoya, A. O. ,2018).

The Gleason score, which is part of the Histological Classification, was explained in detail with the help of literature.

Gleason Score (Grading System for Prostate Cancer)

In 1966, Donald Gleason proposed a method called the Gleason score to grade prostatic carcinomas. This method aims to measure the aggressiveness of the malignancy with tumor morphology. Although the Gleason grading system has changed many times over time, its basis is based on the histological growth grades of prostate carcinomas. The Gleason score (GS) is obtained by obtaining the first and second most frequent samples in a tumor (Chen, H., et al., 2016).

The Gleason score method is a scoring method used to determine the distribution and spreading speed of cancer cells and shows the degree of differentiation of prostate cancer cells. This score varies between 2 and 10. In prostate cancer, Gleason score 6 represents the best cancer that can be detected and the lowest degree (Stage I). When the Gleason score is 9-10, it represents the most advanced stage of prostate cancer (Stage V) (Tagai, E. K., et al., 2019).

Table 2.6. Gleason Scoring System and Prostate Cancer Stages (Tagai, E. K., et al., 2019).

Stage I	Gleason score<6
Stage II	Gleason score<7
Stage III	Gleason score<7
Stage IV	Gleason score<8
Stage V	Gleason score<10

The Gleason score system is one of the most important factors determining the prognosis (prediction) of treatment results in prostate cancer. Each stage of prostate cancer and the Gleason score provide information about the disease. When the Gleason score is <6, the tissue of the tumor cell has changed considerably, is less aggressive. In addition, cancerous cells are less prone to growth. When the Gleason score is <7-8, the tissue of the tumor cell has changed moderately and is moderately aggressive. In addition, although cancerous cells are prone to growth, they do not spread very much. When the Gleason score is determined as <10, the tumor tissue has changed little or not at all. It is very aggressive. Cancerous cells tend to both grow and spread very quickly (Epstein, J. I., et al., 2016).

2.4.4.3. Molecular Classification of Prostate Cancer

Genetic factors and familial inheritance are important risks of prostate cancer, and 10% of people with prostate cancer have familial inheritance as the cause of cancer. Germline mutations are 9% in these cancer cases. Prostate cancer has a complex molecular pathogenesis. Genes associated with prostate cancer include; tumor suppressor genes (BRCA2, BRCA1, TP53, PTEN), AR, CHEK2, KLK3, PALB2, ATM, HOXB13, TMPRSS2-ERG. BRCA2, BRCA1 genes are genes that actively play a role in the DNA repair process, and the PALB2 gene helps DNA repair together with the BRCA2 gene. PALB2 gene mutation is associated with high-risk prostate cancer. Patients with this gene variation have a Gleason score of 8-10 for prostate cancer. The ATM gene controls the cellular DNA damage response mechanism and cell division. Loss and deletion of tumor suppressor genes TP53 and PTEN are genetic disorders in prostate cancer. The growth of prostate cancer cells depends on the transcriptional activity of the Androgen Receptor (AR). CHEK2's function is to regulate the cell cycle and is associated with hereditary prostate cancer as a result of mutation in the gene. HOXB13 mutation is associated with an increased risk of prostate cancer and early diagnosis. TMPRSS2-ERG; TMPRSS2 is a fusion gene with an androgen-regulated serine protease and ETS transcription factor ERG and has an important role in prostate carcinogenesis (Konac, E., & Sozen, 2014), (Wokołorczyk, D., et al., 2021), (Finch, A., et al., 2022).

Table 2.7. Genes involved in prostate cancer (Konac, E., & Sozen, 2014).

GENE	LOCATION	GENOMIC IRREGULARITY	FEATURE
Androgen Receptors (AR)	Xq11	Amplification Mutation	It is seen in 58% of castration-resistant prostate cancers
BRCA1	17q21	Deletion	Causes aggressive, resistant prostate cancer
BRCA2	13q12.3	Deletion	Causes aggressive, resistant prostate cancer
PTEN	10q23	Deletion Mutation	Early stage with 40% copy number loss
TP53	17p31	Deletion Mutation	It is the most mutated gene in cancer, with 40% deletion
TMPRSS2-ERG	Chromosome 21	Gene Fusion	It is seen in 50% of metastatic prostate cancer
KLK3	19q13.33	Somatic Mutation	Causes aggressive, resistant prostate cancer

It can lose PTEN alleles located at the 10q23 location. This loss occurs most often after TMPRSS2-ERG rearrangement. PTEN loss leads to Prostatic Intraepithelial Neoplasia (PIN) type lesions, Invasive Prostatic Adenocarcinoma and Metastatic Prostatic Cancer. Prostatic Intraepithelial Neoplasia (PIN) can be considered as a pre-cancer of the prostate with the possibility of developing into prostate cancer over time (Ratnacaram, C. K., et al., 2008).

Kallikrein-3 (KLK3) gene is expressed in high amounts in the prostate epithelium with androgen signal. Serine proteases from the KLK family play a role in prostate cancer. Kallikrein-3 (KLK3) gene is also known as Prostate Specific Antigen (PSA) (Mamidi, T. K. K., et al., 2019).

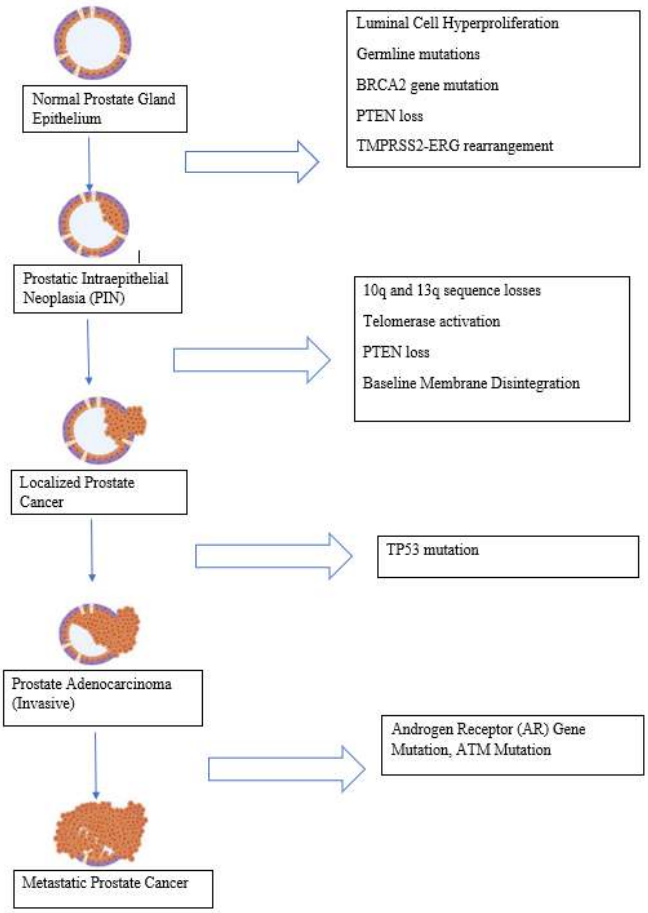

Figure 2.11. Molecular and cellular progression stages of prostate cancer (Canesin, G., 2021).

2.4.4.4. Pathological Classification of Prostate Cancer

The purpose of pathological classification is to analyze the spreading status and aggressiveness of tumoral cancer tissues under the microscope. Pathological classification of prostate cancer is used together with the Gleason score method. Histopathological detection of prostate cancer is based on the benign or malignant status of tissues taken from prostate cancer cells with microscopic images. The Gleason score method is also used to estimate the aggressiveness and spreading rate of prostate cancer (Cimadamore, A., et al., 2020).

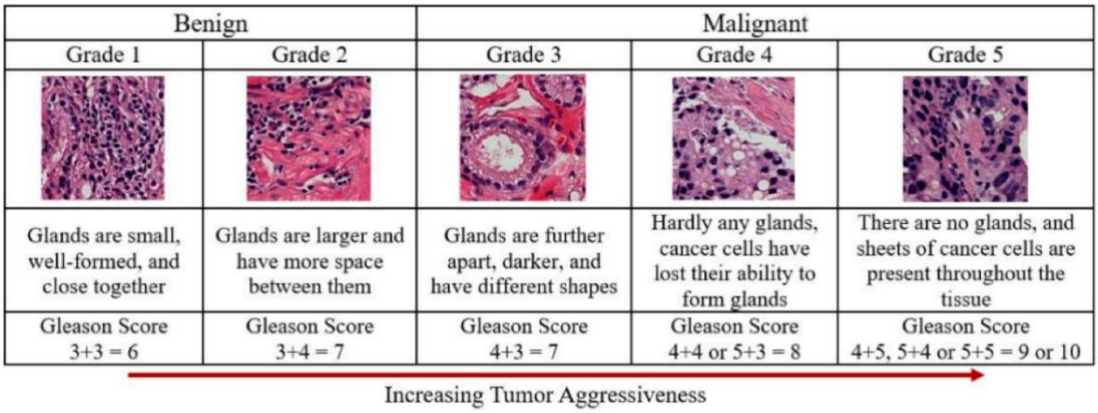

Figure 2.12. Images of all grades from Grade1 to Grade5 were scanned at 40x optical magnification (Bhattacharjee, S., et al., 2019).

In Grade 1, the prostate glands are well-formed, small, and close together. In Grade 2, the prostate glands are larger and slightly farther apart. In Grade 3, the prostate glands are farther apart and darker and differently shaped. In Grade 4, cancerous cells have covered the prostate gland, and in Grade 5, the prostate glands are absent.

2.4.4.5. Stage Groups in Prostate Cancer

The classification of prostate cancer according to stages varies between I (1) and IV (4). Stage II is divided into subcategories such as IIA, IIB and IIC according to its characteristics, while Stage III is divided into subclasses IIIA, IIIB and IIIC. The rule in the general stages of prostate cancer is that the lower the number, the better the prostate cancer. As the number increases, it is accepted that the cancer has spread and metastasized to other areas. In addition, a letter that is earlier represents a lower level (Cheng, L., et al., 2012).

Stage I

• Cancer cells are small and confined to the prostate.

• The doctor cannot detect the tumor by manual examination or obtain images with a transrectal ultrasound.

• The PSA level is low.

• Cancer cells have not spread to the lymph nodes and have not metastasized to other organs.

• The Gleason score is 6 or lower.

Stage IIA

• Cancer cells are still confined to the prostate and have not spread.

• The tumor can be felt with a digital rectal exam

• The PSA level is below a certain threshold.

• The Gleason score is 6 or lower.

Stage IIB

• Cancer cells are larger and may have spread to all parts of the prostate.

• Cancer cells have not spread beyond the prostate.

• The tumor can be seen with a digital rectal exam and transrectal ultrasound.

• PSA level is less than 20 ng/ml.

• Gleason score is 7.

Stage IIC

• Cancer cells are larger and may have spread to both parts of the prostate.

• Cancer cells are confined to the prostate.

• Gleason score is between 7 and 8.

Stage IIIA

• Cancer cells have spread beyond the prostate, beyond the prostate capsule. It may have spread to the seminal vesicles.

• The PSA level is higher.

• The Gleason score is 8 or lower.

• The cancer cells have not spread to the lymph nodes.

Stage IIIB

• Cancer cells have spread to the seminal vesicles and other nearby areas (rectum, bladder, pelvic wall).

• The Gleason score is 8 or lower.

• The PSA level may be any value.

Stage IIIC

• Cancer cells have spread to the seminal vesicles and other nearby areas (rectum, bladder, pelvic wall, etc.).

• Gleason score is 8 or lower.

• PSA level may be any value.

• Cancer cells may or may not have spread to the lymph nodes.

Stage IV

• Cancer cells have spread to all organs of the body except the prostate gland.

• Cancer cells have spread to the lymph nodes.

• PSA levels can be anywhere.

• Cancer cells have spread to organs of the body such as the lungs and liver.

• Gleason score is 10 or lower.

Table 2.8. Prostate Cancer Stages and TNM staging (Caglic, I., et al., 2019).

Stage I	T1-2	N0	M0
Stage IIA	T1-2	N0	M0
Stage IIB	T1-2	N0	M0
Stage IIC	T1-2	N0	M0
Stage IIIA	T1-2	N0	M0
Stage IIIB	T3-4	N0	M0
Stage IIIC	Any T	N0	M0
Stage IVA	Any T	N1	M0

Stage IVB	Any T	Any N	M1

2.5. Prostate Cancer Treatment Methods

The variability and unstable characteristics of prostate cancer biology, early stage diagnosis for prostate cancer treatment, long and short term risk factors of treatment processes, difficulties in definitive diagnosis of prostate cancer, even though there are a diagnosis made at the right time and the right treatment to be applied, the survival rates of the patient with prostate cancer in the first 5 years or even 5 to 10 years are quite high. The use of internationally used TNM staging systems, statistics and reports are also extremely important for doctors to determine the areas where the cancer has spread and to determine the appropriate and critical treatments to be applied to the patients. There are many different prostate cancer treatments, and whether the patient responds positively to the treatment is also monitored. Treatments that can be applied against prostate cancer include surgical intervention, radiotherapy, hormone therapy, chemotherapy and patient follow-up. Surgical intervention or radical prostatectomy treatment options can be applied for prostate cancer that is in an advanced stage but remains local. The cancerous cells must not have spread outside the prostate tissue and have not spread. Radiotherapy method can be applied in addition to surgical intervention for prostate cancer detected in the early stage. If prostate cancer is at a stage that cannot be resolved with surgery and radiation or radiation therapy, hormone therapy is applied. A patient with advanced prostate cancer, such as stage 4, may also receive chemotherapy with this treatment (Haydaroğlu, A., et al., 2019), (Anagnostou, T., et al., 2003).

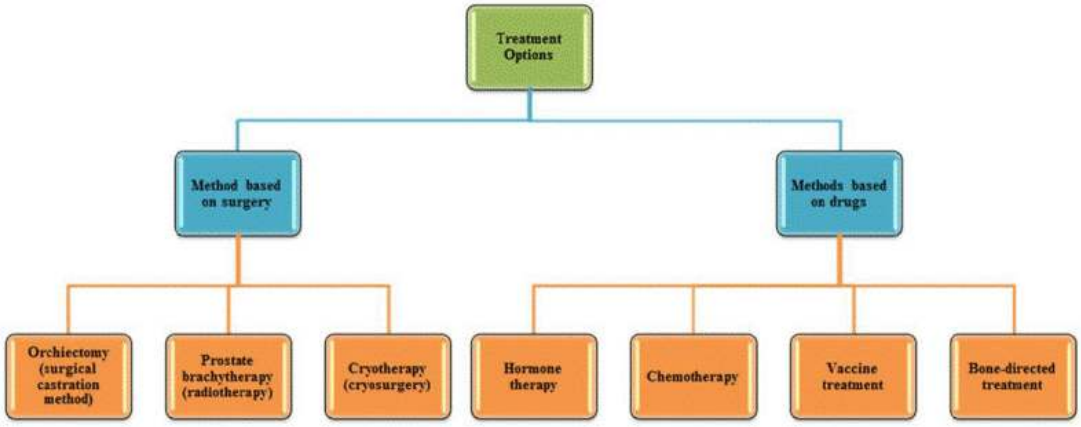

Figure 2.13. The treatment methods of prostate cancer (Elancheran, R., et al., 2015).

2.5.1. Surgical Methods

There are 3 different surgical methods preferred for early stage prostate cancer patients. These can be listed as open, laparoscopic and robotic methods. In addition to using chemotherapy and radiotherapy methods to reduce the tumor mass beforehand and then performing the procedure, surgery can be used together with other methods or surgery can be preferred alone (Costello, A. J., 2020).

The surgical method is based on the removal of the prostate gland tissue or tumor from the body where cancerous cells have spread. The number of prostate cancer patients preferring this method is increasing day by day. Robotic surgery can be used for hard-to-reach areas. This method is preferred over laparoscopic and open surgery methods. Laparoscopic surgery involves the removal of prostate tissue with a minimally invasive method. This method has advantages such as smaller scars, less pain and suffering, and faster recovery for the patient (Baykara, O., 2016), (Karadağ, M. A., et al., 2015), (Bozdoğan, Ş. N., & Koçaşlı, S., 2022).

2.5.2. Radiotherapy

Radiation therapy is a method of treating cancerous cells associated with prostate cancer using intense and high beams. It is aimed to destroy tumor cells, prevent their proliferation or shrink them by keeping all cells exposed to high radiation at a minimum level. Radiation therapy may be preferred according to the stage of prostate cancer and other factors. Radiotherapy is applied to prostate cancer patients

at certain intervals for the self-repair process of healthy tissues in the patient and for an efficient treatment process (Zaorsky, N. G., et al., 2013).

There are two types of radiotherapy for prostate cancer. These are external radiotherapy and brachytherapy. External radiotherapy is the method of applying high-energy X-rays to the patient from outside the tissue, from a certain and appropriate distance. Brachytherapy radiotherapy is the method of applying high-energy X-rays to the patient by placing them inside the tissue. In some cases, doctors aim to shrink the tumor mass by applying radiotherapy to the patient. In addition, hormone therapy is also preferred with radiotherapy (Lee, C. T., et al., 2005), (Podder, T. K., et al., 2018), (Schaeffer, E., et al., 2021).

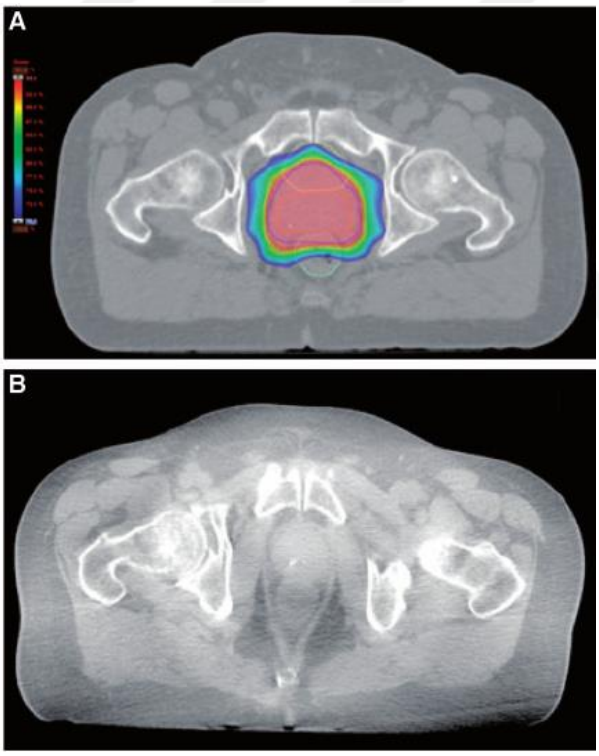

Figure 2.14. Radiotherapy treatment plan applied to a prostate cancer patient with an appropriate dose and post-radiotherapy with Cone Beam Computed Tomography (CBCT) method (Høyer, M. et al., 2011).

2.5.3. Hormone Therapy

Hormone therapy (Androgen Deprivation Therapy) method is to suppress androgen hormones that prostate cancer patients have and stop them. The purpose of this method is to encourage androgen hormones to cause cell growth and spread by

encouraging prostate cancer. Hormone therapy alone may not be enough for prostate cancer patients. This method is used in conjunction with chemotherapy or radiotherapy methods (Sharifi, N., et al., 2005).

The body's androgen hormones are divided into 2, testosterone and dihydrotestosterone (DHT). Although androgen hormones are produced by the testicles, the adrenal glands can also produce some of this hormone. Hormone therapy applied to reduce the levels of androgen hormones and prevent their use by cancer cells is of 4 different types (Sharifi, N., et al., 2005).

1. Orchiectomy (Surgical Castration)

The testicles largely meet the production of androgen hormones. Orchiectomy is the surgical removal of one or two testicles from the body. In metastatic prostate cancer, androgen suppression therapy and orchiectomy are indispensable methods (Garje, R., et al., 2020).

2. LHRH Agonists (Luteinizing Hormone Releasing Hormone) Agonists

This treatment method changes the production and levels of testosterone hormone, stimulates the pituitary gland region in the brain to increase testosterone hormones, and then reduces them again. A flare period occurs due to the sudden increase in testosterone hormone. In addition, testosterone hormone production can be stopped without the need for orchiectomy. Leuprolide acetate or goserelin active ingredients are used. These drugs are administered subcutaneously every 3 or 6 months (Fujii, Y., et al., 2008).

3. LHRH Antagonist (Luteinizing Hormone Releasing Hormone) Antagonist

The aim of this treatment method is to change and reduce testosterone hormone levels more stably without a flare period. Degarelix is an LHRH antagonist drug (10.1080/14656566.2017.1328056).

4. CYP17 suppressor

Even though LHRH agonists and LHRH antagonist drugs suppress this

hormone for prostate cancer treatment by changing the levels of testosterone hormone produced in the testicles, the adrenal glands continue to produce testosterone hormone in the body. Hormones formed in small amounts can trigger prostate cancer growth. The aim of CYP17 suppressor drugs is to block the CYP17 enzyme that helps cells synthesize and produce androgen hormone. Zytiga (Abiraterone Acetate) is a CYP17 suppressor. This drug can be used for patients with advanced prostate cancer (Attard, G., et al., 2009).

5. Anti-Androgens (Therapies Interfering with Androgen Function)

Androgen hormones work by binding to androgen receptors located in prostate cells. Anti-androgen drugs prevent androgens from binding to receptor proteins. Bicalutamide and Flutamide drugs are among the anti-androgens (Huang, J., et al., 2022).

Androgen Deprivation Therapy has some side effects on patients.

These side effects;

- Hot flushes
- Exhaustion
- Depression
- Loss of sexual desire
- Weight gain
- High cholesterol levels
- Decreased muscle mass

Table 2.9. Classification of drugs used in prostate cancer hormone therapy (Huang, J., et al., 2022), (Dhawan, M., et al., 2016), (Erdkamp, F., et al., 2014).

LHRH Agonists	**LHRH Antagonists**	**CYP17 inhibitors**	**Anti-Androgens**
Leuprolide acetate	Degareliks	Zytiga (Abiraterone Acetate)	Bicalutamide
Goserelin	Abarelix	Galeterone	Flutamide

Triptorelin	Ganirelix		Darolutamide
Buserelin			Enzalutamide
			Apalutamide

2.5.4 Chemotherapy Treatment

Chemotherapy treatment method is used for cancer disease. The aim of this method, which is a drug treatment, is to prevent or stop the growth of metastatic and dispersed cancer cells (Gilligan, T., & Kantoff, P. W., 2002).

Although the chemotherapy treatment method in prostate cancer gave negative results at first, new agent development studies continued. Docetaxel drug was the first agent with positive results in metastatic castration-resistant prostate cancer (mCRPC). This method also showed positive effects against complaints of prostate cancer patients such as bone pain, etc. and was used in cases where other prostate cancer treatment methods were ineffective. Cabazitaxel and Docetaxel are the most widely known chemotherapy drugs. Cisplatin, Mitoxantrone and Etoposide drugs are also used for the same method.

Chemotherapy has been used since the 1980s and is used for advanced prostate cancer patients, but it is also used in combination with hormone therapy or radiotherapy methods. It is also preferred for patients who have not been treated with hormone therapy (Nader, R., et al., 2018), (Quinn, D. I., et al., 2017).

CHAPTER III. MATERIALS AND METHODS

In this theoretical study, the receptors and genes that cause prostate cancer were modeled in the presence of different ligands and new generation prostate cancer drugs by means of high computational computers. Using Molecular Docking (MD) and Molecular Dynamics Simulation (MDS) methods, the activities of prostate cancer-related AR (Androgen Receptor) gene (PDB ID: 1E3G and 8E1A), KLK3/PSA (Prostate-Specific Antigen) gene (PDB ID: 2ZCH and 2ZCL) receptors with natural agents, IC50 values, traditional drug values and interactions with new drugs approved by FDA specific for prostate cancer were evaluated. Ligand data were obtained from programs such as PubChem and ChEMBL.

In this study, 1E3G, 8E1A, 2ZCH and 2ZCL receptors were used for literature research of prostate cancer from RCSB PDB (Research Collaboratory for Structural Bioinformatics Protein Data Bank) site. ChEMBL and DrugBank codes of ligands used for protein receptors were obtained from UniProtKB (Universal Protein Resource Knowledgebase) database which contains comprehensive protein sequences and information.

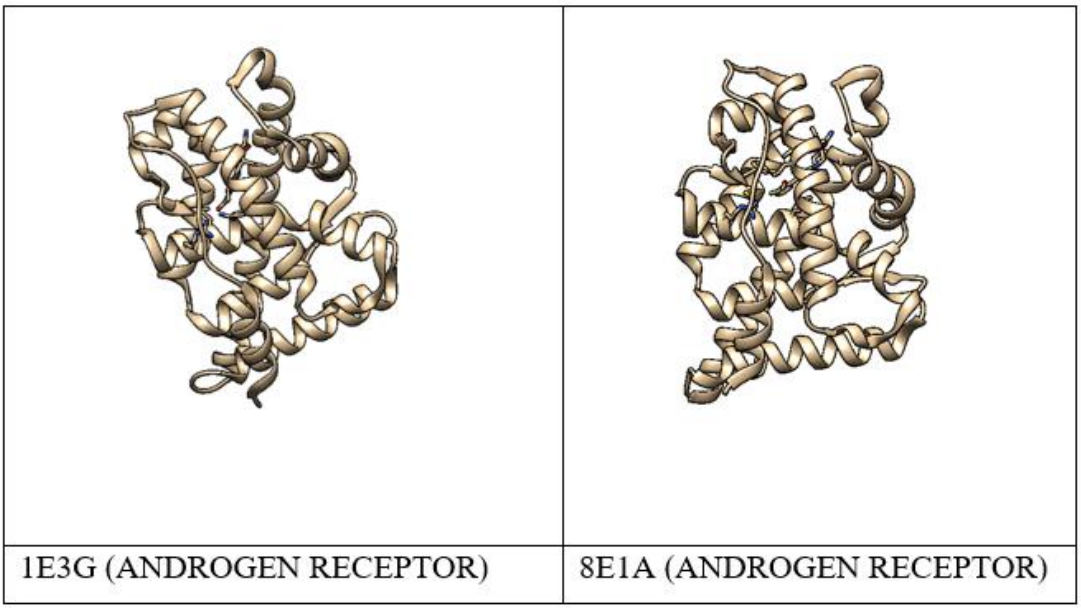

Figure 3.1. 3D image of 1E3G and 8E1A receptors obtained from UCSF Chimera

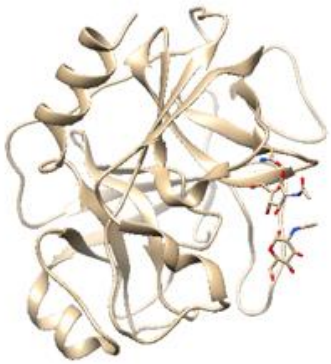	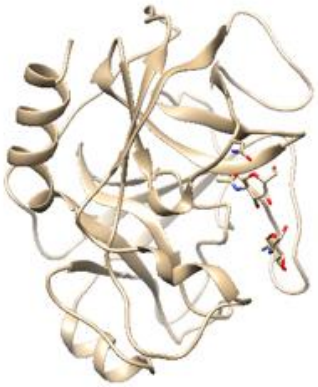
2ZCH (PROSTATE SPECIFIC ANTIGEN)	2ZCL (PROSTATE SPECIFIC ANTIGEN)

Figure 3.2. 3D image of 2ZCH and 2ZCL receptors obtained from UCSF Chimera

In addition, ligands containing the lowest IC50 values were obtained from the ChEMBL database. Simulation was provided with water and ions. For each of 1E3G, 8E1A, 2ZCH and 2ZCL receptors, 72 ligands with IC50 values between 0.0 and 3200.0 from ChEMBL, 30 Natural agent, 67 traditional prostate cancer drugs and 11 new prostate cancer drugs were studied. Among the ligands docked to protein receptors, the ligands with the best results and the lowest binding energies were selected. Autodock Vina and Autodock Tools were used for receptor and ligand dockings. The GROMACS program was used for Molecular Dynamics Simulation (MDS). Calculations were performed via the National High Performance Computing Center (UHeM). After Molecular Dynamics Simulations, RMSD (Root Mean Square Deviation), RMSF (Root Mean Square Fluctuation), Radius of Gyration (Rg), SASA (Solvent Accessible Surface Area), ADMET (Absorption, Distribution, Metabolism, Excretion, and Toxicity) analyses were performed.

3.1. New Prostate Cancer Drugs

New prostate cancer drugs approved by the FDA; Abiraterone, Olaparib, Pylarify, Rucaparib and Locametz were selected as the main ligands. Their molecular structures and formulas were obtained from the PubChem database.

Abiraterone is a prostate cancer drug and is a part of hormone therapy for male patients. The working mechanism of the Abiraterone drug is based on stopping the progression of prostate cancer by preventing the production of the testosterone hormone in the body. Abiraterone is a selective inhibitor of CYP17. Olaparib is a prostate cancer drug and is used for male patients in cases where hormone therapy does not work. Olaparib drug provides control of cancer. Olaparib drug is a PARP inhibitor. Pylarify is a prostate cancer drug and is an agent used for male patients with metastatic prostate cancer, used to find metastatic tumors and their locations in the body. Rucaparib is a prostate cancer drug and is an anticancer agent used for male patients. This drug acts by showing cytotoxic effects against tumor cells and is a PARP inhibitor. Locametz is a prostate cancer drug and is used for male patients. The mechanism of action of Locametz is to try to detect whether prostate cancer is present by binding to cells that overexpress PSMA. In addition, the Gallium-68 atom contained in the drug is a β+ emitting radionuclide and this feature is used for PET.

3.2. Protein Preparation

By looking at the genes and proteins directly and most related to prostate cancer, AR (Androgen Receptor) (8E1A and 1E3G), KLK3 (Prostate Specific Antigen) (2ZCH and 2ZCL) were obtained from the RCSB PDB protein data bank database in PDB format and recorded for use in the Autodock Tools program. The structures obtained in the PDB format are X-Ray crystallography structures, and unwanted parts may be included in the protein while the 3D structure is being formed. For the optimization of the proteins to be used in Autodock Tools, water molecules were removed, hydrogen atoms were added, Kollman charges were added and the structure of the protein was optimized.

3.3. Ligand Preparation

New prostate cancer drugs approved by FDA; Abiraterone, Olaparib, Pylarify, Rucaparib and Locametz were selected as main ligands. Natural agents such as Apigenin and Quercetin, traditional drugs such as Estrone, Docetaxel and IC50 drugs were selected as ligands. Their molecular structures and formulas were obtained from PubChem database. CHEMBL codes of receptor and ligand chemical structures are shown in Table. Autodock Vina and Autodock Tools programs were prepared for

molecular docking.

Table 3.1. CHEMBL codes of New Prostate Cancer Drugs, natural agents, traditional drugs and IC50 drugs.

RECEPTOR	1E3G (AR)	8E1A (AR)	2ZCH (KLK3)	2ZCL (KLK3)
NEW DRUG	CHEMBL254328 CHEMBL521686 CHEMBL4297334 CHEMBL1173055 CHEMBL5095039	CHEMBL254328 CHEMBL521686 CHEMBL4297334 CHEMBL1173055 CHEMBL5095039	CHEMBL254328 CHEMBL521686 CHEMBL4297334 CHEMBL1173055 CHEMBL5095039	CHEMBL254328 CHEMBL521686 CHEMBL4297334 CHEMBL1173055 CHEMBL5095039
Natural Drug	CHEMBL28 CHEMBL50	CHEMBL50	CHEMBL50	CHEMBL50
Ligand	CHEMBL1405	CHEMBL1405	CHEMBL3545252	CHEMBL3545252
IC50	CHEMBL182412	CHEMBL267270	CHEMBL446790	CHEMBL446790

3.4. Protein-Ligand Docking

The optimized structures of the prepared protein receptors and ligands were provided with the AutoDock Tools and AutoDock Vina programs used for molecular docking studies. A grid box was defined for the ligands to be placed by docking by targeting the active sites or ligand binding sites of 1E3G, 8E1A, 2ZCL and 2ZCH receptors. The center of the grid box was defined with X-Y-Z dimensions. Simulation studies were performed to observe the binding affinity values and interactions of the ligands through the grid box located within the target protein receptors.

3.5. Autodock Tools and Molecular Docking Procedure with Autodock

Autodock Tools and Autodock Vina programs are basically software programs that provide protein-ligand simulation for molecular docking and approximation studies of a selected ligand into the target protein or gene at the atomic level. They are programs that pave the way for the discovery of new drugs by using molecules that have the potential to be drugs. There are differences between Autodock Tools and Autodock Vina programs. Autodock Vina does not use a grid box and works by selecting atom types. In addition, the Autodock Vina program can use multiple threads and multiple CPUs.

PDB (Protein Data Bank) and PDBQT (Protein Data Bank Partial Charge and Atom Type) formats of receptors and ligands were prepared for the Autodock Tools program. 1E3G, 8E1A, 2ZCL and 2ZCH molecules were obtained from the RCSB PDB database in PDB format. Water atoms and unwanted molecules in proteins were removed. Polar hydrogen atoms were included. 1E3G, 8E1A, 2ZCL and 2ZCH proteins were optimized. Kollman charges were loaded to spread the charge gap to all atoms. Kollman charges were included after the hydrogen atoms. Kollman charges are calculated using the AMBER force field and the orbital electron density of the molecule, while Gasteiger charges are calculated using the atomic electron density of the molecule. These charges are important for the structural binding poses and binding energies of the selected ligand to 1E3G, 8E1A, 2ZCL and 2ZCH proteins. The binding affinities of the ligands to prostate cancer-related protein receptors were obtained in silico using AutoDock Vina and Autodock Tools programs.

The appropriate geometries and 3D structures of selected natural agents and traditional drugs were downloaded from the PubChem database. ChEMBL coded ligands selected from the UniProt database were obtained. FDA approved drugs for prostate cancer were determined from the Cancer.gov website. Considering the ligand binding sites and active sites of 1E3G, 8E1A, 2ZCH and 2ZCL protein receptors, the grid boxes required for correct binding of ligands and increasing ligand binding optimizations were determined with Chimera Tools and AGFR programs. The X-Y-Z coordinate dimensions and centers of the grid boxes were adjusted to include the active sites and ligand sites, and the center coordinates were determined.

In addition, all dimensions of the grid boxes, taking into account the coordinates including the active areas, are shown in the table below.

Table 3.2. Centers, dimensions and coordinates of the grid box of receptors and ligands with AutoDock Vina and Autodock Tools

RECEPTOR	Center_X	Center_Y	Center_Z
1E3G (AR)	0.601	30.314	4.266
8E1A (AR)	16.669	8.943	9.708
2ZCH (KLK3)	-40.988	-32.42	-20.378
2ZCL (KLK3)	-31.372	-34.260	-18.427

LIGAND	Size_X	Size_Y	Size_Z
ABIRATERONE	60	60	60
OLAPARIB	60	60	60
RICAPARIB	30	30	30
PYLARIFY	60	60	60
LOCAMETZ	30	30	30

The dimensions of the grid box and the determination of ligand docking parameters were provided by using AutoDock Vina and AutoDock Tools programs. In ligand selection, the lowest energy ligand bindings were taken into account with these parameters.

100 binding modes were set to see the most probable binding modes and the energy range was determined as 4.

As a result, 1E3G, 8E1A, 2ZCH and 2ZCL receptors and ligand files prepared for molecular dockings were loaded into folders in order. Grid boxes and coordinates were set. The binding modes determined for docking were calculated.

Ligand binding energies (in kcal/mol) were calculated for the receptors. The most probable and highly effective binding conformations and binding sites, hydrophobic and hydrophilic interactions were examined with analyses.

3.6. Procedure for Molecular Dynamics Simulations with GROMACS Program

Tutorial

The GROMACS program was used to calculate Molecular Dynamics Simulations (MDS). Calculations were performed for this program via the National Center for High Performance Computing (UHeM). The structures of the determined proteins and ligands were loaded into folders, respectively. The interactions of proteins and ligands with each other, protein-ligand binding conformations, stability behaviors and docking analyses were calculated in a biological simulation.

The binding patterns of new prostate cancer drugs and ligands approved by the FDA to the target protein receptors and the resulting energies of the bindings and the structural and biological properties of the bindings were explained.

The complexes of protein-ligand structures obtained from AutoDock Vina and AutoDock Tools and giving the best binding results were saved as PDB files. The correct binding forms and atomic structures of the protein-ligand structures were checked in UCSF Chimera. They were saved for GROMACS with PDB or GRO formats.

Selected ligands obtained from PubChem, CheMBL or DrugBank databases were prepared by editing and minimizing in Chimera Tools program and made suitable for GROMACS program. Protein receptors prepared for MD simulation were saved. The best scoring protein-ligand structures selected according to their binding energies were loaded as Pose1.pdb files. LIG files of selected ligands were obtained as (LIG.mol2, LIG.rtf, LIG.pdb, LIG.crd, LIG.itp, LIG.par, LIG,psf) using SwissParam program. The GROMACS program and the files required for molecular dynamics simulations (EM.mdp, ions.mdp, MD.mdp, NPT.mdp, NVT.mdp, sort_mol2_bonds.pl) were downloaded from GitHub GROMACS Protein-Ligand file. The pose1.pdb file, prepared protein receptors and ligand files, and all files required for GROMACS were transferred to the National Center for High Performance Computing (UHeM) database.

The force fields used in the simulations (CHARMM, AMBER, GROMOS etc.) need to be polarized for accurate and appropriate simulations. The commonly used force field CHARMM was used for this molecular dynamics study because it contains parameters for structures such as proteins and lipids. CHARMM27 and TIP3P were selected to create the topology of the structure.

Table 3.3. Descriptions of ligand files and GitHub GROMACS Protein-Ligand files

File name	File Type	Explanation
LIG.pdb	PDB (Protein Data Bank File)	Contains three-dimensional coordinates of each atom in molecular structures
LIG.mol2	mol2 file	It includes the bonds and coordinates of the molecular structure
LIG.rtf	RTF (Residual Topology File)	Explains ligand topology in terms of the angles of atoms and the bonds they are bonded to
LIG.CRD	CRD (Coordinate File)	Covers atomic coordinates of molecular structures
LIG.itp	ITP (Include Topology Parameter File)	Covers coordinates and bonds of molecular structures
LİG.PAR	PAR (Parameter File)	Includes parameters of the force field
LIG.psf	PSF (Protein Structure File)	The dihedral angles of the protein structure include its bonds
sort_mol2_bonds.pl	Perl Script	Used to sort bond information in MOL2 files
MD.mdp	Molecular Dynamics File	It includes information such as time, step, temperature and pressure required for the molecular dynamics process.
EM.mdp	EM (Energy Minimization) File)	It is used for the energy minimization process
NVT.mdp	Constant Number, Volume and Temperature File	Used for temperature balance process
NPT.mdp	Constant Number, Pressure and Temperature File	Used for pressure balance process

iyonlar.mdp	Ion Addition File	Used in the ion addition process for the simulation process

In addition, after all topology files were created for the protein-ligand complex, TIP3P water model was selected for the efficiency of the process and water molecules were added. A box was created to cover all atoms, ions and water molecules. The edges of the cubic box were calculated as 2 nm. Solvation and ion addition processes were applied. For the energy minimization process, EM.mdp was selected as the parameter file from GROMACS' mdrun commands in the UHeM database with the sbatch file and command. PME (Particle Mesh Ewald) step was selected for the electrostatic interaction process. For the temperature balance process and stabilization, NVT.mdp was selected as the parameter file from GROMACS' mdrun commands in the UHeM database with the sbatch file and command. For the pressure balance process and stabilization, NPT.mdp was selected as the parameter file from GROMACS' mdrun commands in the UHeM database with the sbatch file and command. The durations of the NVT.mdp and NPT.mdp files were used as 100 ps.

For the NVT.mdp file, the temperature thermostat parameter tcoupl = V-rescale was used. For the NPT.mdp file, the NPT.mdp pcoupl = Parrinello-Rahman parameter was used. After the NVT temperature and NPT pressure balancing processes, the MD.mdp was selected as the parameter file from the GROMACS mdrun commands in the UHeM database with the sbatch file and command.

For each of the simulations, 50 ns MD processes were obtained for the analyses by running 0.002 femtoseconds and 25,000,000 steps.

3.7. Molecular Dynamics Simulations Procedure Tutorial 5 (Protein-Ligand Complex) Analysis

3.7.1. Clustering Analysis (Framework Selection)

Clustering analysis was applied to determine the different conformational changes of protein-ligand complexes. The aim of clustering analysis is to obtain the desired conformational changes group by group. RMSD values of each protein-ligand complex structure were calculated and RMSD matrix was obtained. According to

clustering analysis, representative frames of the clusters were determined (Mistry, J., et al., 2014).

3.7.2. RMSD (Mean Square Deviation)

The structural changes that will occur in the protein-ligand complex over time were tried to be predicted with the RMSD value. With this value, the differences between the actually observed value and the predicted values of the created model were measured. The RMSD value is calculated with the following formula (Vlasiou, M. C., et al., 2024).

di: is the distance between atoms,

i: in two structures and

N: is the total number of equivalent atoms,

$$RMSD = \sqrt{\frac{\sum_{i=1}^{N} di^2}{N}}$$

The gmx_mpi rms -s MD.tpr -f MD_center.xtc -o rmsd.xvg -tu ns command was run from the GROMACS Codes file and the RMSD.xvg result was obtained as the output of the command.

3.7.3. RMSF (Root Mean Square Fluctuations)

RMSF value is used to determine the fluctuation of an atom group in a molecular dynamics simulation process. It determines the flexibility states of different regions of the protein structure by determining the movements of atom groups in fixed-variable regions. It provides information about the deviation positions. RMSF calculates atom i, which is a group T structure (Vlasiou, M. C., et al., 2024).

$$RMSF = \sqrt{\frac{1}{T}\sum_{j=1}^{T}\left[\vec{r}_{j,i} - \frac{1}{T}\sum_{k=1}^{T}\vec{r}_{k,i}\right]^2}$$

3.7.4. Hydrogen Bond Analysis (H-Bond)

It indicates the numbers and positions of all hydrogen bonds that can be formed within 0.35 nm between protein and ligand structures in the MDS process. Hydrogen bond analysis was determined (Bizzarri, A. R., et al., 1995).

r_DA: is the donor-acceptor distance,

θ_(DHA:) is the donor-hydrogen-acceptor angle,

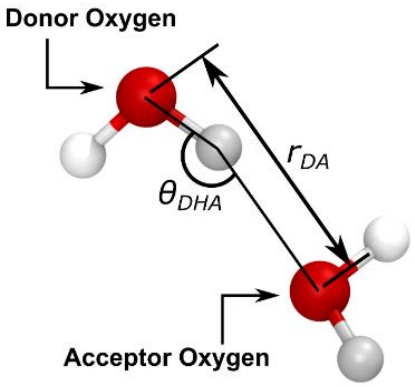

Figure 3.3. Illustration of the identification of hydrogen bonds with donor and acceptor atoms in an MDS process (Bizzarri, A. R., et al., 1995).

The gmx_mpi hbond -s MD.tpr -f MD_center.xtc -num hb.xvg -tu ns command was run from the GROMACS Codes file and the result hb00.xvg was obtained as the output of the command.

3.7.5. Radius of gyration (Rg)

Rg is defined as the root mean square distance of the atomic groups of a molecule to the center of mass. It is evaluated to observe the compactness and conformational change of the molecular structure.

The Rg value is calculated with the following formula (Vlasiou, M. C., et al., 2024).

mi: is the same mass,

ri: is the variable distance,

$$Rg^2 = \frac{\sum m_i {r_i}^2}{\sum m_i}$$

The gmx_mpi gyrate -s MD.tpr -f MD_center.xtc -o gyrate1.xvg -tu ns

command was run from the GROMACS Codes file and the gyrate1.xvg result was obtained as the output of the command.

3.7.6. SASA (Solvent Accessible Surface Area)

SASA, which is the solvent accessible surface area, is used to determine the solvent exposure rates of protein and ligand complexes. It indicates whether the protein and ligand are flexible and suitable for binding. The van der Waals radius of the water molecule (~1.4 Å) is used for SASA calculations (Ausaf Ali, S., et al., 2014).

gmx_mpi sasa -f MD.xtc -s MD.tpr -n index.ndx -o sasa1.xvg -odg odg1.xvg -tu ns command was run for protein-ligand from the GROMACS Codes file. The output of the command was sasa1.xvg. gmx_mpi sasa -f MD.xtc -s MD.tpr -n index.ndx -o sasa2.xvg -odg odg2.xvg -tu ns command was run only for protein from the GROMACS Codes file. The output of the command was sasa2.xvg.

3.7.7. ADMET (Absorption, Distribution, Metabolism, Excretion, and Toxicity)

ADMET (Absorption, Distribution, Metabolism, Elimination, Toxicity) is a method used in drug design and is used to evaluate whether molecules or ligands related to diseases that are being evaluated and investigated are drug candidates.

Absorption properties show how much of the drug candidate is absorbed and at what rate. Distribution properties show the distribution areas and speed of the drug candidate in the body. Metabolism properties show the mechanism of action of the drug candidate or whether it is used as an activator or inhibitor. Elimination properties show how long it takes for the drug candidate to be eliminated from the body. Toxicity properties show whether the drug has a toxic effect on body organs or causes irritation (Roy, K. (Ed.)., 2015).

CHAPTER IV. RESEARCH, FINDINGS AND DISCUSSION

In this thesis study, which is about the structures of new prostate cancer drugs that have been discovered as a solution to prostate cancer and approved by the FDA, conformational changes, molecular docking and molecular dynamics simulations of protein-ligand complexes were analyzed.

After a meticulous and detailed literature review, androgen receptors (1E3G, 8E1A), prostate specific antigen receptors (2ZCH and 2ZCL) were selected as the most effective genes on prostate cancer and the active sites of these receptors were taken as basis for the molecular docking study. A total of 11 new prostate cancer drugs, 30 natural agents, 67 traditional drugs and 72 ChEBML ligands available in the literature were studied for each receptor. Molecular docking results of the receptors with Autodock Vina and Autodock Tools programs are shown in APPENDIX I).

Based on the obtained molecular docking results, 5 new drugs (vs), 4 natural agents, 4 traditional drugs and 3 ChEMBL ligands with the lowest binding energy score, best efficiency and highest ligand binding energy were determined.

Molecular dynamics simulations were performed after protein-ligand docking simulations. Among these, the most suitable protein-ligand pairs were selected according to the lowest binding energy scores based on molecular docking results and prepared for the molecular dynamics simulation process.

A specific modeling study was performed by examining the selected receptors, genes and ligands together with the Molecular Dynamics Simulation method, and observing the structural properties of drugs effective in prostate cancer treatment.

In this study, we performed molecular dynamics simulations after molecular docking to analyze the effects of new prostate cancer drugs currently approved by the FDA on prostate cancer and at what molecular level they interact.

4.1. Molecular Docking Findings

Parameters such as binding energies, physicochemical properties, molecular interactions and biological properties at molecular level of molecules were obtained by molecular docking, respectively. Two different programs were used for molecular docking and docking operations: Autodock Vina and Autodock Tools. The main purpose of the Autodock Tools program was to support the results obtained from Autodock Vina and to see the features that Autodock Vina could not provide. Molecular docking studies were performed using androgen receptors (1E3G and 8E1A), KLK3 gene (2ZCH) receptor and KLK3 gene (2ZCL) receptors and FDA-approved new prostate cancer drugs determined as a result of the literature search for prostate cancer. Protein receptor structures to be used for docking (1E3G, 8E1A, 2ZCH and 2ZCL) were obtained from the Protein Data Bank (PDB). The structures of the drugs and ligands were obtained from PubChem.

Table 4.1. Receptor-ligand structures with lowest binding energy with AutoDock Vina and AutoDock Tools.

Receptor	**Drugs and Ligands**	**Minimum Binding Energy (kcal/mol)**
1E3G (AR)	CHEMBL182412 (Preclinical)	-11.0
	Apigenin	-10.0
	CHEMBL1387	-10.9
8E1A (AR)	CHEMBL267270 (Preclinical)	-11.3
	Baicalin	-10.0
	CHEMBL425863	-10.8
2ZCH (KLK3)	CHEMBL446790	-10.4
	Epigallocatechin-3-gallate (EGCG)	-9.3
	CHEMBL428647	-9.8
2ZCL (KLK3)	CHEMBL446790	-9.6
	Astragaloside	-10.2
	CHEMBL3545252	-9.8

Binding affinity values (kcal/mol) for the selected receptor-ligand pair among drug-ligands are shown in Table 4.1. (The results of ligand docking to receptors with Autodock Vina and AutoDock Tools programs are shown in Appendix I).

Among the new prostate cancer drugs approved by the FDA, Abiraterone, Olaparib, Rucaparib, Pylarify and Locametz were selected as prostate cancer-specific drugs.

4.1.1. Molecular Docking Studies of 1E3G (AR) Receptor with Drugs and Ligands

Androgen receptor gene allows expression of some genes in men. Hormones that bind to androgen receptors are testosterone and dihydrotestosterone. This receptor ensures the development of male individuals. Androgen Insensitivity Syndrome occurs in case of androgen receptor gene deficiency. Due to the major role of androgen receptor in the progression and growth of prostate cancer, it continues to be examined with increasing interest for drugs developed for treatment purposes. Therefore, detailed examination and analysis of molecules that bind to 1E3G receptor is of great importance in the discovery of new drugs or potential drug candidates in the treatment of prostate cancer.

New drug molecules were used in this thesis study. According to RCSB PDB data, 1E3G is provided with ligands from R1881molecule. AutoDock Vina was used for molecular docking studies where the structures of ligand-receptor complexes are flexible or stable. Tight docking and blind docking studies were performed with AutoDock Tools.

The most suitable grid box dimensions and coordinates determined for molecular docking studies are shown in Table 4.2. for 1E3G receptor. Docking parameters are shown in Table 4.2. After completing the necessary steps in the AutoDock program for 1E3G receptor, it was run in **5 steps**, **50, 25 steps** were given to the population size, **150 and 100 steps** were given to the population size, and **300** was given to the population size.

Table 4.2. Grid box parameter file of 1E3G receptor and ligands with AutoDock Vina.

GRID PARAMETER FILE				
Macromolecule	**1E3G (AR)**			
Models	Rucaparib	Apigenin	CHEMBL182412	Estrone
# of grind points in xyz	30 30 30	60 60 60	60 60 60	60 60 60
Spacing (Å)	0.5	0.5	0.5	0.5
xyz grid-center coordinates	0.601	0.601	0.601	0.601
	30.314	30.314	30.314	30.314
	4.266	4.266	4.266	4.266
# of torsional degrees of freedom	5			
Temperature (K)	298.15			
Charges	gasteiger			

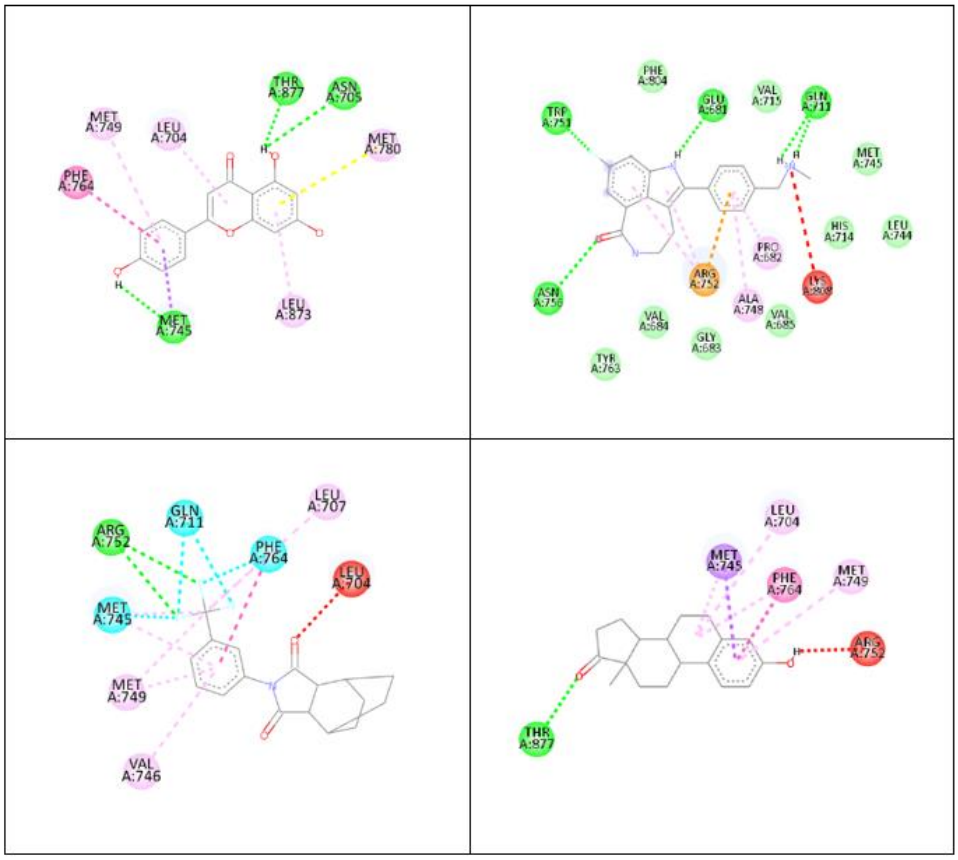

Figure 4.1. 2D ligand-protein diagram using Discovery Studio program showing amino acid transfers between 1E3G receptor and Apigenin, Rucaparib, CHEMBL182412, Estrone ligands, respectively.

Dark green bonds represent conventional hydrogen bonds, light green bonds represent van der Waals bonds, light pink bonds represent pi-alkyl bonds, light purple bonds represent pi-sigma bonds, yellow bonds represent pi-sulfur bonds, blue bonds represent halogen bonds, red bonds represent unfavorable bonds, and dark pink bonds represent pi-pi bonds.

Hydrogen bonds are the strongest specific bonds and are critical for the structural integrity of molecules. They are important for protein folding, protein stability, and specific ligand interactions. Halogen bonds are between the ligand and protein molecules and strengthen the binding affinities of the ligand to the target protein. Noncovalent interactions such as Pi-Pi interactions and alkyl interactions contribute to the binding and stabilizing power of the ligand. Van der Waals bonds are important for high specificity even in the presence of weak interactions in protein-ligand docking (Chen, C., Li, et al., 2009), (Terefe, E. M., & Ghosh, A., 2022), (Celis-Barros, C., et al., 2015), (Sahputra, I. H., & Echtermeyer, A., 2021).

Figure 4.1. shows the 2D protein-ligand interactions of four different ligand types that give the lowest binding energies with the 1E3G receptor. These ligands are the Natural agent; Apigenin, the New Prostate Cancer Drug; Rucaparib, the CHEMBL182412 coded ligand with IC50 activity, and the traditional prostate cancer drug Estrone.

According to Figure 4.1. there are hydrogen bonds, Pi-Pi T-shaped and Pi-Alkyl interactions, Pi-Sulfur bonds between 1E3G receptor and Apigenin. Apigenin binds very strongly to 1E3G receptor via hydrogen bonds with amino acids MET745, ASN705 and THR877. This interaction increases the effect of Apigenin to function as an effective inhibitor. There are Pi-Alkyl interactions between 1E3G receptor and Apigenin with amino acids LEU873, LEU704, MET749 and Pi-Sulfur bond with MET780. Alkyl-like interactions of Apigenin with LEU873 and other hydrophobic amino acids prove the hydrophobic attraction.

There are hydrogen bonds, Pi-Cation and Pi-Alkyl interactions, unfavorable positive-positive bonds between 1E3G receptor and Rucaparib. Rucaparib binds very strongly to 1E3G receptor via hydrogen bonds with amino acids ASN756, TRP751,

GLU681, GLN711. This interaction increases the effect of Rucaparib to act as an effective inhibitor. There are Pi-Alkyl interactions between 1E3G receptor and Rucaparib with amino acids ALA748 and PRO682 and Pi-Cation bond with ARG752. Alkyl-like interactions of Rucaparib with ALA748 and other hydrophobic amino acids prove hydrophobic attraction. Van der Waals interactions occurred between 1E3G and Rucaparib with amino acids VAL684, GLY683 and HIS714.

In addition, according to Figure 4.1. there are hydrogen bonds, halogen and Pi-Alkyl interactions, unfavorable acceptor-acceptor bonds between 1E3G receptor and CHEMBL182412. CHEMBL182412 binds very strongly to 1E3G receptor via hydrogen bonds with ARG752 amino acid. This interaction increases the effect of CHEMBL182412 to function as an effective inhibitor. CHEMBL182412 contributes to the binding energy by forming a halogen bond with MET745, PHE764 and GLN711, and halogen bonds are critical specifically for ligand types containing fluorine atoms. CHEMBL182412, which forms halogen bonds with MET745, PHE764 and GLN711, provides additional stabilization and stability in the binding site. The interactions of MET749, VAL746, LEU707 indicate hydrophobic interactions with the alkyl group atoms of aromatic rings of the ligand molecule, supporting the strong binding of CHEMBL182412 to the 1E3G receptor.

There are hydrogen bonds, Pi-Pi T-shaped, Pi-Alkyl interactions, Pi-Sulfur and Pi-Sigma bonds between 1E3G receptor and Estrone. Estrone binds very strongly to 1E3G receptor via hydrogen bonds with THR877 amino acid. This interaction enhances the effect of Estrone to act as a potent inhibitor. There are unfavorable donor-donor bonds with ARG752. MET749, MET745, LEU704 and PHE764 interactions indicate hydrophobic interactions with alkyl group atoms of aromatic rings of ligand molecule. It supports the strong binding of Estrone to 1E3G receptor.

4.1.2. Molecular Docking Studies of 8E1A (AR) Receptor with Drugs and Ligands

The androgen receptor gene allows the expression of some genes in men. The hormones that bind to androgen receptors are testosterone and dihydrotestosterone. This receptor ensures the development of the male individual. Androgen Insensitivity

Syndrome occurs in the absence of the androgen receptor gene. Due to the major role of the androgen receptor in the progression and growth of prostate cancer, it continues to be examined with increasing interest for drugs developed for therapeutic purposes. Therefore, detailed examination and analysis of molecules that bind to the 8E1A receptor is of great importance in the discovery of new drugs or potential drug candidates in the treatment of prostate cancer.

New drug molecules were used in this thesis study. According to RCSB PDB data, 8E1A is provided with ligands from 3E0 molecule. AutoDock Vina was used for molecular docking studies where the structures of ligand-receptor complexes are flexible or stable. Tight docking and blind docking studies were performed with AutoDock Tools.

The most suitable grid box dimensions and coordinates determined for molecular docking studies are shown in Table 4.3. for 8E1A receptor. Docking parameters are shown in Table 4.3. After completing the necessary steps in the AutoDock program for 8E1A receptor, it was run in 5 steps, 50, 25 steps were given to the population size, 150 and 100 steps were given to the population size, and 300 was given to the population size.

Table 4.3. Grid box parameter file of 8E1A receptor and ligands with AutoDock Vina.

GRID PARAMETER FILE				
Macromolecule	**8E1A (AR)**			
Models	Baicalin	Olaparib	CHEMBL267270	Mibolerone
# of grind points in xyz	40 40 40	20 20 20	30 30 30	30 30 30
Spacing (Å)	0.5	0.5	0.5	0.5
xyz grid-center coordinates	16.669	16.669	16.669	16.669
	8.943	8.943	8.943	8.943
	9.708	9.708	9.708	9.708
# of torsional degrees of freedom	5			
Temperature (K)	298.15			
Charges	gasteiger			

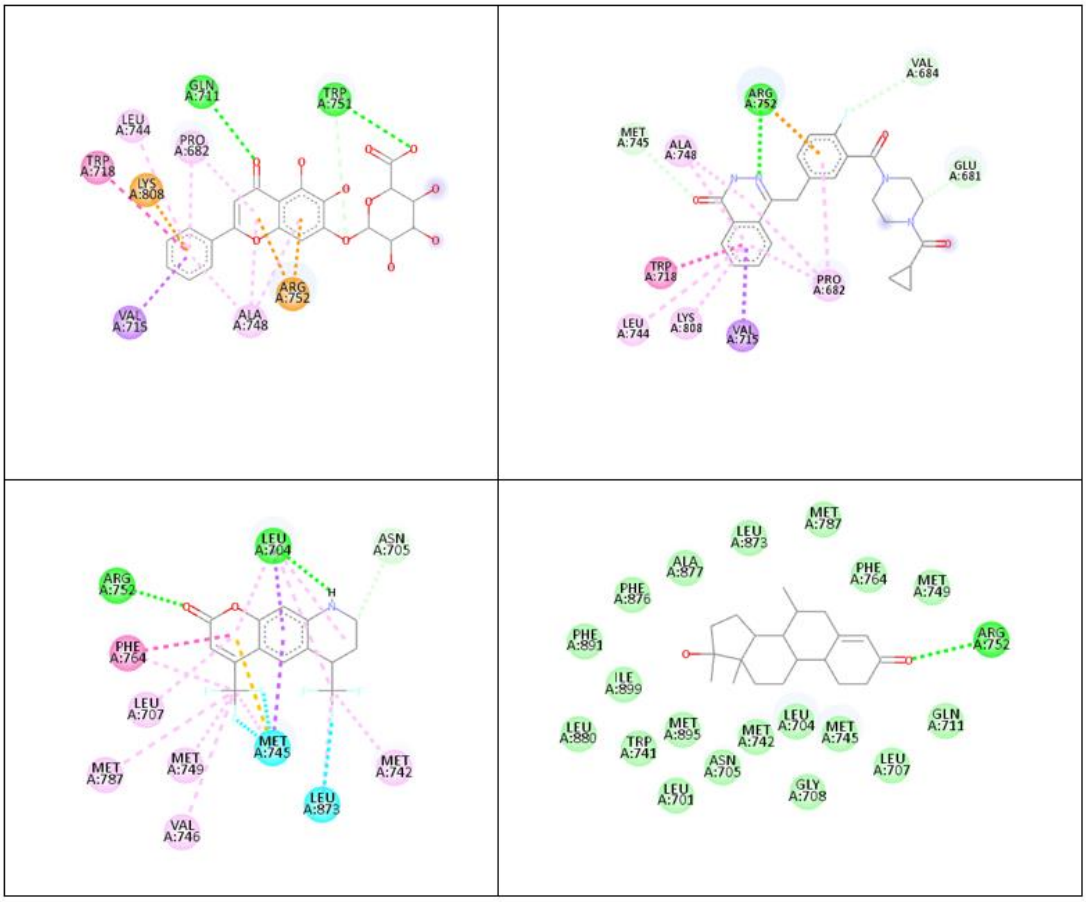

Figure 4.2. 2D ligand-protein interaction diagram with Discovery Studio program showing amino acid interactions between 8E1A receptor and Baicalin, Olaparib, CHEMBL267270, Mibolerone ligands, respectively.

Figure 4.2. shows the protein-ligand interactions of four different ligand types that give the lowest binding energies with 8E1A receptor in 2D form. These ligands are; Natural agent; Baicalin, New Prostate Cancer Drug; Olaparib, IC50 activity CHEMBL267270 coded ligand and traditional prostate cancer drug Mibolerone.

Dark green bonds represent conventional hydrogen bonds, light green bonds represent van der Waals bonds, light pink bonds represent pi-alkyl bonds, light purple bonds represent pi-sigma bonds, yellow bonds represent pi-sulfur bonds, blue bonds represent halogen bonds, red bonds represent unfavorable bonds, and dark pink bonds represent pi-pi bonds.

According to Figure 4.2., there are hydrogen bonds, Pi-Pi T-shaped and Pi-Alkyl interactions, Pi-Cation bonds between 8E1A receptor and Baicalin. Baicalin binds very strongly to 8E1A receptor via hydrogen bonds with amino acids TRP751

and GLN711. This interaction increases the effect of Baicalin to function as an effective inhibitor. There are Pi-Alkyl interactions between 8E1A receptor and Baicalin with amino acids LEU744, ALA748, PRO682 and TRP718 and Pi-Cation bond with LYS808 and ARG752. Alkyl-like interactions of Baicalin with VAL715 and other hydrophobic amino acids prove the hydrophobic attraction.

There are hydrogen bonds, Pi-Cation and Pi-Alkyl interactions between 8E1A receptor and Olaparib. Olaparib binds very strongly to 8E1A receptor via hydrogen bond with amino acid ARG752. This interaction enhances the effect of Olaparib to act as an effective inhibitor. There are Pi-Alkyl interactions between 8E1A receptor and Olaparib with amino acids LYS808, LEU744, PRO682 and ALA748 and Pi-Sigma bond with VAL715. Alkyl-like interactions of Olaparib with VAL684 and other hydrophobic amino acids prove hydrophobic attraction.

In addition, according to Figure 4.2., there are hydrogen bonds, halogen and Pi-Alkyl interaction bonds between 8E1A receptor and CHEMBL267270. CHEMBL267270 binds very strongly to 8E1A receptor via hydrogen bonds with amino acids ARG752 and LEU704. This interaction increases the effect of CHEMBL267270 to function as an effective inhibitor. CHEMBL267270 contributes to the binding energy by forming halogen bonds with MET745 and LEU873, and the halogen bonds are critical specifically for ligand varieties containing fluorine atoms. CHEMBL267270, which forms halogen bonds with MET745 and LEU873, provides additional stabilization and stability in the binding site. MET742, MET749 VAL746, LEU707 interactions indicate hydrophobic interactions with alkyl group atoms of aromatic rings of the ligand molecule. Supports the strong binding of CHEMBL267270 to the 8E1A receptor.

There are strong hydrogen bonding interactions between the 8E1A receptor and Mibolerone. Mibolerone binds very strongly to the 8E1A receptor via hydrogen bonding with the amino acid ARG752. This interaction enhances the effect of Mibolerone to act as a potent inhibitor. Van der Waals interactions occurred between the amino acids LEU707, LEU873, MET787 between 8E1A and Mibolerone.

4.1.3. Molecular Docking Studies of 2ZCH (KLK3) Receptor with Drugs

and Ligands

Prostate Specific Antigen (kallikrein-related peptidase 3/KLK3) gene is detected in the blood as a glycoprotein enzyme encoded in humans and has made a great difference in both the detection and treatment of prostate cancer. Due to the great role of prostate specific antigen in the progression and detection of prostate cancer, it continues to be examined with increasing interest for drugs developed for treatment purposes. Therefore, detailed examination and analysis of molecules binding to 2ZCH (KLK3) receptor is of great importance in the discovery of new drugs or potential drug candidates in the treatment of prostate cancer.

New drug molecules were used in this thesis study. According to RCSB PDB data, 2ZCH is provided with ligands from NDG molecule. AutoDock Vina was used for molecular docking studies where the structures of ligand-receptor complexes are flexible or stable. Tight docking and blind docking studies were performed with AutoDock Tools.

The most suitable grid box dimensions and coordinates determined for molecular docking studies are shown in Table 4.4. for 2ZCH receptor. Docking parameters are shown in Table 4.4. After completing the necessary steps in AutoDock program for 2ZCH receptor, it was run **in 5 steps, 50, 25 steps** were given to the population size, **150 and 100 steps** were given to the population size, and **300** was given to the population size.

Table 4.4. Grid box parameter file of 2ZCH receptor and ligands with AutuDock Vina.

GRID PARAMETER FILE				
Macromolecule	**2ZCH (KLK3)**			
Models	EGCG	Olaparib	Fukugetin	Paclitaxel
# of grind points in xyz	30 30 30	60 60 60	90 90 90	60 60 60
Spacing (Å)	0.5	0.5	0.5	0.5
xyz grid-center coordinates	-40.988	-40.988	-40.988	-40.988
	-32.42	-32.42	-32.42	-32.42
	-20.378	-20.378	-20.378	-20.378
# of torsional degrees of freedom	5			
Temperature (K)	298.15			
Charges	gasteiger			

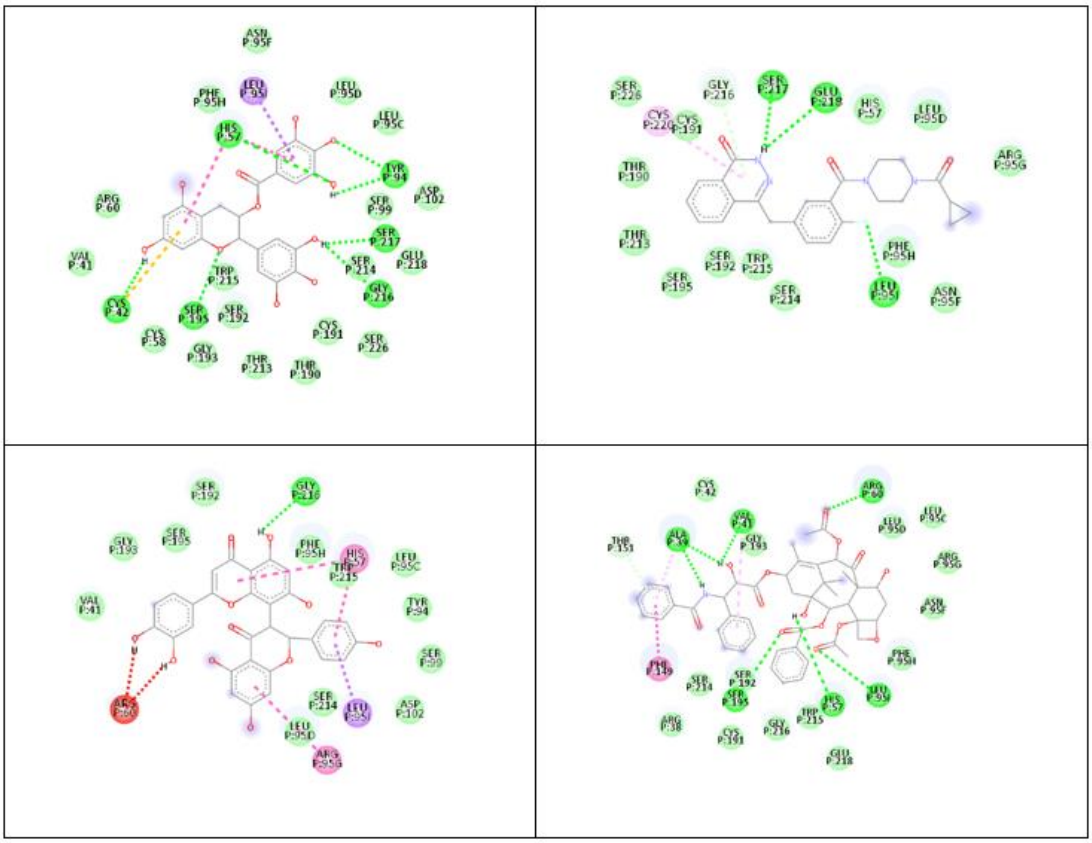

Figure 4.3. 2D ligand-protein interaction diagram with Discovery Studio program showing amino acid interactions between EGCG, Olaparib, Fukugetin, Paclitaxel ligands with 2ZCH receptor, respectively.

Figure 4.3. shows the protein-ligand interactions of four different ligand types that give the lowest binding energies with 2ZCH receptor in 2D form. These ligands are Natural agent; EGCG, New Prostate Cancer Drug; Olaparib, IC50 activity CHEMBL446790 coded (Fukugetin) ligand and traditional prostate cancer drug Paclitaxel.

Dark green bonds represent conventional hydrogen bonds, light green bonds represent van der Waals bonds, light pink bonds represent pi-alkyl bonds, light purple bonds represent pi-sigma bonds, yellow bonds represent pi-sulfur bonds, blue bonds represent halogen bonds, red bonds represent unfavorable bonds, and dark pink bonds represent pi-pi bonds.

According to Figure 4.3., there are hydrogen bonds, Pi-Pi T-shaped and Pi-

Sulfur interactions, Van der Waals interactions, Pi-Sigma bonds between 2ZCH receptor and EGCG. EGCG binds very strongly to 2ZCH receptor via hydrogen bonds with SER217, TYR94, SER195 and HIS57 amino acids. This interaction increases the effect of EGCG to function as an effective inhibitor. There are Pi-Alkyl interactions between 2ZCH receptor and EGCG with CYS42 and HIS57 amino acids. Alkyl-like interactions with hydrophobic amino acids prove hydrophobic attraction. Van der Waals interactions occurred between 2ZCH and EGCG with CYS191, LEU95C, ASP102 amino acids.

Hydrogen bonds, Van der Waals interactions and Pi-Alkyl interactions exist between the 2ZCH receptor and Olaparib. Olaparib binds very strongly to the 2ZCH receptor via hydrogen bonds with amino acids SER217, GLU218 and LEU951. This interaction enhances the effect of Olaparib to act as a potent inhibitor. Pi-Alkyl interactions exist between the 2ZCH receptor and Olaparib with the amino acid CYS220. Alkyl-like interactions with hydrophobic amino acids suggest hydrophobic attraction. Van der Waals interactions exist between Olaparib and amino acids SER214, SER192, SER195 and THR213.

In addition, according to Figure 4.3., there are hydrogen bonds, Van der Waals interactions, Pi-Sigma and Pi-Alkyl interaction bonds between 2ZCH receptor and CHEMBL446790 (Fukugetin). Fukugetin binds very strongly to 2ZCH receptor via hydrogen bonds with amino acid GLY216. This interaction enhances the effect of CHEMBL446790 to function as an effective inhibitor. The interactions between CHEMBL446790 and LEU951, HIS57, ARG95 amino acids indicate hydrophobic interactions with alkyl group atoms of aromatic rings of the ligand molecule. This supports the strong binding of CHEMBL446790 to 2ZCH receptor. CHEMBL446790 (Fukugetin) has Van der Waals interactions with amino acids VAL41, SER192, SER195 and ASP102.

There are strong hydrogen bonding interactions and Van der Waals interactions between the 2ZCH receptor and Paclitaxel. Paclitaxel binds very strongly to the 2ZCH receptor via hydrogen bonds with the amino acids LEU951, SER192, HIS57, ALA39 and VAL41. This interaction enhances the effect of Paclitaxel to act as a potent inhibitor. Paclitaxel has Van der Waals interactions with the amino acids VAL41,

ASN95F, PHE95H, ARG95G, CYS191.

4.1.4. Molecular Docking Studies of 2ZCL (KLK3) Receptor with Drugs and Ligands

Prostate Specific Antigen (kallikrein-related peptidase 3/KLK3) gene is detected in the blood as a glycoprotein enzyme encoded in humans and has made a great difference in both the detection and treatment of prostate cancer. Due to the great role of prostate specific antigen in the progression and detection of prostate cancer, it continues to be examined with increasing interest for drugs developed for treatment purposes. Therefore, detailed examination and analysis of molecules binding to 2ZCL (KLK3) receptor is of great importance in the discovery of new drugs or potential drug candidates in the treatment of prostate cancer.

New drug molecules were used in this thesis study. According to RCSB PDB data, 2ZCL is provided with ligands from NAG molecule. AutoDock Vina was used for molecular docking studies where the structures of ligand-receptor complexes are flexible or stable. Tight docking and blind docking studies were performed with AutoDock Tools.

The most suitable grid box dimensions and coordinates determined for molecular docking studies are shown in Table 4.5. for 2ZCL receptor. Docking parameters are shown in Table 4.5. After completing the necessary steps in AutoDock program for 2ZCL receptor, it was run **in 5 steps, 50, 25 steps** were given to the population size, **150 and 100 steps** were given to the population size, and **300** was given to the population size.

Table 4.5. Grid box parameter file of 2ZCL receptor and ligands with AutuDock Vina.

GRID PARAMETER FILE				
Macromolecule	**2ZCL (KLK3)**			
Models	EGCG	Olaparib	Fukugetin	Paclitaxel
# of grind points in xyz	30 30 30	60 60 60	90 90 90	60 60 60
Spacing (Å)	0.5	0.5	0.5	0.5
xyz grid-center coordinates	-40.988	-40.988	-40.988	-40.988
	-32.42	-32.42	-32.42	-32.42
	-20.378	-20.378	-20.378	-20.378
# of torsional degrees of freedom	5			

Temperature (K)	298.15
Charges	gasteiger

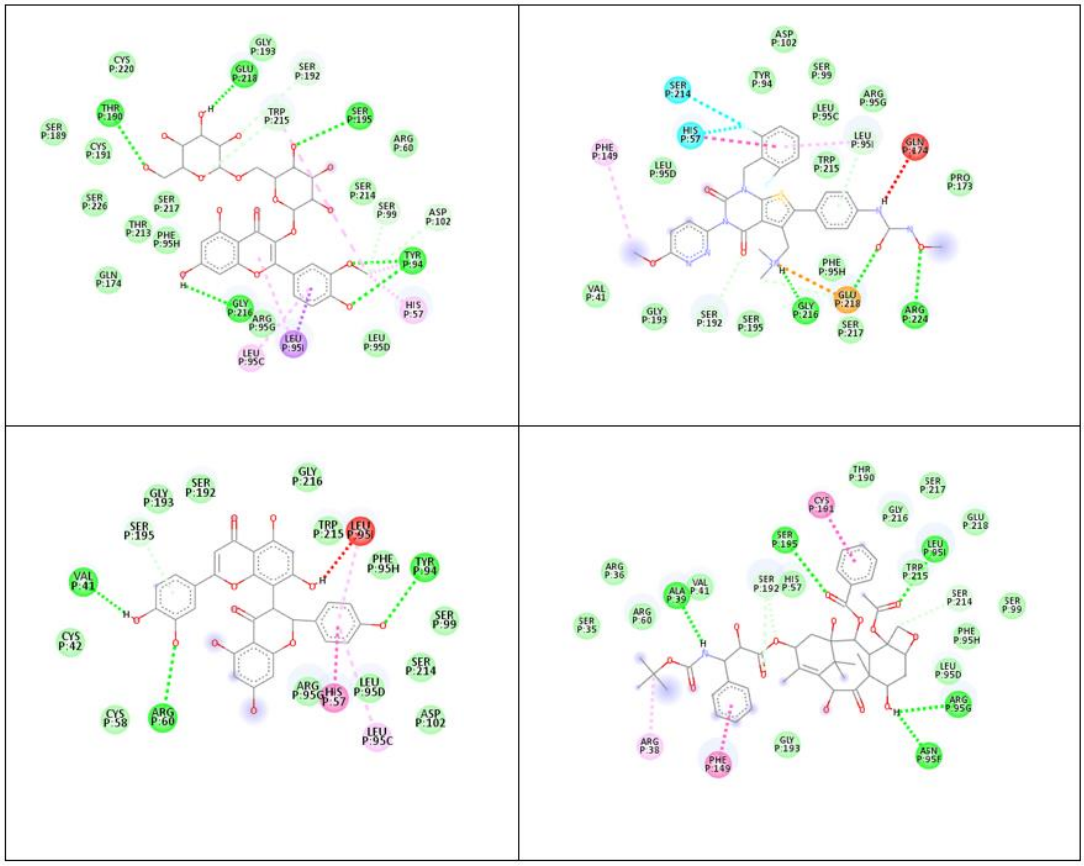

Figure 4.4. 2D ligand-protein interaction diagram with Discovery Studio program showing amino acid interactions between 2ZCL receptor and Astragaloside, Orgovyx, Fukugetin, Docetaxel ligands, respectively.

Figure 4.4. shows the protein-ligand interactions of four different ligand types that give the lowest binding energies with 2ZCL receptor in 2D form. These ligands are; Natural agent; Astragaloside, New Prostate Cancer Drug; Orgovyx, IC50 activity CHEMBL446790 coded (Fukugetin) ligand and traditional prostate cancer drug; Docetaxel.

Dark green bonds represent conventional hydrogen bonds, light green bonds represent van der Waals bonds, light pink bonds represent pi-alkyl bonds, light purple

bonds represent pi-sigma bonds, yellow bonds represent pi-sulfur bonds, blue bonds represent halogen bonds, red bonds represent unfavorable bonds, and dark pink bonds represent pi-pi bonds.

According to Figure 4.4., there are hydrogen bonds, Van der Waals interactions, Pi-Alkyl and Pi-Sigma bonds between the 2ZCL receptor and Astragaloside. Astragaloside binds very strongly to the 2ZCL receptor via hydrogen bonds with amino acids GLU218, THR190, GLY216 and SER195. This interaction increases the effect of Astragaloside to act as an effective inhibitor. There are Pi-Alkyl interactions between the 2ZCL receptor and Astragaloside with amino acids LEU95C, LEU95I and HIS57. Alkyl-like interactions with amino acids showing hydrophobic properties prove hydrophobic attraction. Astragaloside has Van der Waals interactions with amino acids GLN174, SER214, ARG60 and SER189.

Hydrogen bonds, Van der Waals interactions, Pi-Alkyl and halogen interactions exist between the 2ZCL receptor and Orgovyx. Orgovyx binds very strongly to the 2ZCL receptor via hydrogen bonding with amino acids ARG224 and GLY216. This interaction enhances the effect of Orgovyx to function as an effective inhibitor. Orgovyx forms halogen bonds with HIS57 and SER214, contributing to the binding energy, and halogen bonds are critical specifically for ligands containing fluorine atoms. Orgovyx forms halogen bonds with HIS57 and SER214, providing additional stabilization and stability at the binding site. There are unfavorable donor-donor interactions between the 2ZCL receptor and Orgovyx with amino acid GLN174. Alkyl-like interactions between the amino acid PHE149 of Orgovyx provide hydrophobic attraction, and Orgovyx has Van der Waals interactions with the amino acids PRO173, SER195 and LEU95C.

In addition, according to Figure 4.4., hydrogen bonds, Van der Waals interactions and Pi-Alkyl interaction bonds exist between 2ZCL receptor and CHEMBL446790 (Fukugetin). Fukugetin binds very strongly to 2ZCL receptor via hydrogen bonds with amino acids TYR94, ARG60 and VAL41. This interaction enhances the effect of CHEMBL446790 to function as an effective inhibitor. The interactions between CHEMBL446790 and amino acids HIS57 and LEU95C indicate hydrophobic interactions with alkyl group atoms of aromatic rings of the ligand

molecule, supporting the strong binding of CHEMBL446790 to 2ZCL receptor. CHEMBL446790 (Fukugetin) has Van der Waals interactions with amino acids CYS58, SER195 and LEU95D.

There are strong hydrogen bonding interactions and Van der Waals interactions between the 2ZCL receptor and Docetaxel. Docetaxel binds very strongly to the 2ZCL receptor via hydrogen bonds with the amino acids SER195, ASN95F and ALA39. This interaction enhances the effect of Docetaxel to act as a potent inhibitor. The interactions between Docetaxel and the amino acids CYS191 and PHE149 reflect hydrophobic interactions with the alkyl group atoms of the aromatic rings of the ligand molecule. Docetaxel has Van der Waals interactions with the amino acids GLY193, SER99 and LEU95D.

4.2. Molecular Dynamics Simulations Results (Stability of Ligand Receptor Complexes)

Molecular dynamics studies were performed to see the dynamic shape changes that occur in the structure in order to understand that the ligand or drug candidates change their conformations according to selective proteins by detecting kinetic energy changes. The force values acting on each atom were calculated according to the energy values. An environment closer to biological systems was obtained by modeling the movement of protein-ligand pairs in water molecules over time with molecular dynamics simulations. Thus, it was seen that efficient dynamic results could be obtained if the necessary parameters were added to the polarized force fields in the modeling of the dynamic structures of disordered and rapidly folding proteins. In addition, the parameters used in all MD simulations are shown in **Table 4.6.**

Table 4.6. MD simulation parameters.

Temperature	300 K
Force Field	Charmm27
Solvent	TIP3P
Cubic Box Boundary	2.0 nm

MD simulations were performed by adjusting the thermostat based on fixed particle number, fixed volume, and fixed temperature and NVT balancing was performed with 100 ps for system balancing. In order to control the density according to fixed particle number, NPT balancing was performed with 100 ps and then thermodynamic conditions were provided.

The protocol of the codes used to perform MD simulations is shown in APPENDIX I. In addition, RMSD (root mean square deviation), RMSF (root mean square fluctuations), RG (Radius of Gyration), SASA (solvent accessible surface area), MSD (mean square displacement) and ADMET (Absorption, Distribution, Metabolism, Excretion, and Toxicity) analyses were performed for the simulations performed with these codes used for each protein-ligand complex, and 50 ns simulations were recorded for each ligand and drug complexes with UHeM (The National Center for High Performance Computing).

4.2.1. Molecular Dynamics Simulations of 1E3G, 8E1A, 2ZCH and 2ZCL Receptors with Abiraterone Drug

First, the RMSD (Root Mean Square Deviation) value was plotted to obtain the conformational changes of the molecules from their initial positions to their final positions due to Abiraterone drug and 1E3G, 8E1A, 2ZCH and 2ZCL receptors during the molecular dynamics simulation and to monitor the changes during this process and to see how it stabilizes. In addition, the Figure 4.5. shows the root-mean-square deviation (RMSD) over time during the molecular dynamics (MD) simulations of 1E3G, 8E1A, 2ZCH and 2ZCL receptors due to Abiraterone drug.

During the simulation process, lower and less displayed RMSD values indicate that the protein-ligand complexes to which they are bound are more stable, while higher resulting RMSD values indicate that there are more structural changes in the protein-ligand complexes and more mobility during the simulation process.

The RMSD values for the 1E3G receptor showed a lot of mobility over time. This indicates that Abiraterone drug is not tightly bound to the protein and its conformational changes are high. Although the RMSD values for the 2ZCH receptor

fluctuated between 10,000 and 15,000 ps, they remained stable between 15,000 and 50,000 ps. It exhibited a very stable structure throughout the simulation. The RMSD values for the 2ZCL receptor remained stable between approximately 15,000 and 50,000 ps. It exhibited a very stable structure throughout the simulation. The RMSD values for the 8E1A receptor remained stable between 30,000 and 50,000 ps and between 10,000 and 20,000 ps. The results suggested that the 1E3G receptor underwent more conformational changes throughout the simulation and that the binding stability with Abiraterone drug may be lower than other receptors.

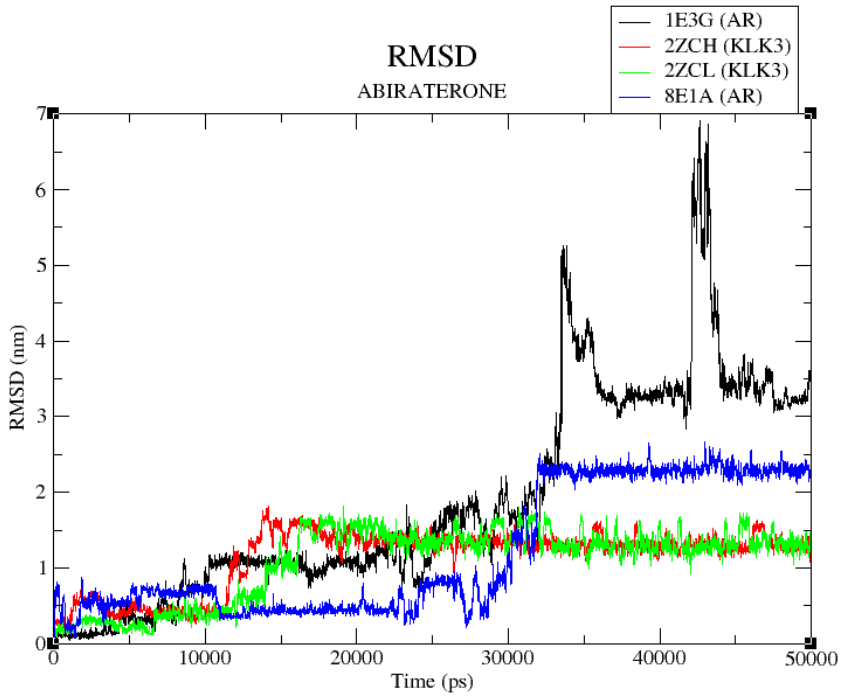

Figure 4.5. RMSD analysis results graph of 1E3G (AR), 8E1A (AR), 2ZCH (KLK3) and 2ZCL (KLK3) receptors bound to Abiraterone drug in MD simulation.

As a result, Abiraterone was most stable and tightly bound to 2ZCH and 2ZCL receptors. While 8E1A receptor showed moderately stable binding, 1E3G receptor showed the least stable binding.

The RMSF value measures how much each structure deviates and moves away from its reference position during the simulation. This value is used to determine the flexibility and dynamics of atoms in certain regions.

In addition, the Figure 4.6. shows the atomic root-mean-square deviations (RMSF) of the drug Abiraterone bound to the 1E3G, 2ZCH, 2ZCL and 8E1A receptors.

RMSF values are generally below 0.1 nm for 1E3G, but exceed 0.5 nm. The 1E3G receptor has high RMSF values, indicating that it is unstable and exhibits high flexibility when bound to the receptor.

RMSF values for 2ZCH are generally between 0.1 and 0.2 nm. The 2ZCH receptor has lower RMSF values, indicating that it is stable and not very flexible when bound to the receptor. RMSF values for 2ZCL are generally between 0.1 and 0.2 nm. The 2ZCL receptor has lower RMSF values, indicating that it is stable and not very flexible when bound to the receptor. RMSF values are generally below 0.1 nm for 8E1A, but exceed 0.5 nm. The 8E1A receptor has higher RMSF values, indicating that it is unstable and not very flexible when bound to the receptor.

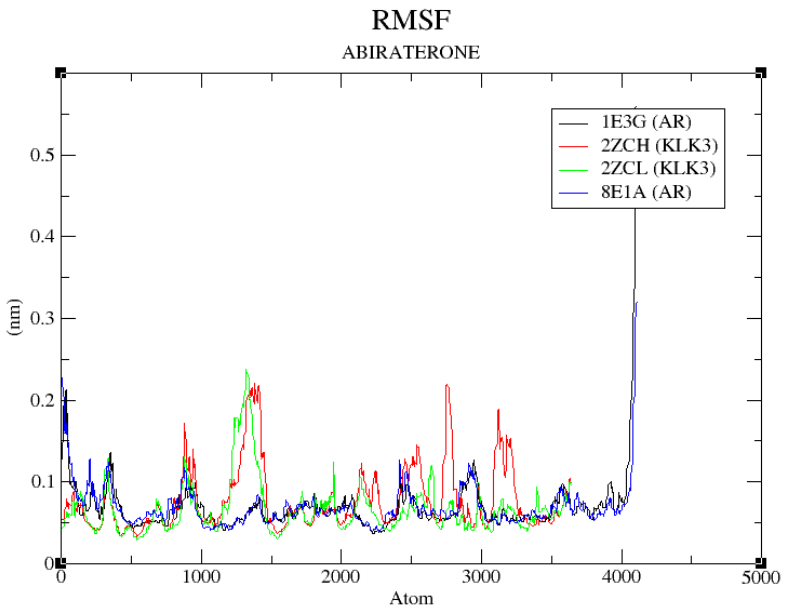

Figure 4.6. MD simulation, RMSF analysis results graph of Abiraterone drug bound to 1E3G (AR), 2ZCH (KLK3), 2ZCL (KLK3) and 8E1A (AR) receptors.

As a result, RMSF peaks are observed in similar regions for 1E3G and 8E1A receptors. These regions indicate that Abiraterone drug is more flexible or mobile in

these receptors. In addition, 2ZCL has the lowest RMSF values, indicating that this ligand exhibits the most stable binding and its conformational change is very small. The results based on RMSF graph are consistent with RMSD analyses.

The radius of gyration analyzes the stability of the protein-ligand structure and the compactness of the complex.

The similar Rg values of 2ZCH and 2ZCL with Abiraterone indicate that these structures have similar stability. The lower Rg values of these structures indicate that these complexes have a more compact structure with the drug. The similar Rg values of 1E3G and 8E1A with Abiraterone indicate that these structures have similar stability.

The radius of gyration, Rg values during molecular simulation are shown in Figure 4.7.

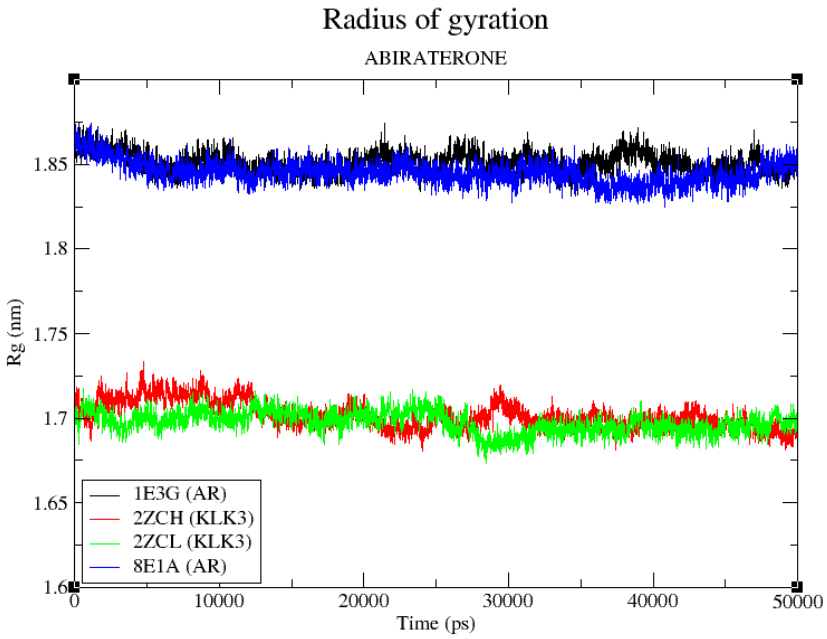

Figure 4.7. Graph of Rg analysis results bound to 1E3G, 2ZCH, 2ZCL and 8E1A receptors for Abiraterone drug in MD simulation.

As a result, according to these results, the Rg values of the protein-ligand complexes remained constant over time and did not create much fluctuations. The complexes with abiraterone drug reached the highest stability with 2ZCH and 2ZCL

receptors during the simulation process.

The SASA (Solvent Accessible Surface) method is used to calculate the surface area of a biomolecular structure that is accessible to a solvent (Erol, M., 2023).

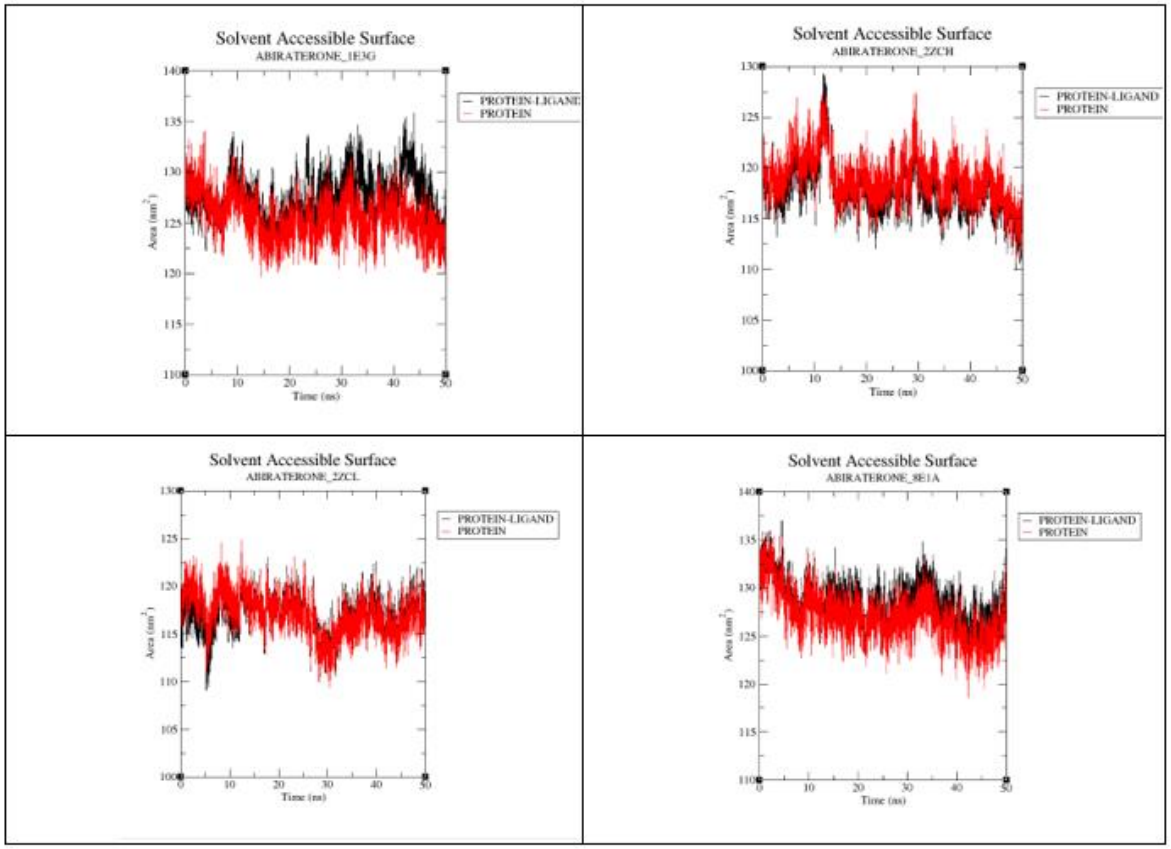

Figure 4.8. Results of SASA bound to 1E3G (AR), 2ZCH (KLK3), 2ZCL (KLK3) and 8E1A (AR) receptors with Abiraterone drug during MD simulation.

SASA values of four receptors (1E3G, 2ZCH, 2ZCL and 8E1A) structures were determined with the drug abiraterone. The SASA value due to the interaction of abiraterone with 1E3G and 8E1A is greater than the other receptors (2ZCH, 2ZCL).

The protein-ligand (nm\S2\N)- protein (nm\S2\N) value of 1E3G with abiraterone is 2. The protein-ligand (nm\S2\N)- protein (nm\S2\N) value of 2ZCH with abiraterone is -0.846. The protein-ligand (nm\S2\N)- protein (nm\S2\N) value of 2ZCL with abiraterone is -0.092. The protein-ligand (nm\S2\N)- protein (nm\S2\N) value of 8E1A with abiraterone is 1.262.

The results showed that with the Abiraterone drug, 2ZCH and 2ZCL had less

conformational change. These receptors had a better docking and interaction with the drug.

4.2.2. Molecular Dynamics Simulations of 1E3G, 8E1A, 2ZCH and 2ZCL Receptors with the Drug Olaparib

Firstly, the RMSD (Root Mean Square Deviation) value was plotted to obtain the conformational changes of the molecules from their initial positions to their final positions depending on the drug Olaparib and 1E3G, 8E1A, 2ZCH and 2ZCL receptors throughout the molecular dynamics simulation and to monitor the changes during this process and to see how it stabilizes. In addition, figure .. shows the root-mean-square deviation (RMSD) with respect to 1E3G, 8E1A, 2ZCH and 2ZCL receptors depending on the time during the molecular dynamics (MD) simulations.

During the simulation process, lower and less shown RMSD values indicate that they are more stable in the protein-ligand complexes they bind to, while higher RMSD values indicate that there are more structural changes in the protein-ligand complexes and that they are more mobile during the simulation process.

RMSD values for the 1E3G receptor showed a lot of mobility and fluctuations over time. This shows that Olaparib does not bind tightly to this protein and that its conformational changes are too much. RMSD values for the 2ZCH receptor remained constant between 0 and 0.5 nm and also remained stable between 10,000 and 50,000 ps. It exhibited a very stable structure throughout the simulation. RMSD values for the 2ZCL receptor remained constant between 0 and 0.25 nm and remained stable between 0 ps and 50,000 ps. It exhibited the most stable structure throughout the simulation. It remained stable at almost all time intervals. This suggests that Olaparib binds tightly to the 8E1A receptor. The results suggest that the 1E3G receptor underwent more conformational changes throughout the simulation and that its binding stability with Olaparib may be lower than other receptors.

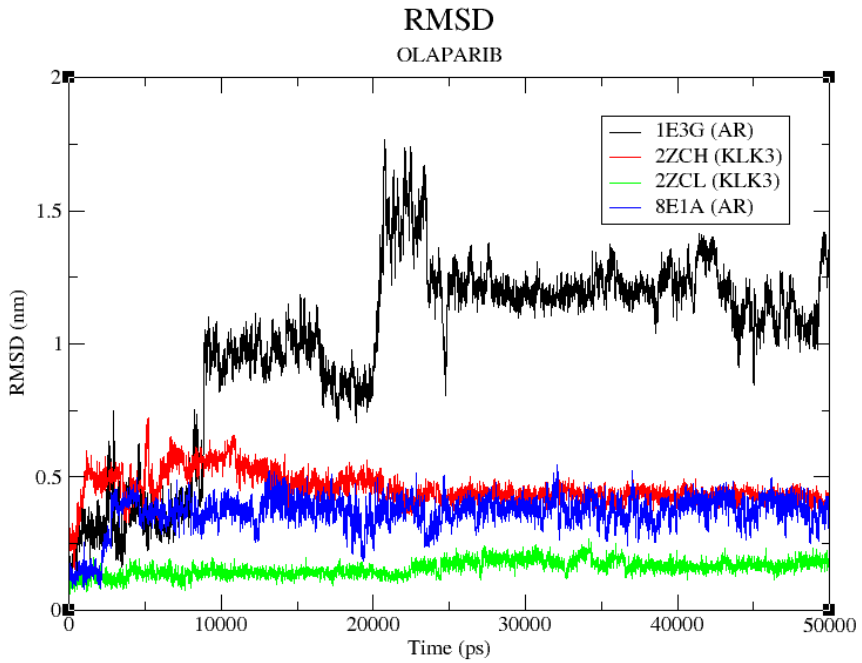

Figure 4.9. RMSD analysis results graph of 1E3G (AR), 8E1A (AR), 2ZCH (KLK3) and 2ZCL (KLK3) receptors bound to Olaparib drug in MD simulation.

As a result, Olaparib bound most stably and tightly to the 2ZCL, 2ZCH and 8E1A receptors. It showed the least stable binding to the 1E3G receptor.

The RMSF value measures how much each structure deviates and moves away from its reference position during the simulation. This value is used to determine the flexibility and dynamics of atoms in certain regions.

In addition, Figure 4.10. shows the atomic root-mean-square deviations (RMSF) of the drug Olaparib bound to the 1E3G, 2ZCH, 2ZCL and 8E1A receptors.

RMSF values are generally below 0.2 nm for 1E3G but increase towards 0.5 nm. The 1E3G receptor has high RMSF values, indicating that it is unstable and has high flexibility when binding to the receptor. RMSF values for 2ZCH generally fluctuate between 0.1-0.3 nm, while the 2ZCH receptor has lower RMSF values. This indicates that it is stable and does not exhibit high flexibility when binding to the receptor. RMSF values for 2ZCL generally fluctuate between 0.1-0.3 nm, while the 2ZCL receptor has lower RMSF values. This indicates that it is stable and does not

exhibit high flexibility when binding to the receptor. The 8E1A receptor has high RMSF values below 0.2 nm but increase towards 0.5 nm. The 8E1A receptor has high RMSF values, indicating that it is unstable and exhibits too much flexibility when binding to the receptor.

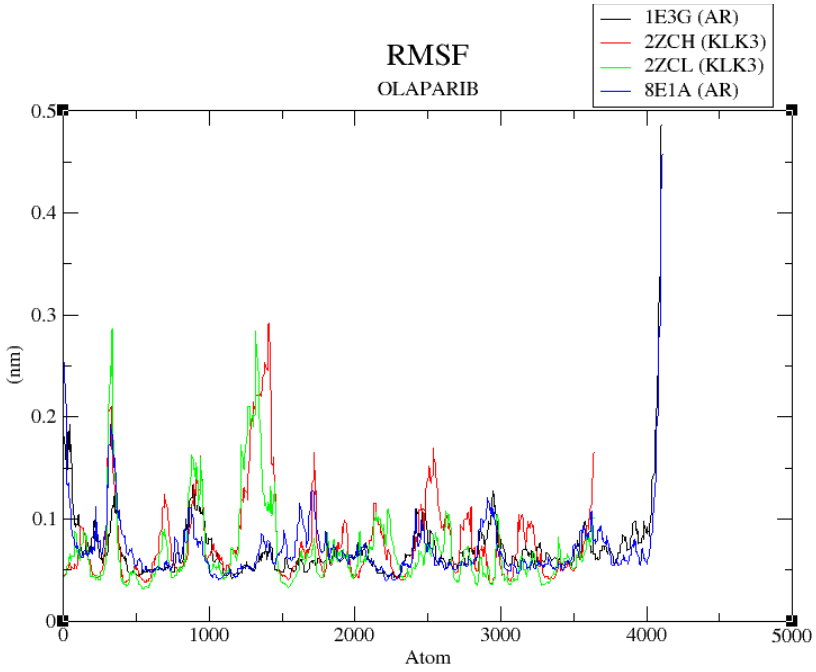

Figure 4.10. RMSF analysis results graph of Olaparib drug bound to 1E3G (AR), 2ZCH (KLK3), 2ZCL (KLK3) and 8E1A (AR) receptors in MD simulation.

As a result, RMSF peaks are observed in similar regions for 1E3G and 8E1A receptors. These regions indicate that Olaparib drug is more flexible or mobile in these receptors. In addition, 2ZCL has the lowest RMSF values, indicating that this ligand exhibits the most stable binding and its conformational change is minimal. The results based on the RMSF plot are consistent with the RMSD analyses.

The radius of gyration analyzes the stability of the protein-ligand structure and the compactness of the complex.

Similar Rg values of 2ZCH and 2ZCL with olaparib indicate that these structures have similar stability. The lower Rg values of these structures indicate that these complexes have a more compact structure with the drug. Similar Rg values of 1E3G and 8E1A with olaparib indicate that these structures have similar stability.

The radius of gyration, Rg values during molecular simulation are shown in Figure 4.11.

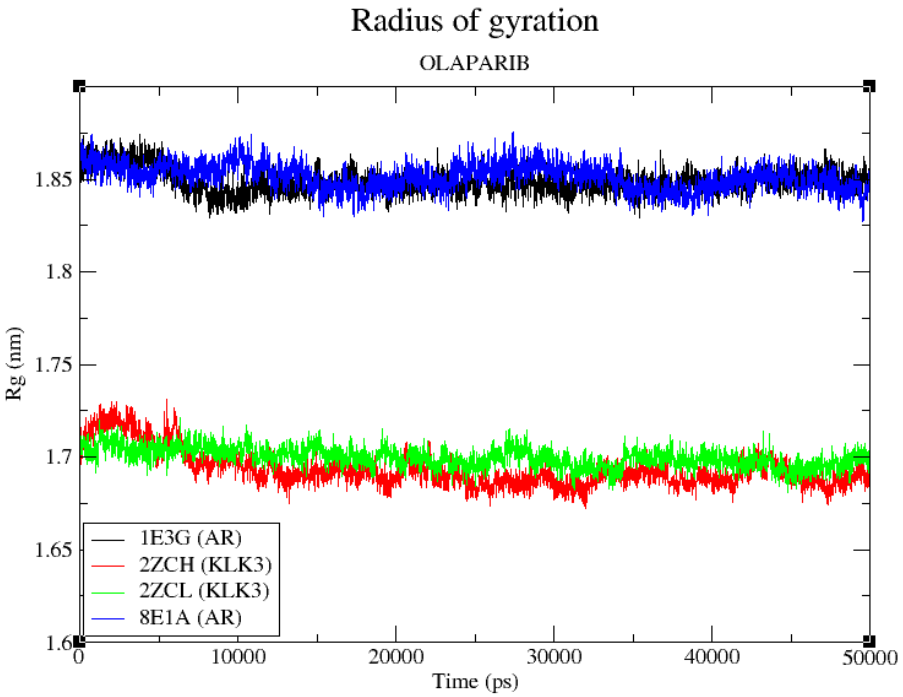

Figure 4.11. Graph of Rg analysis results for Olaparib drug bound to 1E3G, 2ZCH, 2ZCL and 8E1A receptors in MD simulation.

As a result, according to these results, the Rg values of the protein-ligand complexes remained constant over time and did not create much fluctuations. The

complexes with olaparib reached the highest stability with 2ZCH and 2ZCL receptors during the simulation process.

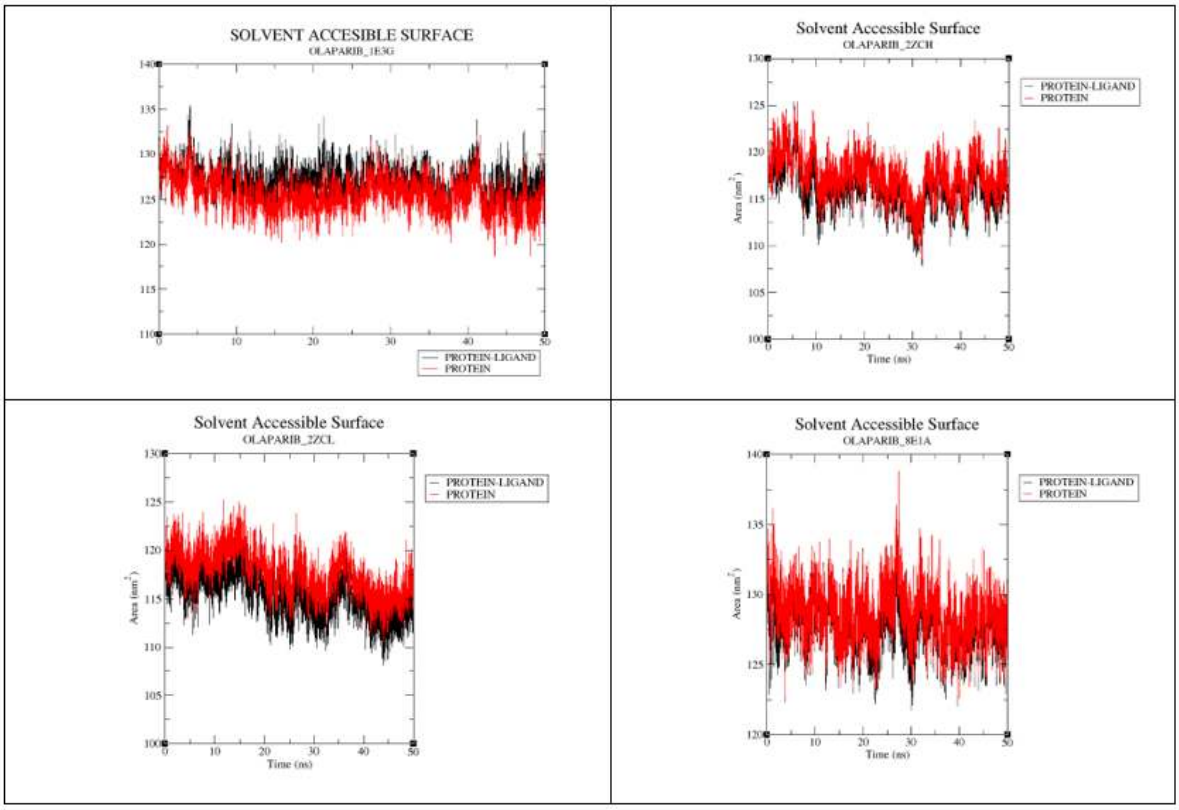

Figure 4.12. Results of SASA bound to 1E3G (AR), 2ZCH (KLK3), 2ZCL (KLK3) and 8E1A (AR) receptors with Olaparib drug during MD simulation.

The SASA (Solvent Accessible Surface) method is used to calculate the surface area of a biomolecular structure that is accessible to a solvent (Erol, M., 2023).

The SASA values of the four receptors (1E3G, 2ZCH, 2ZCL and 8E1A) structures were determined with the drug olaparib. The SASA value due to the interaction of olaparib with 1E3G and 8E1A is greater than the other receptors (2ZCH, 2ZCL).

The protein-ligand (nm\S2\N)- protein (nm\S2\N) value of 1E3G with olaparib is 1.477. The protein-ligand (nm\S2\N)- protein (nm\S2\N) value of 2ZCH with olaparib is -1.033. The protein-ligand (nm\S2\N)- protein (nm\S2\N) value of 2ZCL with olaparib is -2.435. The protein-ligand (nm\S2\N)- protein (nm\S2\N) value of 8E1A with olaparib is -0.763.

The results showed that with the drug Olaparib, 2ZCH and 2ZCL had less conformational changes. With the drug, these receptors had a better docking and

interaction.

4.2.3. Molecular Dynamics Simulations of 1E3G, 8E1A, 2ZCH and 2ZCL Receptors with the Drug Pylarify

First, the RMSD (Root Mean Square Deviation) value was plotted to obtain the conformational changes of the molecules from their initial positions to their final positions due to the Pylarify drug and the 1E3G, 8E1A, 2ZCH and 2ZCL) receptors during the molecular dynamics simulation and to monitor the changes during this process and to see how they stabilize. In addition, the figure.. shows the root-mean-square deviation (RMSD) over time during the molecular dynamics (MD) simulations according to the Pylarify drug and the 1E3G, 8E1A, 2ZCH and 2ZCL) receptors.

During the simulation process, lower and less shown RMSD values indicate that the protein-ligand complexes they bind are more stable, while higher RMSD values indicate that there are more structural changes in the protein-ligand complexes and that they are more mobile during the simulation process.

For the 1E3G receptor, the RMSD values remained constant between 0 and 0.25 nm and remained stable between 0 ps and 50,000 ps. It exhibited the most stable structure throughout the simulation. This shows that the Pylarify drug binds tightly to this receptor and does not have any conformational changes. For the 2ZCH receptor, the RMSD values remained constant between 0 and 0.75 nm and remained stable between 15,000 and 35,000 ps. It exhibited a stable structure throughout the simulation. The RMSD values for the 2ZCL receptor showed that it underwent more conformational changes throughout the simulation. For the 8E1A receptor, the RMSD values remained constant between 0 and 0.5 nm. Fluctuations between 10,000 and 20,000 ps are present. The results suggest that the 2ZCL receptor undergoes more conformational changes throughout the simulation and its binding stability with the Pylarify drug may be lower than other receptors.

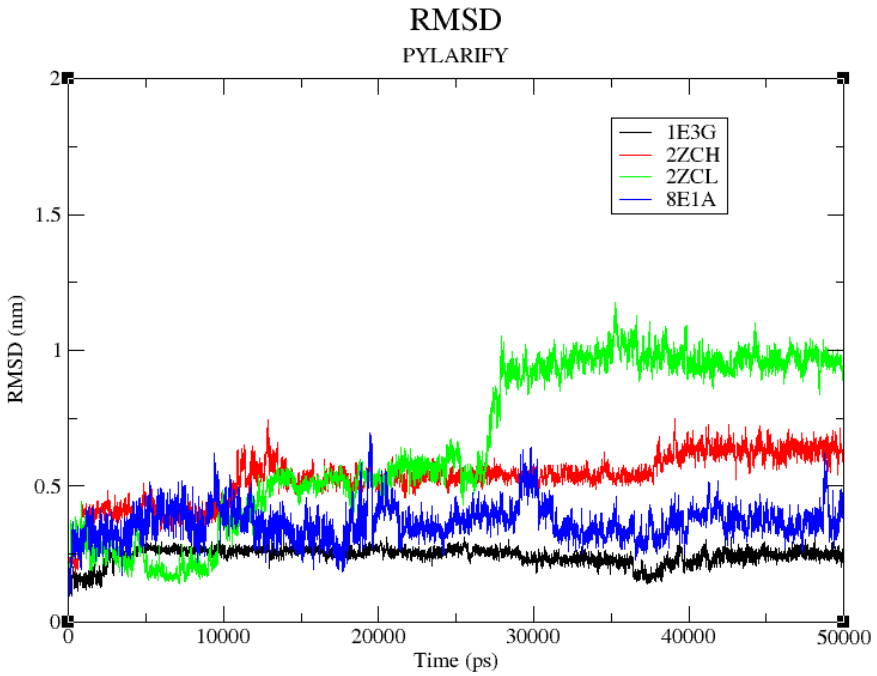

Figure 4.13. RMSD analysis results graph of 1E3G (AR), 8E1A (AR), 2ZCH (KLK3) and 2ZCL (KLK3) receptors bound to Pylarify drug in MD simulation.

As a result, Pylarify showed the most stable and tight binding to the 1E3G (AR) receptor. It showed the least stable binding to the 2ZCL receptor.

The RMSF value measures how much each structure deviates and moves away from its reference position during the simulation. This value is used to determine the flexibility and dynamics of the atoms in certain regions.

In addition, the figure shows the atomic root-mean-square deviations (RMSF) of the drug Pylarify bound to the 1E3G, 2ZCH, 2ZCL and 8E1A receptors.

RMSF values are generally below 0.2 nm for 1E3G and exceed 0.4 nm. The 1E3G receptor has high RMSF values, indicating that it is unstable and has high flexibility when binding to the receptor. RMSF values for 2ZCH generally fluctuate between 0.2-0.4 nm, while the 2ZCH receptor has lower RMSF values and is more stable. This indicates that it is stable and does not exhibit high flexibility when binding to the receptor. RMSF values for 2ZCL generally fluctuate between 0.1-0.2 nm, while the 2ZCL receptor has lower RMSF values. This indicates that it is stable and does not

exhibit high flexibility when binding to the receptor. The 8E1A receptor has high RMSF values below 0.2 nm but exceed 0.5 nm. The 8E1A receptor has high RMSF values, indicating that it is unstable and exhibits too much flexibility when binding to the receptor.

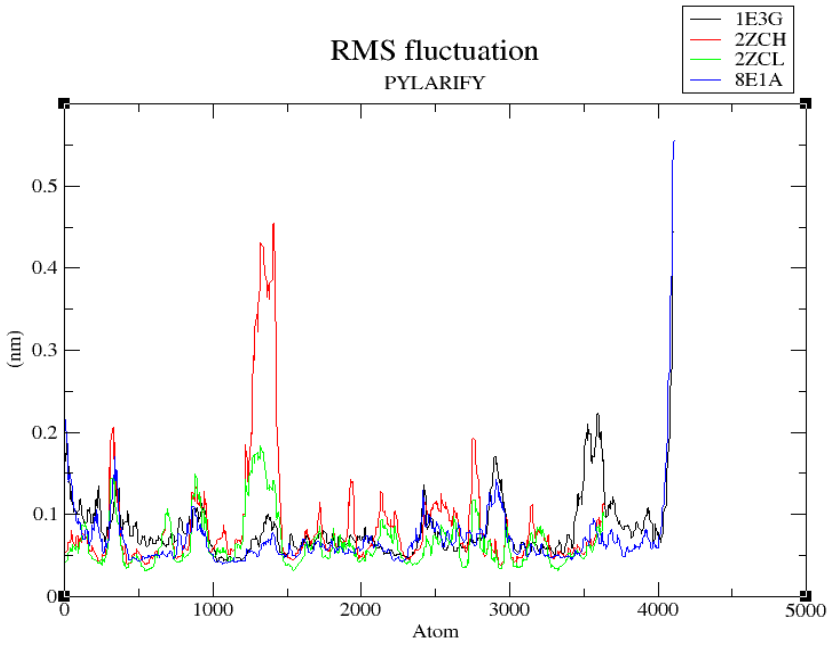

Figure 4.14. RMSF analysis results graph of Pylarify drug bound to 1E3G (AR), 2ZCH (KLK3), 2ZCL (KLK3) and 8E1A (AR) receptors in MD simulation.

As a result, RMSF peaks are observed in similar regions for 1E3G and 8E1A receptors. These regions indicate that Pylarify is more flexible or mobile in these receptors. In addition, RMSF values for 2ZCL generally fluctuate between 0.1-0.2 nm, but it has the lowest RMSF values, indicating that this ligand exhibits the most stable binding and its conformational change is minimal.

The radius of gyration analyzes the stability of the protein-ligand structure and the compactness of the complex.

The similar Rg values of 2ZCH and 2ZCL with Pylarify indicate that these structures have similar stability. The lower Rg values of these structures indicate that these complexes have a more compact structure with the drug. The similar Rg values of 1E3G and 8E1A with Pylarify indicate that these structures have similar stability.

The radius of gyration, Rg values during molecular simulation are shown in Figure 4.15.

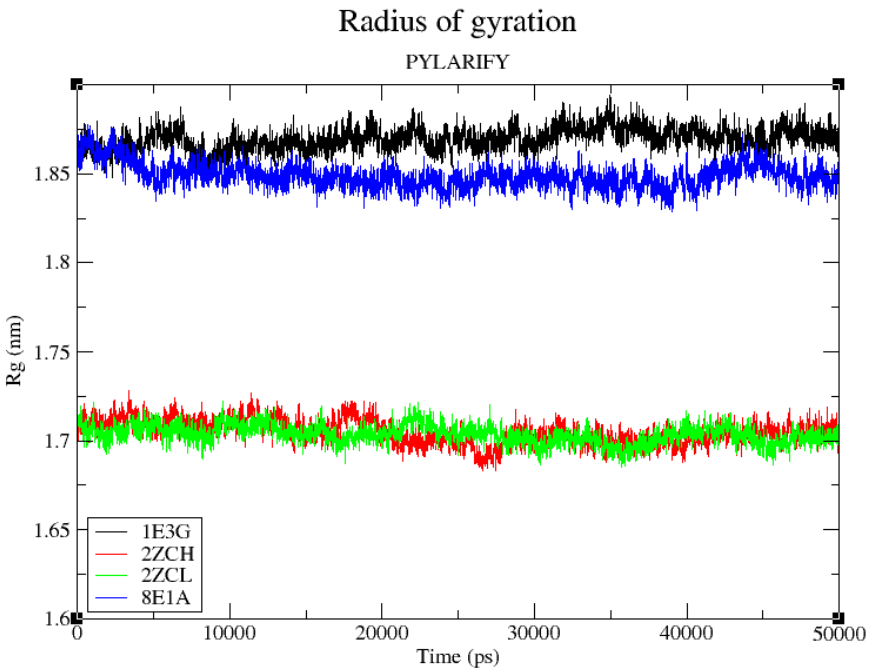

Figure 4.15. Plot of Rg analysis results bound to 1E3G, 2ZCH, 2ZCL and 8E1A receptors for the drug Pylarify in MD simulation.

As a result, according to these results, the Rg values of the protein-ligand complexes remained stable over time and did not create large fluctuations. The most stability during the simulation process of the complexes with the drug Pylarify was reached with the receptors 2ZCH and 2ZCL.

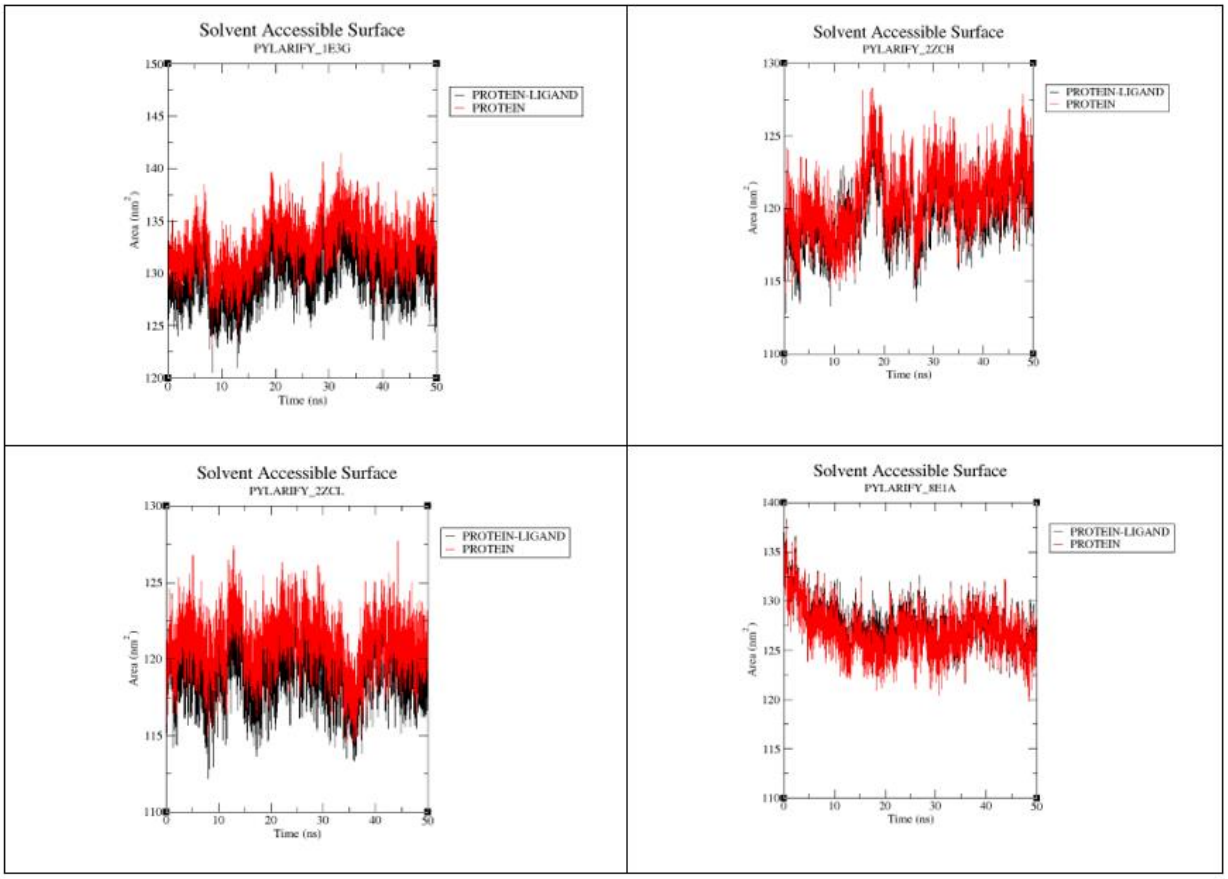

Figure 4.16. Results of SASA bound to 1E3G (AR), 2ZCH (KLK3), 2ZCL (KLK3) and 8E1A (AR) receptors with Pylarify drug during MD simulation.

The SASA (Solvent Accessible Surface) method is used to calculate the surface area of a biomolecular structure accessible by a solvent (Erol, M., 2023).

With Pylarify, the protein-ligand (nm\S2\N)-protein (nm\S2\N) value of 1E3G is -2.897. With Pylarify, the protein-ligand (nm\S2\N)-protein (nm\S2\N) value of 2ZCH is 0.785. With Pylarify, the protein-ligand (nm\S2\N)-protein (nm\S2\N) value of 2ZCL is -1.978. With Pylarify, the protein-ligand (nm\S2\N)-protein (nm\S2\N) value of 8E1A is 0.424.

The SASA values of the structures of four receptors (1E3G, 2ZCH, 2ZCL and 8E1A) were determined with the drug Pylarify. The SASA value due to the interaction of 1E3G and 8E1A with Pylarify is greater than the other receptors (2ZCH, 2ZCL).

The results showed that with Pylarify, 2ZCH and 2ZCL had less

conformational change. These receptors had better docking and interaction with the drug.

4.2.4. Molecular Dynamics Simulations of 1E3G, 2ZCH and 2ZCL Receptors with the Drug Rucaparib

First, the RMSD (Root Mean Square Deviation) value was plotted to obtain the conformational changes of the molecules from their initial positions to their final positions depending on the Rucaparib drug and the 1E3G, 2ZCH and 2ZCL receptors during the molecular dynamics simulation and to monitor the changes during this process and to see how they stabilize. In addition, the figure.. shows the root-mean-square deviation (RMSD) over time during the molecular dynamics (MD) simulations of 1E3G, 2ZCH and 2ZCL receptors depending on the Rucaparib drug.

In the simulation process, lower and less shown RMSD values indicate that the protein-ligand complexes they bind are more stable, while higher RMSD values indicate that there are more structural changes in the protein-ligand complexes and more mobility during the simulation process.

For 1E3G receptor, RMSD values were sufficiently stable between 35,000 and 50,000 ps, but RMSD values showed a lot of mobility over time. This indicates that Rucaparib drug is not tightly bound to the protein and its conformational changes are high. For 2ZCH receptor, RMSD values were sufficiently stable between 0 and 50,000 ps. It exhibited a very stable structure throughout the simulation. For 2ZCL receptor, RMSD values were stable between approximately 0 and 20,000 ps, but had a lot of fluctuations. The results suggested that 2ZCL receptor underwent more conformational changes during the simulation and its binding stability with Rucaparib drug may be lower than other receptors.

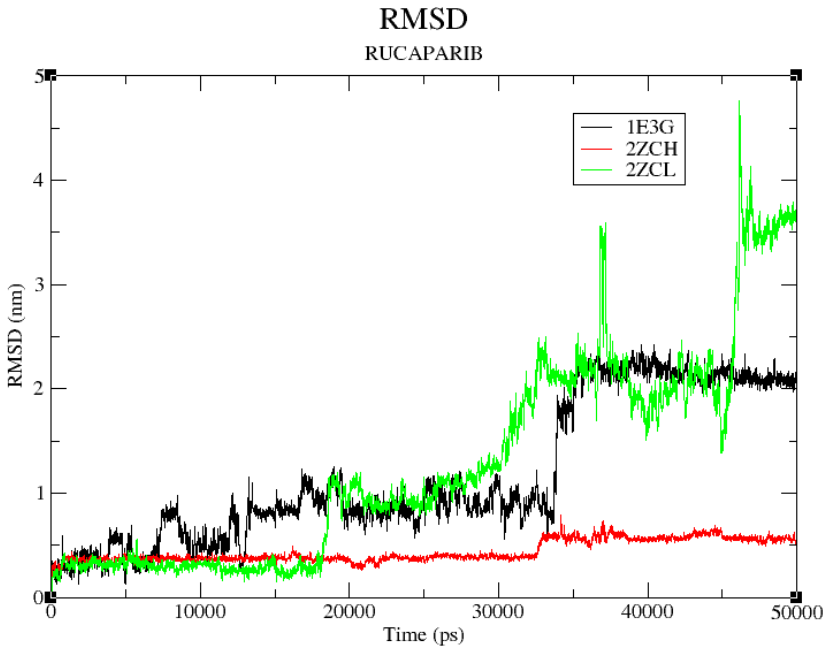

Figure 4.17. RMSD analysis results graph of 1E3G, 2ZCH and 2ZCL receptors bound to Rucaparib drug in MD simulation.

As a result, Rucaparib is the most stable and tightly bound to 2ZCH receptor. It showed moderately stable binding with 1E3G receptor, while 2ZCL receptor showed the least stable binding.

RMSF value measures how much each structure deviates and moves away from the reference position during the simulation. This value is used to determine the flexibility and dynamics of atoms in some regions.

In addition, Figure 4.18. shows the atomic root-mean-square deviations (RMSF) of the drug bound to 1E3G, 2ZCH and 2ZCL receptors of Rucaparib drug.

RMSF values are generally below 0.2 nm for 1E3G but do not exceed 0.3 nm. The 1E3G receptor has low RMSF values, indicating that it is stable and not very flexible when bound to the receptor. RMSF values for 2ZCH are generally between 0.1 and 0.2 nm, but there are small fluctuations. The 2ZCH receptor also has low RMSF values, indicating that it is stable and not very flexible when bound to the receptor. RMSF values for 2ZCL are generally between 0.1 and 0.2 nm. The 2ZCL receptor has higher RMSF values, indicating that it is unstable and not very flexible

when bound to the receptor.

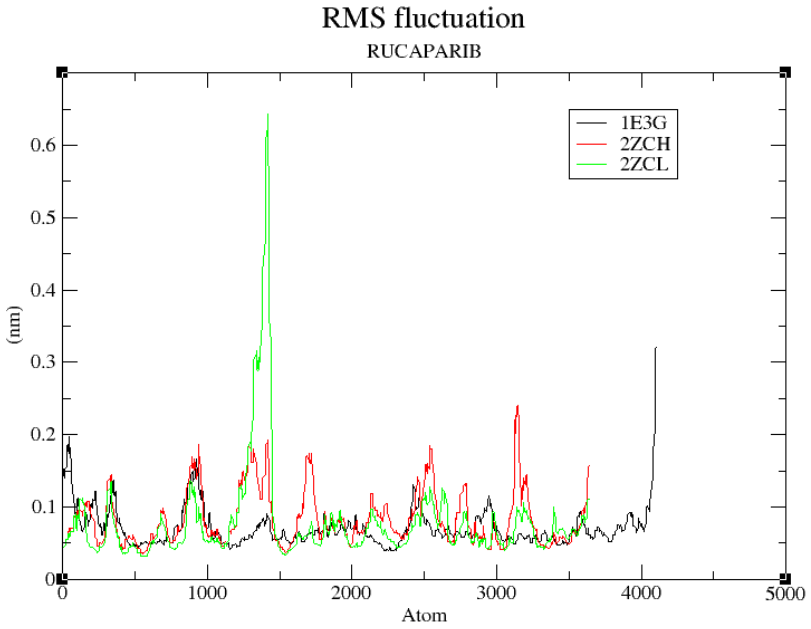

Figure 4.18. RMSF analysis results graph of Rucaparib drug bound to 1E3G, 2ZCH and 2ZCL receptors in MD simulation.

As a result, RMSF peaks are observed in some regions for 2ZCL receptor. These regions indicate that Rucaparib drug is more flexible or mobile in these receptors. In addition, 1E3G has the lowest RMSF values, indicating that this ligand shows the most stable binding and its conformational change is very little. The results based on RMSF graph are quite consistent with RMSD analysis.

The radius of gyration analyzes the stability of the protein-ligand structure and the compactness of the complex.

The similar Rg values of 2ZCH and 2ZCL with Rucaparib indicate that these structures have a similar stability. The lower Rg values of these structures indicate that these complexes have a more compact structure with the drug. The Rg value of 1E3G receptor with Rucaparib is different from other receptors.

The radius of gyration, Rg values during molecular simulation are shown in Figure 4.19.

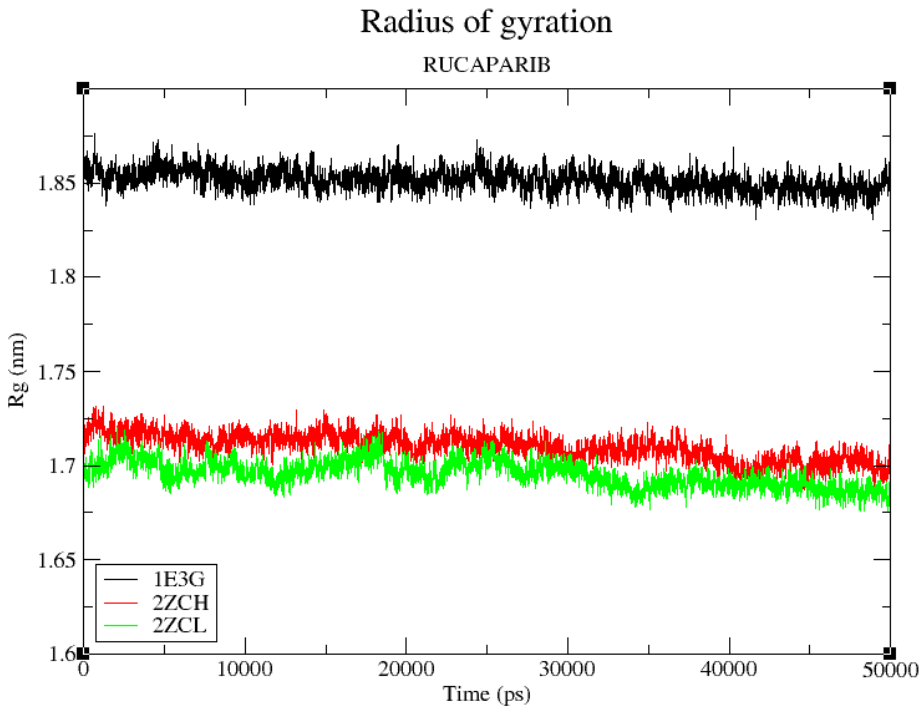

Figure 4.19. Rg analysis results graph for Rucaparib drug in MD simulation, bound to 1E3G, 2ZCH and 2ZCL receptors.

As a result, according to these results, Rg values of protein-ligand complexes remained constant over time and did not create much fluctuations. The most stability of complexes with Rucaparib drug during the simulation process was reached with 2ZCH and 2ZCL receptors.

SASA (Solvent Accessible Surface) method is used to calculate the surface area of a biomolecular structure accessible by a solvent (Erol, M., 2023).

SASA values of three receptor structures (1E3G, 2ZCH and 2ZCL) with Rucaparib drug were determined. SASA value originating from the interaction of Rucaparib with 1E3G receptor is greater than other receptors (2ZCH and 2ZCL).

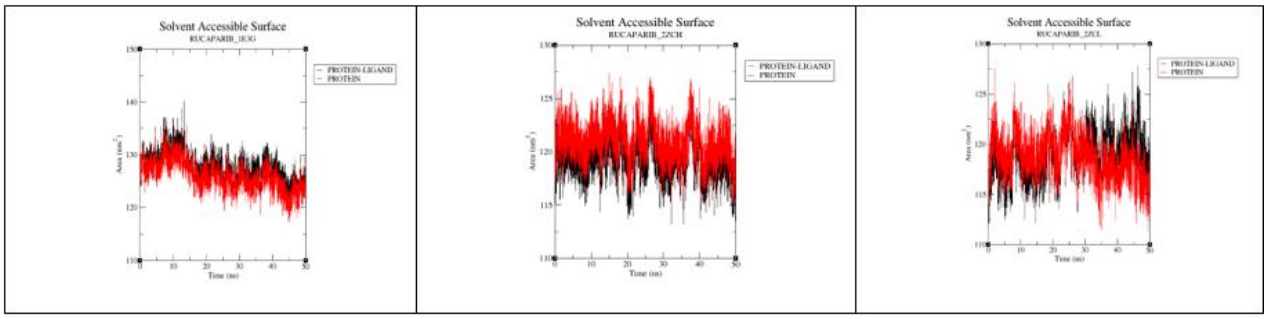

Figure 4.20. SASA results for 1E3G, 2ZCH and 2ZCL receptors with Rucaparib during MD simulation.

Protein-ligand (nm\S2\N)-protein (nm\S2\N) value of 1E3G with Rucaparib is 1.625. Protein-ligand (nm\S2\N)-protein (nm\S2\N) value of 2ZCH with Rucaparib is -1.568. Protein-ligand (nm\S2\N)-protein (nm\S2\N) value of 2ZCL with Rucaparib is 0.307.

The results showed that 2ZCH had less conformational change with Rucaparib. The drug had better docking and interaction with this receptor.

4.2.5 Molecular Dynamics Simulations of 1E3G, 2ZCH, and 2ZCL Receptors with the Locametz Drug

First, the RMSD (Root Mean Square Deviation) value was plotted to obtain the conformational changes of the molecules from their initial positions to their final positions depending on the Rucaparib drug and the 1E3G, 2ZCH and 2ZCL receptors during the molecular dynamics simulation and to monitor the changes during this process and to see how they stabilize. In addition, the figure.. shows the root-mean-square deviation (RMSD) over time during the molecular dynamics (MD) simulations of the Locametz drug-bound 1E3G, 2ZCH and 2ZCL receptors.

In the simulation process, lower and less shown RMSD values indicate that the protein-ligand complexes they bind are more stable, while higher RMSD values indicate that there are more structural changes in the protein-ligand complexes and that they are more mobile during the simulation process.

Although the RMSD values for the 1E3G receptor remained stable from time to time, the RMSD values showed a lot of mobility. This shows that the Locametz drug

does not bind tightly to the protein and that its conformational changes are high. Although the RMSD values for the 2ZCH receptor remained stable from time to time, the RMSD values showed a lot of mobility. The results suggested that the 2ZCH receptor underwent more conformational changes throughout the simulation and that the binding stability with the Locametz drug may be lower than other receptors. The RMSD values for the 2ZCL receptor remained sufficiently stable between 0 and 50,000 ps. It exhibited a very stable structure throughout the simulation.

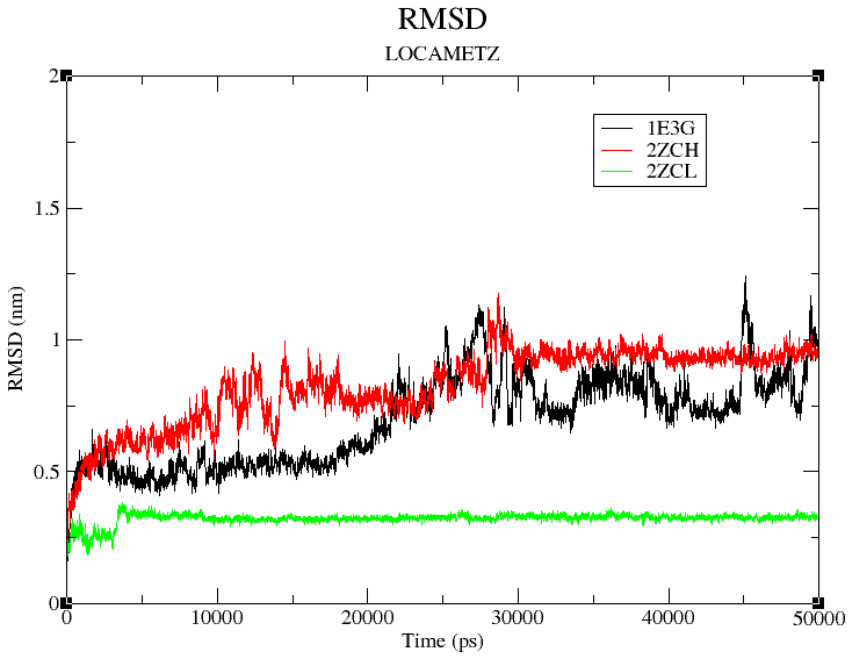

Figure 4.21. RMSD analysis results graph of 1E3G, 2ZCH and 2ZCL receptors bound to Locametz drug in MD simulation.

As a result, Locametz is the most stable and tightly bound to 2ZCL receptor. While 1E3G receptor showed moderately stable binding, 2ZCL receptor showed the least stable binding.

RMSF value measures how much each structure deviates and moves away from the reference position during the simulation. This value is used to determine the flexibility and dynamics of atoms in some regions.

In addition, Figure 4.21. shows the atomic root-mean-square deviations (RMSF) of the drug bound to 1E3G, 2ZCH and 2ZCL receptors of Locametz drug.

RMSF values are generally below 0.2 nm for 1E3G but do not exceed 0.3 nm. The 1E3G receptor has low RMSF values overall, although it does show occasional peaks, indicating that it is stable and does not exhibit much flexibility when bound to the receptor. RMSF values for 2ZCH are generally between 0.1 and 0.2 nm, but there are small fluctuations. The 2ZCH receptor also has low RMSF values, indicating that it is stable and does not exhibit much flexibility when bound to the receptor. RMSF values for 2ZCL are generally between 0.1 and 0.2 nm. The 2ZCL receptor is also stable and does not exhibit much flexibility when bound to the receptor.

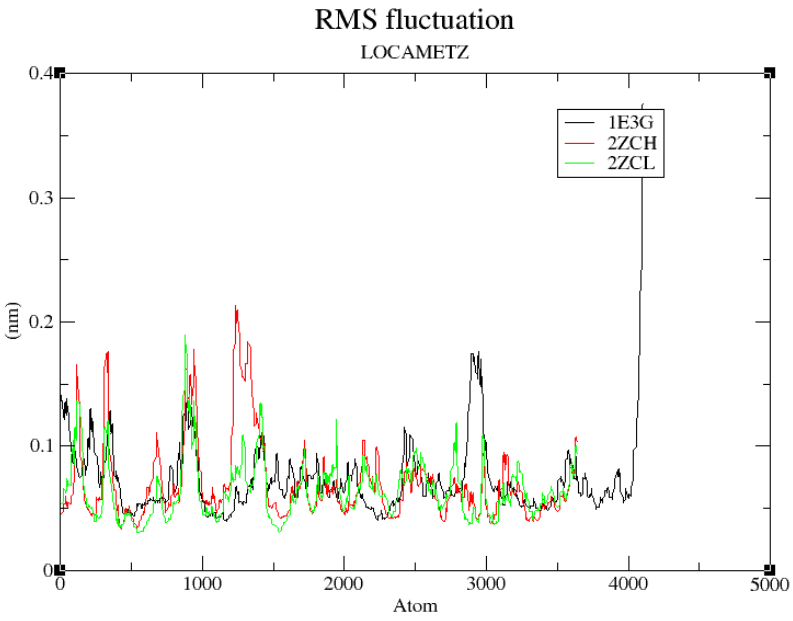

Figure 4.22. RMSF analysis results of Locametz drug bound to 1E3G, 2ZCH and 2ZCL receptors in MD simulation.

As a result, although RMSF peaks are observed in some regions for 1E3G, 2ZCH and 2ZCL receptors, it shows that Locametz drug binds more tightly to these receptors in general. In addition, 2ZCL has the lowest RMSF values, indicating that this ligand shows the most stable binding and its conformational change is very little. The results based on RMSF plot are quite consistent with RMSD analysis.

The radius of gyration analyzes the stability of the protein-ligand structure and the compactness of the complex.

The similar Rg values of Locametz with 2ZCH and 2ZCL indicate that these structures have similar stability. The lower Rg values of these structures indicate that these complexes have a more compact structure with the drug. The Rg value of the 1E3G receptor with Locametz is different from other receptors.

The radius of gyration and Rg values during molecular simulation are shown in Figure 4.23.

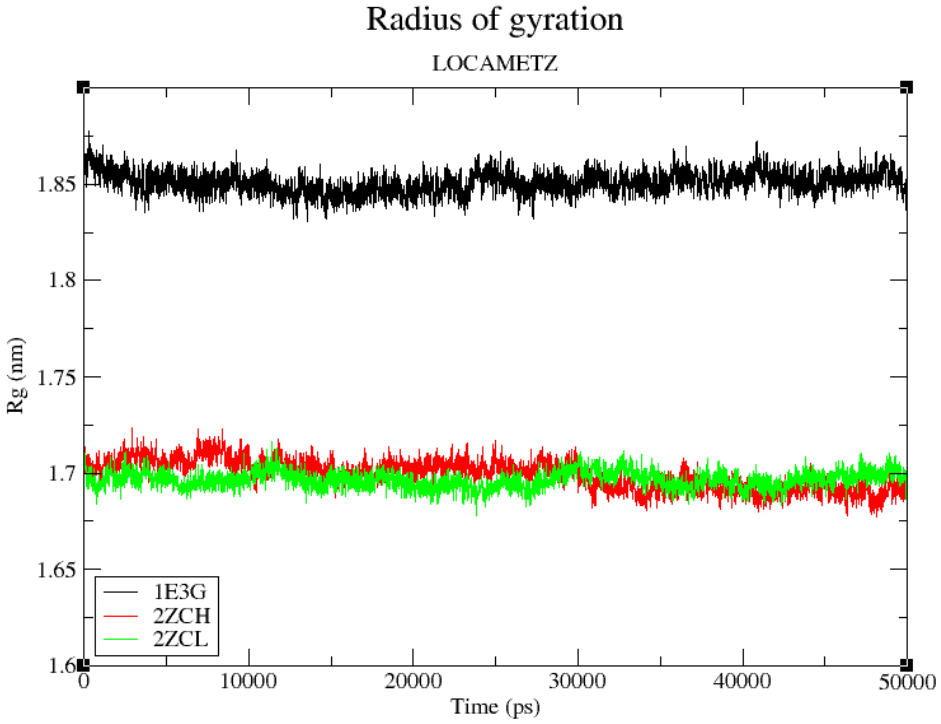

Figure 4.23. Rg analysis results graph for Locametz drug bound to 1E3G, 2ZCH and 2ZCL receptors in MD simulation.

As a result, according to these results, Rg values of protein-ligand complexes remained constant over time and did not create much fluctuations. The most stability of the complexes with Locametz drug was reached with 2ZCH and 2ZCL receptors throughout the simulation process.

The SASA (Solvent Accessible Surface) method is used to calculate the surface area of a biomolecular structure accessible by a solvent (Erol, M., 2023).

SASA values of three receptor structures (1E3G, 2ZCH and 2ZCL) with Locametz drug were determined. The SASA value due to the interaction of Locametz and 1E3G receptor is greater than the other receptors (2ZCH and 2ZCL

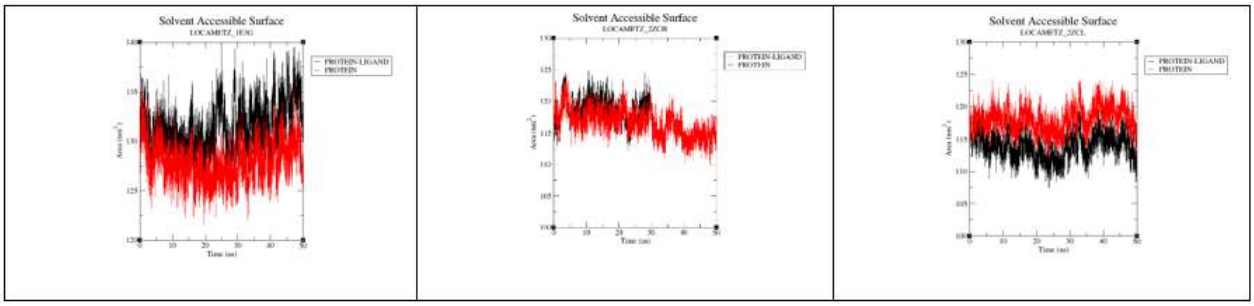

Figure 4.24. SASA results for 1E3G, 2ZCH and 2ZCL receptors with Locametz drug during MD simulation.

Protein-ligand (nm\S2\N)-protein (nm\S2\N) value of 1E3G with Locametz is 3.619.

Protein-ligand (nm\S2\N)-protein (nm\S2\N) value of 2ZCL with Locametz is -4.316.

The results showed that 2ZCL with Locametz drug had less conformational change. The drug had better docking and interaction with this receptor.

4.3. ADMET Data Results with Abiraterone, Olaparib, Pylarify, Rucaparib and Locametz Drugs

ADMET (Absorption, Distribution, Metabolism, Elimination, Toxicity) method is a method used in drug design. This method was used to evaluate the pharmacokinetic properties of drug or ligand candidates and to determine their toxicity properties. It was done through ADMETLab 2.0 web server.

Abbreviations and meanings of Physicochemical Properties are as follows (Xiong, G., et al., 2021).

DEFINITION	EXPLANATION
Flexibility	nRot / nRig
LogS	Water solubility value (Low solubility is a harmful feature and its average values should be between -4 and 0.5 log mol/L)
logP	N-octanol/water partition coefficient (indicates hydrophobic binding property and average values should be between 0-3 log mol/L)
logD	N-octanol/water distribution coefficients at physiological pH (logD7.4) (indicates balance between lipophilicity/ hydrophilicity features and average values should be between 1-3 log mol/L)
Caco-2 Permeability	Cell permeability of human colon adenocarcinoma cell lines (Caco-2) (indicates in vivo drug permeation features and average values should be greater than > -5.15log cm/s)
HIA	Human intestinal absorption (indicates absorption of drug in human intestine features and values are 0-0.3: excellent (green); 0.3-0.7: medium (yellow); 0.7-1.0(++): poor (red)
F20%	The human oral bioavailability 20% (indicates oral bioavailability and values are 0-0.3: excellent (green); 0.3-0.7: medium (yellow); 0.7-1.0(++): poor

	(red)
PPB	Plasma protein binding (indicates binding of drug to proteins in plasma and values are ≤ 90%: excellent (green); otherwise: poor (red)
VD	Volume Distribution (indicates concept regarding the administered dose and the initial concentration in circulation and values are 0.04-20: excellent (green); otherwise: poor (red)

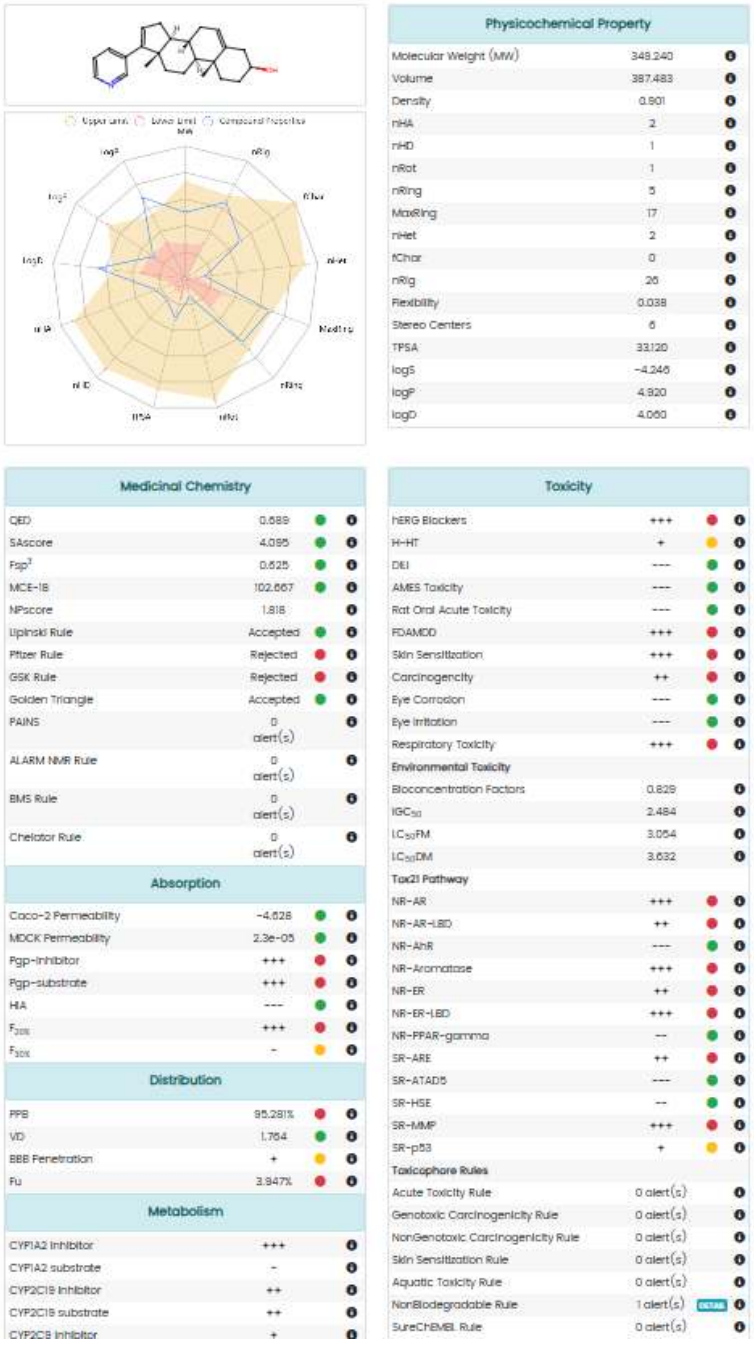

Physicochemical Property	
Molecular Weight (MW)	349.240
Volume	387.483
Density	0.901
nHA	2
nHD	1
nRot	1
nRing	5
MaxRing	17
nHet	2
fChar	0
nRig	26
Flexibility	0.038
Stereo Centers	6
TPSA	33.120
logS	-4.246
logP	4.920
logD	4.060

Medicinal Chemistry	
QED	0.689
SAscore	4.095
Fsp^3	0.625
MCE-18	102.667
NPscore	1.818
Lipinski Rule	Accepted
Pfizer Rule	Rejected
GSK Rule	Rejected
Golden Triangle	Accepted
PAINS	0 alert(s)
ALARM NMR Rule	0 alert(s)
BMS Rule	0 alert(s)
Chelator Rule	0 alert(s)

Absorption	
Caco-2 Permeability	-4.628
MDCK Permeability	2.3e-05
Pgp-inhibitor	+++
Pgp-substrate	+++
HIA	---
$F_{20\%}$	+++
$F_{30\%}$	-

Distribution	
PPB	95.281%
VD	1.764
BBB Penetration	+
Fu	3.947%

Metabolism	
CYP1A2 Inhibitor	+++
CYP1A2 substrate	-
CYP2C19 Inhibitor	++
CYP2C19 substrate	++
CYP2C9 Inhibitor	+

Toxicity	
hERG Blockers	+++
H-HT	+
DILI	---
AMES Toxicity	---
Rat Oral Acute Toxicity	---
FDAMDD	+++
Skin Sensitization	+++
Carcinogencity	++
Eye Corrosion	---
Eye Irritation	---
Respiratory Toxicity	+++
Environmental Toxicity	
Bioconcentration Factors	0.829
IGC_{50}	2.484
$LC_{50}FM$	3.054
$LC_{50}DM$	3.632
Tox21 Pathway	
NR-AR	+++
NR-AR-LBD	++
NR-AhR	---
NR-Aromatase	+++
NR-ER	++
NR-ER-LBD	+++
NR-PPAR-gamma	--
SR-ARE	++
SR-ATAD5	---
SR-HSE	--
SR-MMP	+++
SR-p53	+
Toxicophore Rules	
Acute Toxicity Rule	0 alert(s)
Genotoxic Carcinogenicity Rule	0 alert(s)
NonGenotoxic Carcinogenicity Rule	0 alert(s)
Skin Sensitization Rule	0 alert(s)
Aquatic Toxicity Rule	0 alert(s)
NonBiodegradable Rule	1 alert(s) DETAIL
SureChEMBL Rule	0 alert(s)

Figure 4.25. ADMETLab2.0 results for potential drug candidacy of Abiraterone with the 2ZCH receptor.

Flexibility value is 0.0038. The LogS value of Abiraterone is -4.246 and is high and its water solubility is considered good. The logP value of Abiraterone is 4.920 and is close to the appropriate value. The logD value of Abiraterone is 4.060. The Caco-2 Permeability value of Abiraterone is -4.628 and is a very high value. The drug is suitable for cell permeability. The HIA value of Abiraterone is green (0-0.3: excellent).

It shows that the absorption of this drug in the intestine is good. The F20% value of Abiraterone is red 0.7-1.0(++): poor (red). It shows that the human oral bioavailability of this drug is low. The Plasma protein binding value of Abiraterone is low. The VD value of Abiraterone is 1.764 (green).

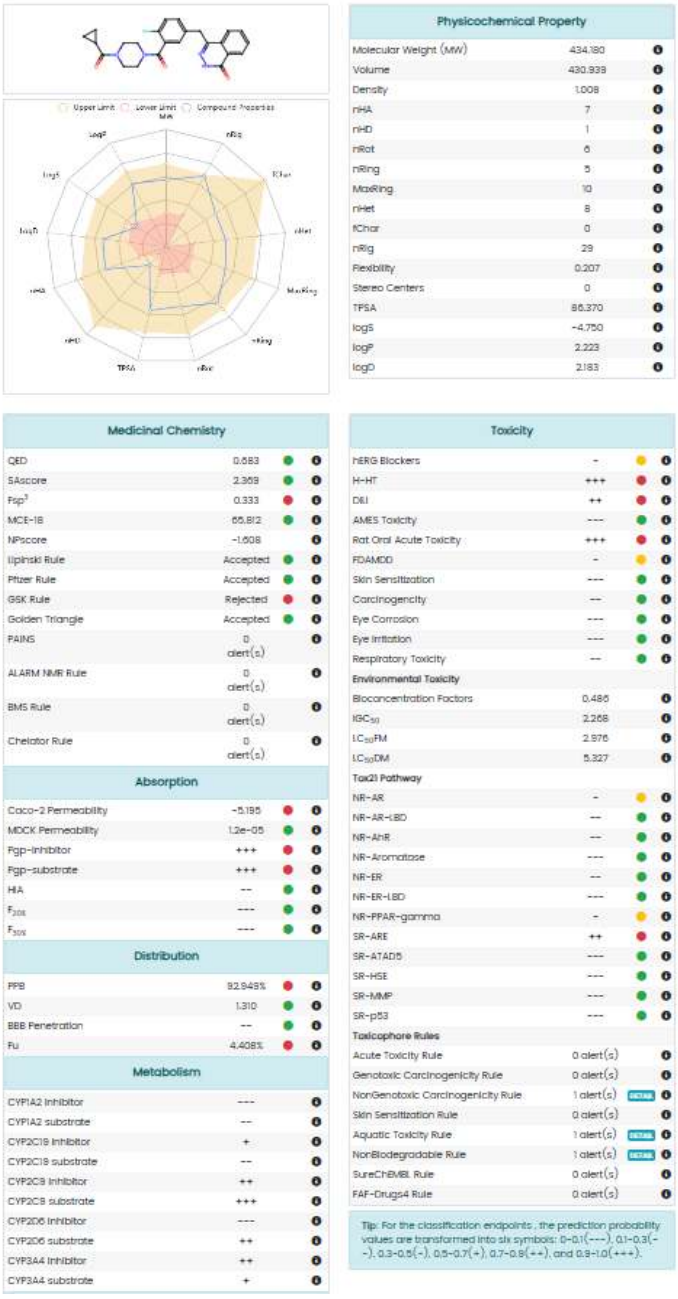

Figure 4.26. ADMETLab2.0 results for potential drug candidacy of Olaparib with the 8E1A receptor.

Flexibility value is 0.207. The LogS value of the drug olaparib is -4.750 and is high and its water solubility is accepted as good. The logP value of the drug olaparib is 2.223 and is at an appropriate value. The hydrophobic binding property of the drug olaparib is good. The logD value of the drug olaparib is 2.183. This value shows that the lipophilicity/hydrophilicity balance of the drug is good. The Caco-2 Permeability value of the drug olaparib is -5.195 and is close to the average value. The drug can be

considered suitable for cell permeability. The HIA value of the drug olaparib is green (0-0.3: excellent). This shows that the absorption of the drug in the intestine is good. The F20% value of the drug olaparib is green 0-0.3: excellent (green). This shows that the human oral bioavailability of the drug is good. The Plasma protein binding value of the drug olaparib is low. The VD value of the drug olaparib is 1.310 (green).

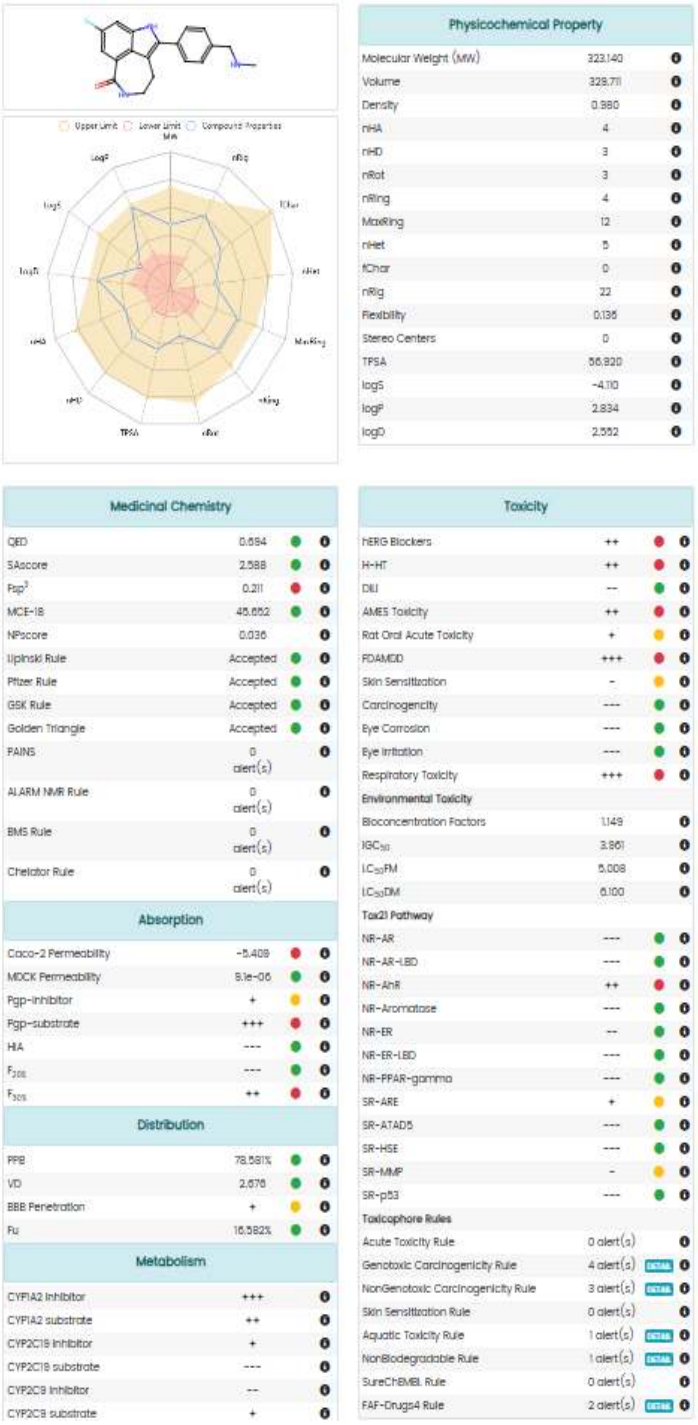

Figure 4.27. ADMETLab2.0 results for potential drug candidacy of Rucaparib with 1E3G receptor.

Flexibility value is 0.136. The LogS value of rucaparib is -4.110 and is high and its water solubility is considered good. The logP value of rucaparib is 2.834 and is at an appropriate value. The hydrophobic binding property of rucaparib is good. The logD value of rucaparib is 2.552. This value shows that the lipophilicity/hydrophilicity balance of the drug is good. The Caco-2 Permeability value of rucaparib is -5.409 and

is close to the average value. The drug can be considered suitable for cell permeability. The HIA value of rucaparib is green (0-0.3: excellent). This shows that the absorption of the drug in the intestine is good. The F20% value of rucaparib is green 0-0.3: excellent (green). This shows that the human oral bioavailability of this drug is good. Plasma protein binding value of Rucaparib drug is 78.581%, which shows that the drug binds well to proteins in plasma. VD value of Rucaparib drug is 2.676 (green).

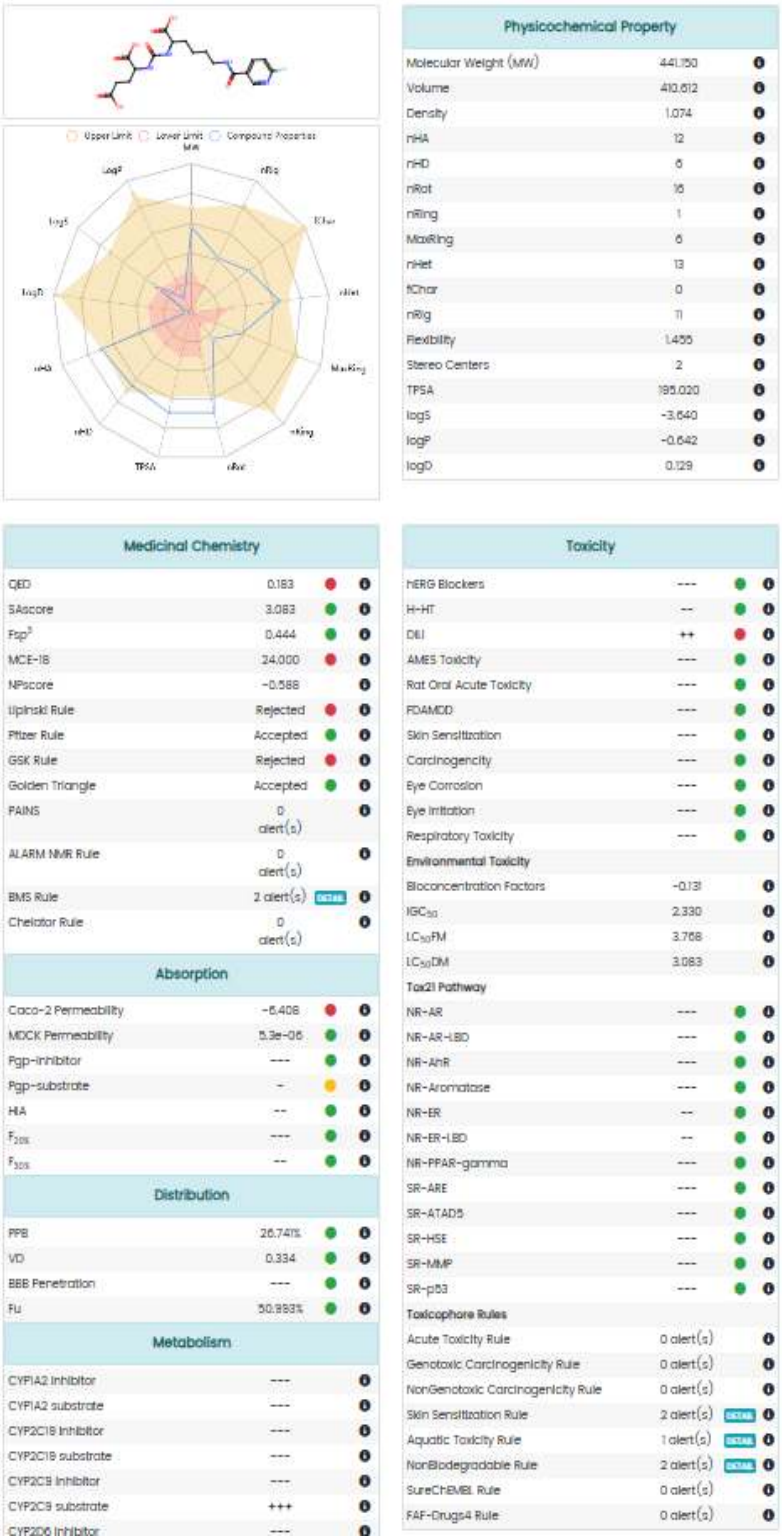

Figure 4.28. ADMETLab2.0 results for potential drug candidacy of Pylarify with the 2ZCL receptor.

Flexibility value is 1.455. The LogS value of Pylarify is -3.640 and is considered high and its water solubility is good. The logP value of Pylarify is -0.642 and is at an appropriate value. The hydrophobic binding property of Pylarify can be

considered appropriate. The logD value of Pylarify is 0.129. This value shows that the lipophilicity/hydrophilicity balance of the drug is good. The Caco-2 Permeability value of Pylarify is -6.408 and is close to the average value. The drug can be considered appropriate for cell permeability. The HIA value of Pylarify is green (0-0.3: excellent). This shows that the drug has good absorption in the intestine. The F20% value of Pylarify is green 0-0.3: excellent (green). This shows that the drug has good human oral bioavailability. The plasma protein binding value of Pylarify is 26.741%, which indicates that the drug binds very well to proteins in plasma. The VD value of Pylarify is 0.334 (green).

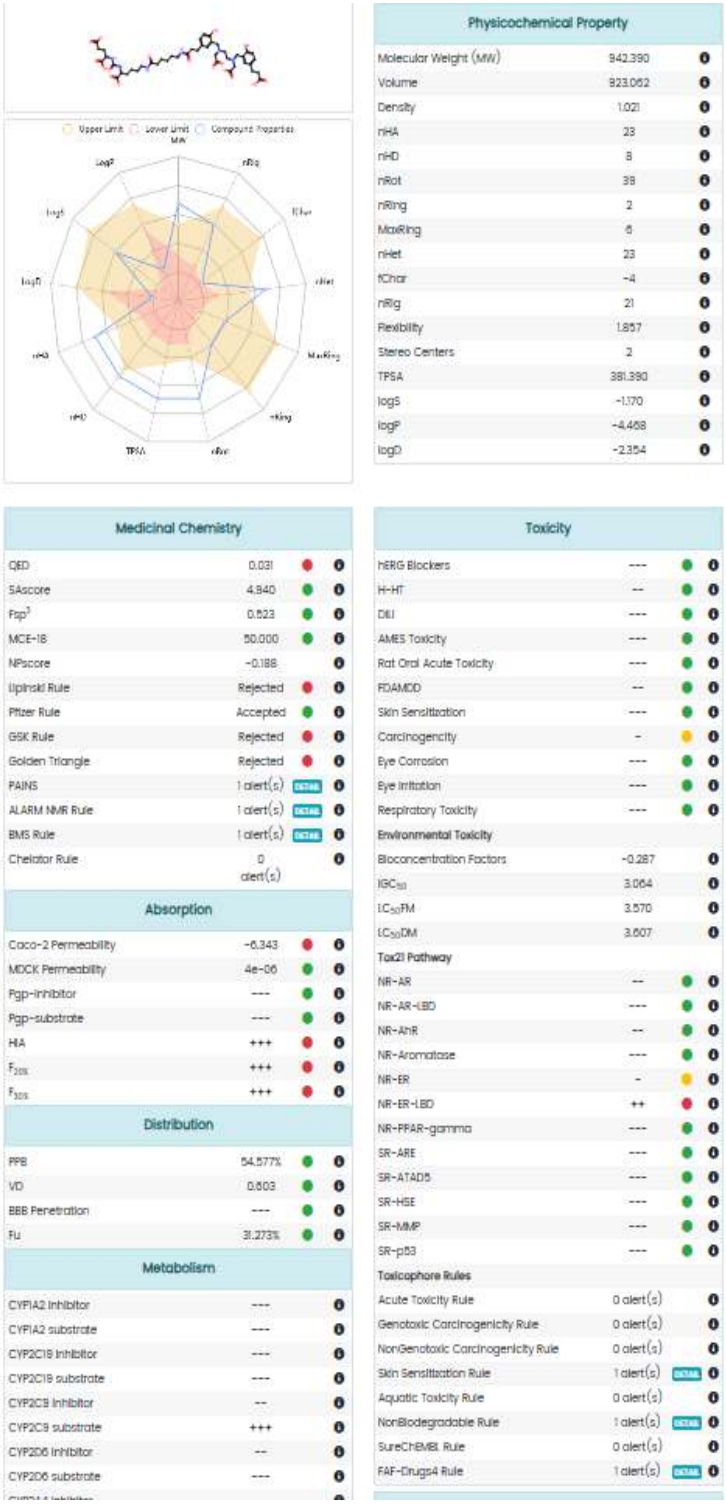

Physicochemical Property	
Molecular Weight (MW)	942.390
Volume	923.062
Density	1.021
nHA	23
nHD	8
nRot	38
nRing	2
MaxRing	6
nHet	23
fChar	-4
nRig	21
Flexibility	1.857
Stereo Centers	2
TPSA	381.390
logS	-1.170
logP	-4.468
logD	-2.354

Medicinal Chemistry		
QED	0.031	
SAscore	4.940	
Fsp3	0.523	
MCE-18	50.000	
NPscore	-0.188	
Lipinski Rule	Rejected	
Pfizer Rule	Accepted	
GSK Rule	Rejected	
Golden Triangle	Rejected	
PAINS	1 alert(s)	DETAIL
ALARM NMR Rule	1 alert(s)	DETAIL
BMS Rule	1 alert(s)	DETAIL
Chelator Rule	0 alert(s)	
Absorption		
Caco-2 Permeability	-6.343	
MDCK Permeability	4e-06	
Pgp-inhibitor	---	
Pgp-substrate	---	
HIA	+++	
$F_{20\%}$	+++	
$F_{30\%}$	+++	
Distribution		
PPB	54.577%	
VD	0.603	
BBB Penetration	---	
Fu	31.273%	
Metabolism		
CYP1A2 Inhibitor	---	
CYP1A2 substrate	---	
CYP2C19 Inhibitor	---	
CYP2C19 substrate	---	
CYP2C9 Inhibitor	--	
CYP2C9 substrate	+++	
CYP2D6 Inhibitor	--	
CYP2D6 substrate	---	

Toxicity		
hERG Blockers	---	
H-HT	--	
DILI	---	
AMES Toxicity	---	
Rat Oral Acute Toxicity	---	
FDAMDD	--	
Skin Sensitization	---	
Carcinogenicity	-	
Eye Corrosion	---	
Eye Irritation	---	
Respiratory Toxicity	---	
Environmental Toxicity		
Bioconcentration Factors	-0.287	
IGC_{50}	3.064	
$LC_{50}FM$	3.570	
$LC_{50}DM$	3.607	
Tox21 Pathway		
NR-AR	--	
NR-AR-LBD	---	
NR-AhR	--	
NR-Aromatase	---	
NR-ER	-	
NR-ER-LBD	++	
NR-PPAR-gamma	---	
SR-ARE	---	
SR-ATAD5	---	
SR-HSE	---	
SR-MMP	---	
SR-p53	---	
Toxicophore Rules		
Acute Toxicity Rule	0 alert(s)	
Genotoxic Carcinogenicity Rule	0 alert(s)	
NonGenotoxic Carcinogenicity Rule	0 alert(s)	
Skin Sensitization Rule	1 alert(s)	DETAIL
Aquatic Toxicity Rule	0 alert(s)	
NonBiodegradable Rule	1 alert(s)	DETAIL
SureCHEMBL Rule	0 alert(s)	
FAF-Drugs4 Rule	1 alert(s)	DETAIL

Figure 4.29. ADMETLab2.0 results for Locametz's potential drug candidacy with the 8E1A receptor.

Flexibility value is 1.857. The LogS value of the Locametz drug is -1.170 and is high and its water solubility was accepted as very good. The logP value of the Locametz drug is -4.468 and is an appropriate value. The hydrophobic binding

property of the Locametz drug can be considered appropriate. The logD value of the Locametz drug is -2.354. This value shows that the lipophilicity/hydrophilicity balance of the drug is poor. The Caco-2 Permeability value of the Locametz drug is -6.343 and is close to the average value. The drug can be considered appropriate for cell permeability. The HIA value of the Locametz drug is red. It shows that the absorption of this drug in the intestines is not good. The F20% value of the Locametz drug is red. 0.7-1.0(++): poor (red). It shows that the human oral bioavailability of this drug is not good. The Plasma protein binding value of the Locametz drug is 54.577% and shows that the binding of the drug to proteins in plasma is very good. The VD value of the drug Locametz is 0.603 (green).

CHAPTER V. CONCLUSION AND RECOMMENDATIONS

In this master's thesis, Molecular Docking, Molecular Dynamics Simulations (MDS) and ADMET studies were extensively conducted to model drugs or ligands with target proteins associated with prostate cancer at an atomistic level, especially by investigating the potential therapeutic effects of drugs newly approved by the FDA for the treatment of prostate cancer.

The findings of this study provide important information about the atomic interactions and mechanisms between selected new FDA-approved drugs (Abiraterone, Olaparib, Pylarify, Rucaparib, and Locametz) and the genes (proteins) most associated with prostate cancer. These genes include the crystal structures of the ligand-binding domains 1E3G and 8E1A (AR) of the androgen receptor, and the crystal structures of Kallikrein-3 Protein (KLK3) 2ZCH and 2ZCL. The binding affinities and potential inhibitory activities of the drugs on these genes were demonstrated. The identified drugs demonstrated high potential and promising binding energies as effective inhibitors in the treatment of prostate cancer. These results provide a basis for further analysis and decision-making processes for optimal ligand-receptor pairs.

Molecular docking result of the drug Abiraterone is -8.7. Molecular docking result of the drug Olaparib is -11.2. Molecular docking result of the drug Rucaparib is -8.8. Molecular docking result of the drug Locametz is -6.9. Molecular docking result of the drug Pylarify is -6.7.

Abiraterone, a new prostate cancer drug, binds to CYP17A1, a member of the P450 enzyme family, with high affinity and inhibits it. This inhibition aims to stop androgen production. Abiraterone, used as a reference drug, and other drugs have the highest binding scores and results with these proteins.

Later, Molecular Dynamics Simulation studies provided important information about the stability and dynamic behavior of receptor-drug complexes in an artificial and simulated biological environment. The stability of these receptor-drug complexes, as shown by the RMSD, RMSF and Radius of Gyration parameters, showed that the

drugs maintained and maintained stable interactions with target proteins throughout the simulation period. The stability of these complexes proved that the drug and ligand components have high therapeutic potential. Based on the results of 180 molecular docking analyses and 25 Molecular Dynamics Simulation Olaparib and Rucaparib yielded the best results.

Finally, the SASA (Solvent Accessible Surface Area) study provided detailed information on the binding flexibility and stability of receptor-drug complexes. The ADMET study provided important results on the metabolism effects and toxicity properties of drugs. The combination of these methods strengthened the reliability of the results and helped to understand the potential role of new prostate cancer drugs in prostate cancer treatment in a comprehensive and comprehensive way.

Overall, this study successfully demonstrated that the new drug components exhibit strong and effective potential as therapeutic components and agents in prostate cancer treatment. The integrated computational approaches used in this study paved the way for future studies in this field by providing efficient and accurate methods for the development of new drug discoveries. In addition, the successful results of the combination studies and atomistic modeling of the components of new prostate cancer drugs, which have also received positive results in clinical trials, support the results of these experiments.

Considering the promising and successful results obtained from this study, new drug discoveries can also be made. Future studies can progress with the discovery of new drug components or the investigation of components found in other natural sources. Synergistic effects and new drug combinations can also increase the effectiveness of treatments. The aim can be to reduce drug-effect side effects. This offers a more successful and comprehensive approach to prostate cancer treatment. Since environmental factors can also change the stability and effectiveness of drug-protein complexes, more Molecular Dynamics Simulations can be performed by including different physiological conditions in the simulation. In order to improve the drug discovery process, other computational techniques such as machine learning algorithms can be combined with existing approaches. These methods can help to more accurately predict the behavior of receptor-ligand complexes and understand their potential. By following these suggestions, future drug discoveries and research can be

built on the findings of this thesis and pave the way for detailed examination and evaluation of the effects of compounds that can be used for potential prostate cancer treatment and their development.

REFERENCES

Açıkgöz, A., Çımrın, D., & Ergör, G. (2018). Meme, prostat, kolorektal ve akciğer kanserlerinde çevresel risk faktörleri ve risk düzeylerinin belirlenmesi: olgu-kontrol çalışması. *Cukurova Medical Journal, 43*(2), 411-421.

Adhyam, M., & Gupta, A. K. (2012). A review on the clinical utility of PSA in cancer prostate. *Indian journal of surgical oncology, 3*, 120-129.

Akki, A. J., Patil, S. A., Hungund, S., Sahana, R., Patil, M. M., Kulkarni, R. V., Raghava Reddy, K., Zameer, F., & Raghu, A. V. (2024). Advances in Parkinson's disease research - A computational network pharmacological approach. *International immunopharmacology*, *139*, 112758. https://doi.org/10.1016/j.intimp.2024.112758

Akın, A. C., Bürçe, B., Çevirici, B., Şahin, B., Şahin, E., & Şahin, Y. (2014). Disiplinler Arası Bir Bilim Dalı: Biyoinformatik.

Anagnostou, T., Remzi, M., Lykourinas, M., & Djavan, B. (2003). Artificial neural networks for decision-making in urologic oncology. *European urology*, *43*(6), 596–603. https://doi.org/10.1016/s0302-2838(03)00133-7

Ashrafizadeh, M., Zhang, W., Tian, Y., Sethi, G., Zhang, X., & Qiu, A. (2024). Molecular panorama of therapy resistance in prostate cancer: a pre-clinical and bioinformatics analysis for clinical translation. *Cancer and Metastasis Reviews, 43*(1), 229-260.

Attard, G., Reid, A. H., Auchus, R. J., Hughes, B. A., Cassidy, A. M., Thompson, E., . . . Arlt, W. (2012). Clinical and biochemical consequences of CYP17A1 inhibition with abiraterone given with and without exogenous glucocorticoids in castrate men with advanced prostate cancer. *The Journal of Clinical Endocrinology & Metabolism, 97*(2), 507-516.

Attard, G., Reid, A. H., A'Hern, R., Parker, C., Oommen, N. B., Folkerd, E., Messiou, C., Molife, L. R., Maier, G., Thompson, E., Olmos, D., Sinha, R., Lee, G., Dowsett, M., Kaye, S. B., Dearnaley, D., Kheoh, T., Molina, A., & de Bono, J. S. (2009). Selective inhibition of CYP17 with abiraterone acetate is highly active in the treatment of castration-resistant prostate cancer. *Journal of clinical oncology : official journal of the American Society of Clinical Oncology*, *27*(23), 3742–3748. https://doi.org/10.1200/JCO.2008.20.0642

Ausaf Ali, S., Imtaiyaz Hassan, M., Islam, A., & Ahmad, F. (2014). A review of methods available to estimate solvent-accessible surface areas of soluble proteins in the folded and unfolded states. *Current Protein and Peptide Science*, *15*(5), 456-476.

Baykara, O. (2016). Kanser Tedavisinde Güncel Yaklaşimlar. *Balıkesir Sağlık Bilimleri Dergisi*, *5*(3), 154-165.

Barclay, P. L., & Zhang, D. Z. (2021). Periodic boundary conditions for arbitrary deformations in molecular dynamics simulations. *Journal of Computational*

Physics, *435*, 110238.

Bhattacharjee, S., Kim, C. H., Park, H. G., Prakash, D., Madusanka, N., Cho, N. H., & Choi, H. K. (2019). Multi-Features Classification of Prostate Carcinoma Observed in Histological Sections: Analysis of Wavelet-Based Texture and Colour Features. *Cancers*, *11*(12), 1937. https://doi.org/10.3390/cancers11121937

Bizzarri, A. R., Wang, C. X., Chen, W. Z., & Cannistraro, S. (1995). Hydrogen bond analysis by MD simulation of copper plastocyanin at different hydration levels. *Chemical physics*, *201*(2-3), 463-472.

Boonsirikamchai, P., Choi, S., Frank, S. J., Ma, J., Elsayes, K. M., Kaur, H., & Choi, H. (2013). MR imaging of prostate cancer in radiation oncology: what radiologists need to know. *Radiographics, 33*(3), 741-761.

Borley, N., & Feneley, M. R. (2008). Prostate cancer: diagnosis and staging. *Asian journal of andrology, 11*(1), 74.

Bozdoğan, Ş. N., & Koçaşlı, S. (2022). Cerrahi sonrası hızlandırılmış iyileşme (ERAS) protokolleri çerçevesinde cerrahi hastasında malnütrisyon. *Türkiye Sağlık Bilimleri ve Araştırmaları Dergisi*, *5*(2), 85-100.

Buyyounouski, M. K., Choyke, P. L., McKenney, J. K., Sartor, O., Sandler, H. M., Amin, M. B., . . . Lin, D. W. (2017). Prostate cancer–major changes in the American Joint Committee on Cancer eighth edition cancer staging manual. *CA: a cancer journal for clinicians, 67*(3), 245-253.

Caglic, I., Kovac, V., & Barrett, T. (2019). Multiparametric MRI - local staging of prostate cancer and beyond. *Radiology and oncology*, *53*(2), 159–170. https://doi.org/10.2478/raon-2019-0021

Canesin, G. (2021). The prostate cancer stem cell niche: Genetic drivers and therapeutic approaches. In *Advances in Stem Cells and their Niches* (Vol. 5, pp. 137-175). Elsevier.

Cassell, A., & Konneh, S. (2024). Unlocking the potential-vitamin D in prostate cancer prevention. *World journal of clinical oncology*, *15*(2), 169–174. https://doi.org/10.5306/wjco.v15.i2.169

Celis-Barros, C., Saavedra-Rivas, L., Salgado, J. C., Cassels, B. K., & Zapata-Torres, G. (2015). Molecular dynamics simulation of halogen bonding mimics experimental data for cathepsin L inhibition. *Journal of computer-aided molecular design*, *29*(1), 37–46. https://doi.org/10.1007/s10822-014-9802-7

Chen, C., Li, W. Z., Song, Y. C., & Yang, J. (2009). Hydrogen bonding analysis of glycerol aqueous solutions: A molecular dynamics simulation study. *Journal of Molecular Liquids*, *146*(1-2), 23-28.

Chen, H., Zhou, L., Wu, X., Li, R., Wen, J., Sha, J., & Wen, X. (2016). The PI3K/AKT pathway in the pathogenesis of prostate cancer. *Front Biosci (Landmark Ed)*, *21*(5),

1084-1091.

Cheng, L., Montironi, R., Bostwick, D. G., Lopez-Beltran, A., & Berney, D. M. (2012). Staging of prostate cancer. *Histopathology*, *60*(1), 87–117. https://doi.org/10.1111/j.1365-2559.2011.04025.x

Ciccotti, G., Dellago, C., Ferrario, M., Hernández, E. R., & Tuckerman, M. E. (2022). Molecular simulations: past, present, and future (a Topical Issue in EPJB). *The European Physical Journal B*, *95*(1), 3.

Cimadamore, A., Scarpelli, M., Raspollini, M. R., Doria, A., Galosi, A. B., Massari, F., Di Nunno, V., Cheng, L., Lopez-Beltran, A., & Montironi, R. (2020). Prostate cancer pathology: What has changed in the last 5 years. *Urologia*, *87*(1), 3–10. https://doi.org/10.1177/0391560319876821

Cosma, G., Acampora, G., Brown, D., Rees, R. C., Khan, M., & Pockley, A. G. (2016). Prediction of pathological stage in patients with prostate cancer: a neuro-fuzzy model. *PloS one*, *11*(6), e0155856.
Costello, A. J. (2020). Considering the role of radical prostatectomy in 21st century prostate cancer care. *Nature Reviews Urology*, *17*(3), 177-188.

Das, S., Talukdar, A. D., Nath, D., & Choudhury, M. D. (2023). Discovery of anticancer therapeutics: Computational chemistry and Artificial Intelligence-assisted approach. In *Computational Methods in Drug Discovery and Repurposing for Cancer Therapy* (pp. 19-41). Academic Press.

David, M., & Leslie, S. (2024). Prostate-Specific Antigen. *StatPearls*.V

Decherchi, S., & Cavalli, A. (2020). Thermodynamics and Kinetics of Drug-Target Binding by Molecular Simulation. *Chemical reviews*, *120*(23), 12788–12833. https://doi.org/10.1021/acs.chemrev.0c00534

Demirbaş, N., & Onmaz, M. (2021). Sağlık inanç modeli ile erkeklerin prostat kanseri taramalarına ilişkin inanç ve algı düzeyleri ile etkileyen faktörlerin değerlendirilmesi. *Türkiye Aile Hekimliği Dergisi, 25*(4), 137-144.

Denmeade, S. R., & Isaacs, J. T. (2002). A history of prostate cancer treatment. *Nat Rev Cancer, 2*(5), 389-396. doi:10.1038/nrc801

Dhawan, M., & Ryan, C. J. (2016, August). Utility of novel androgen receptor therapies in the real world: A nuanced approach. In *Urologic Oncology: Seminars and Original Investigations* (Vol. 34, No. 8, pp. 340-347). Elsevier.

Dnyandev, K. M., Babasaheb, G. V., Chandrashekhar, K. V., Chandrakant, M. A., & Vasant, O. K. (2021). A review on molecular docking. *Int. Res. J. Pure Appl. Chem*, *22*, 60-68.

Donati, O. F., Jung, S. I., Vargas, H. A., Gultekin, D. H., Zheng, J., Moskowitz, C. S., . . . Akin, O. (2013). Multiparametric prostate MR imaging with T2-weighted, diffusion-weighted, and dynamic contrast-enhanced sequences: are all pulse sequences

necessary to detect locally recurrent prostate cancer after radiation therapy? *Radiology, 268*(2), 440-450.

Duan, Y., Wilkosz, P., Crowley, M., & Rosenberg, J. M. (1997). Molecular dynamics simulation study of DNA dodecamer d (CGCGAATTCGCG) in solution: conformation and hydration. *Journal of molecular biology*, *272*(4), 553-572.

Du, X., Li, Y., Xia, Y. L., Ai, S. M., Liang, J., Sang, P., Ji, X. L., & Liu, S. Q. (2016). Insights into Protein-Ligand Interactions: Mechanisms, Models, and Methods. *International journal of molecular sciences*, *17*(2), 144. https://doi.org/10.3390/ijms17020144

Düzgün, D. (2024). The Role of Parabens in Bladder Cancer.

Elancheran, R., Maruthanila, V. L., Ramanathan, M., Kabilan, S., Devi, R., Kunnumakara, A., & Kotoky, J. (2015). Recent discoveries and developments of androgen receptor based therapy for prostate cancer. *MedChemComm*, *6*(5), 746-768.
Elshakre, M. E., Noamaan, M. A., Moustafa, H., & Butt, H. (2020). Density Functional Theory, Chemical Reactivity, Pharmacological Potential and Molecular Docking of Dihydrothiouracil-Indenopyridopyrimidines with Human-DNA Topoisomerase II. *International Journal of Molecular Sciences*, *21*(4), 1253. doi:10.3390/ijms21041253

Epstein, J. I., Zelefsky, M. J., Sjoberg, D. D., Nelson, J. B., Egevad, L., Magi-Galluzzi, C., ... & Klein, E. A. (2016). A contemporary prostate cancer grading system: a validated alternative to the Gleason score. *European urology*, *69*(3), 428-435.

Erdkamp, F., Boone, N., Janknegt, R., & Zambon, V. (2014). GnRH agonists and antagonists in prostate cancer. *Gene Biosimilars Initiative J*, *3*, 133-42.

Eren, D., & Yalçın, İ. (2020). RASYONEL İLAÇ TASARIMINDA MOLEKÜLER MEKANİK VE MOLEKÜLER DİNAMİK YÖNTEMLERİN KULLANILMA AMACI. Journal of Faculty of Pharmacy of Ankara University, 44(2), 334-355.v doi: 10.33483/jfpau.688351

Erol, M. (2023). In silico evaluation of sars-cov-2 papain-like protease inhibitory activity of some fda-approved drugs. *Journal of Faculty of Pharmacy of Ankara University*, *47*(3), 978-986.

Feng, X., Zahed, H., Onwuka, J., Callister, M. E., Johansson, M., Etzioni, R., & Robbins, H. A. (2024). Cancer stage compared with mortality as end points in randomized clinical trials of cancer screening: a systematic review and meta-analysis. *JAMA*.

Finch, A., Clark, R., Vesprini, D., Lorentz, J., Kim, R. H., Thain, E., ... & Narod, S. A. (2022). An appraisal of genetic testing for prostate cancer susceptibility. *NPJ Precision Oncology*, *6*(1), 43.

Fujii, Y., Yonese, J., Kawakami, S., Yamamoto, S., Okubo, Y., & Fukui, I. (2008). Equivalent and sufficient effects of leuprolide acetate and goserelin acetate to suppress

serum testosterone levels in patients with prostate cancer. *BJU international*, *101*(9), 1096–1100. https://doi.org/10.1111/j.1464-410X.2007.07374.x

Furtado, P., Lima, M. V. A., Nogueira, C., Franco, M., & Tavora, F. (2011). Review of small cell carcinomas of the prostate. *Prostate Cancer*, *2011*(1), 543272.

Fu, Y., Lei, Y., Wang, T., Patel, P., Jani, A. B., Mao, H., . . . Yang, X. (2021). Biomechanically constrained non-rigid MR-TRUS prostate registration using deep learning based 3D point cloud matching. *Medical image analysis, 67*, 101845.
Gandaglia, G., Leni, R., Bray, F., Fleshner, N., Freedland, S. J., Kibel, A., . . . La Vecchia, C. (2021). Epidemiology and prevention of prostate cancer. *European urology oncology, 4*(6), 877-892.

Garje, R., Chennamadhavuni, A., Mott, S. L., Chambers, I. M., Gellhaus, P., Zakharia, Y., & Brown, J. A. (2020). Utilization and Outcomes of Surgical Castration in Comparison to Medical Castration in Metastatic Prostate Cancer. *Clinical genitourinary cancer*, *18*(2), e157–e166. https://doi.org/10.1016/j.clgc.2019.09.020

Geavlete, P. A. (Ed.). (2016). Retrograde Ureteroscopy: Handbook of Endourology.

Gençhellaç, H., & Yılmaz, E. (2015). Prostat görüntüleme. *Türk Radyoloji Seminerleri, 3*(1), 138-148.
Gürkan, Ç., Budak, A., Karatas, H., & Akın, K. (2024). Segmentation of prostate zones on a novel MRI database using Mask R-CNN: An implementation on PACS system. *Journal of the Faculty of Engineering and Architecture of Gazi University, 39*(3), 1401-1416.

Gilligan, T., & Kantoff, P. W. (2002). Chemotherapy for prostate cancer. *Urology*, *60*(3 Suppl 1), 94–100. https://doi.org/10.1016/s0090-4295(02)01583-2

Gürkan, Ç., Budak, A., Karataş, H., Akın, K. (2024). Mask R-CNN kullanılarak yeni bir MRG veri tabanında prostat bölgelerinin segmentasyonu: PACS sistemi üzerinde bir uygulama. Gazi Üniversitesi Mühendislik Mimarlık Fakültesi Dergisi, 39(3), 1401-1416. https://doi.org/10.17341/gazimmfd.1153507

Haydaroğlu, A., Yalman, D., Özkök, S., Gökmen, E., Şen, S., Kumbaracı, B. S., ... & Caner, A. (2019). Ege Üniversitesi Hastanesinde erkek genital sistem kanserlerinin epidemiyolojik ve genel sağ kalım özellikleri. *Ege Tıp Dergisi*, 120-125.

He, H., Yang, W., Shi, Y., Chen, X., Chen, X., Hu, X., ... & Yu, L. (2024). Design and synthesis of the first PARP-1 and proteasome dual inhibitors to treat breast cancer. *European Journal of Medicinal Chemistry*, *264*, 115943.

Henttu, P., Liao, S. S., & Vihko, P. (1992). Androgens up-regulate the human prostate-specific antigen messenger ribonucleic acid (mRNA), but down-regulate the prostatic acid phosphatase mRNA in the LNCaP cell line. *Endocrinology*, *130*(2), 766–772. https://doi.org/10.1210/endo.130.2.1370795

Hernndez-Santoyo, A., Yair, A., Altuzar, V., Vivanco-Cid, H., & Mendoza-Barrer, C. (2013). Protein-Protein and Protein-Ligand Docking. InTech. doi: 10.5772/56376

Huang, J., Lin, B., & Li, B. (2022). Anti-Androgen Receptor Therapies in Prostate Cancer: A Brief Update and Perspective. *Frontiers in oncology*, *12*, 865350. https://doi.org/10.3389/fonc.2022.865350

Humphrey P. A. (2017). Histopathology of Prostate Cancer. *Cold Spring Harbor perspectives in medicine*, *7*(10), a030411. https://doi.org/10.1101/cshperspect.a030411

Hünenberger, P. H. (2005). Thermostat algorithms for molecular dynamics simulations. *Advanced computer simulation: Approaches for soft matter sciences I*, 105-149.

Hollingsworth, S. A., & Dror, R. O. (2018). Molecular Dynamics Simulation for All. *Neuron*, *99*(6), 1129–1143. https://doi.org/10.1016/j.neuron.2018.08.011

Høyer, M., Thor, M., Thörnqvist, S., Søndergaard, J., Lassen-Ramshad, Y., & Paul Muren, L. (2011). Advances in radiotherapy: from 2D to 4D. *Cancer imaging : the official publication of the International Cancer Imaging Society*, *11 Spec No A*(1A), S147–S152. https://doi.org/10.1102/1470-7330.2011.9036

James, N. D., Tannock, I., N'Dow, J., Feng, F., Gillessen, S., Ali, S. A., . . . Xie, L.-P. (2024). The Lancet Commission on prostate cancer: planning for the surge in cases. *The Lancet, 403*(10437), 1683-1722. doi:10.1016/S0140-6736(24)00651-2

Jenča, A., Mills, D. K., Ghasemi, H., Saberian, E., Jenča, A., Karimi Forood, A. M., . . . Zare-Zardini, H. (2024). Herbal Therapies for Cancer Treatment: A Review of Phytotherapeutic Efficacy. *Biologics: Targets and Therapy*, 229-255.

Kabasakal, L., Demirci, E., Nematyazar, J., Akyel, R., Razavi, B., Ocak, M., ... & Kural, A. R. (2017). The role of PSMA PET/CT imaging in restaging of prostate cancer patients with low prostate-specific antigen levels. *Nuclear Medicine Communications*, *38*(2), 149-155.

Karadağ, M. A., Çeçen, K., Demir, A., Bağcıoğlu, M., Kocaaslan, R., & Sofikerim, M. Focal Treatment Alternatives in Prostate Cancer. *Kafkas Journal of Medical Sciences*, (1), 18-24.

Karalar, M., Gercek, O., Yazar, V. M., & Ulusoy, K. (2024). PROSTAT İĞNE BİYOPSİLERİ VE RADİKAL PROSTATEKTOMİ PATOLOJİ SONUÇLARININ KARŞILAŞTIRILMASI. *Kocatepe Tıp Dergisi, 25*(2), 235-240.

Kilinç, M. F., Karakan, T., Özer, E., Demir, D. O., Aydogmus, Y., & Doluoglu, Ö. G. (2016). Combined Radiation and Hormonal Therapy for Squamous Cell Carcinoma of the Prostate: A Case Report and Review of the Literature. *Journal of Urological Surgery, 3*(3), 98.

Koçak, T., & Tek, N. A. (2022). Prostat Kanseri Etiyoloji ve Tedavisinde Beslenmenin Rolü. *Gümüşhane Üniversitesi Sağlık Bilimleri Dergisi, 11*(3), 1247-1256.

Konac, E., & Sozen, T. E. V. F. İ. K. (2014). Molecular biology in diagnosis and treatment of prostate cancer. *UROONKOLOJI BULTENI-BULLETIN OF UROONCOLOGY*, (4).

Książek, I., Ligęza, A., Drzymała, F., Borek, A., Miszczyk, M., Francuz, M. R., . . . Zapała, Ł. (2024). Role of Lutetium Radioligand Therapy in Prostate Cancer. *Cancers, 16*(13), 2433.

Kumari, R., Kumar, R., Open Source Drug Discovery Consortium, & Lynn, A. (2014). g_mmpbsa--a GROMACS tool for high-throughput MM-PBSA calculations. *Journal of chemical information and modeling*, *54*(7), 1951–1962. https://doi.org/10.1021/ci500020m

Küçükulu, M. (2012). Prostat kanseri için üç boyutlu konformal radyoterapi ile yoğunluk ayarlı radyoterapinin karşılaştırılması.

Lang, J., McClure, T. D., & Margolis, D. J. (2024). MRI–Ultrasound Fused Approach for Prostate Biopsy—How It Is Performed. *Cancers, 16*(7), 1424.

Lee, C. T., Dong, L., Ahamad, A. W., Choi, H., Cheung, R., Lee, A. K., Horne, D. F., Jr, Breaux, A. J., & Kuban, D. A. (2005). Comparison of treatment volumes and techniques in prostate cancer radiation therapy. *American journal of clinical oncology*, *28*(6), 618–625. https://doi.org/10.1097/01.coc.0000172281.32437.d4

Lindahl E. R. (2008). Molecular dynamics simulations. *Methods in molecular biology (Clifton, N.J.)*, *443*, 3–23. https://doi.org/10.1007/978-1-59745-177-2_1

Liu, Z., Li, J., Liu, J., Liu, Y., Nie, W., Han, L., Li, Y., & Wang, R. (2015). Cross-Mapping of Protein - Ligand Binding Data Between ChEMBL and PDBbind. *Molecular informatics*, *34*(8), 568–576. doi: 10.1002/minf.201500010

Longoria, O., Beije, N., & de Bono, J. S. (2024). PARP inhibitors for prostate cancer. *Seminars in oncology*, *51*(1-2), 25–35

Mamidi, T. K. K., Wu, J., & Hicks, C. (2019). Interactions between germline and somatic mutated genes in aggressive prostate cancer. *Prostate Cancer*, *2019*(1), 4047680.

McNeal, J. E. (1988). Normal histology of the prostate. *The American journal of surgical pathology, 12*(8), 619-633.
Mistry, J., Sarkis, J., & Dhavale, D. G. (2014). Multi-criteria analysis using latent class cluster ranking: An investigation into corporate resiliency. *International Journal of Production Economics*, *148*, 1-13.

Musser, J. E., Assel, M., Mashni, J. W., Sjoberg, D. D., & Russo, P. (2014). Adult prostate sarcoma: the Memorial Sloan Kettering experience. *Urology*, *84*(3), 624–628. https://doi.org/10.1016/j.urology.2014.05.036

Mu, Yuguang, Kosov, Daniil S., and Stock, Gerhard (2003) *Conformational dynamics*

of trialanine in water. 2. Comparison of AMBER, CHARMM, GROMOS, and OPLS force fields to NMR and infrared experiments. Journal of Physical Chemistry Part B, 107 (21). pp. 5064-5073.

Nader, R., El Amm, J., & Aragon-Ching, J. B. (2018). Role of chemotherapy in prostate cancer. *Asian journal of andrology*, *20*(3), 221–229. https://doi.org/10.4103/aja.aja_40_17

O'Malley, D. M., Krivak, T. C., Kabil, N., Munley, J., & Moore, K. N. (2023). PARP inhibitors in ovarian cancer: a review. *Targeted oncology*, *18*(4), 471-503.

Oselusi, S. O., Dube, P., Odugbemi, A. I., Akinyede, K. A., Ilori, T. L., Egieyeh, E., Sibuyi, N. R., Meyer, M., Madiehe, A. M., Wyckoff, G. J., & Egieyeh, S. A. (2024). The role and potential of computer-aided drug discovery strategies in the discovery of novel antimicrobials. *Computers in biology and medicine*, *169*, 107927. https://doi.org/10.1016/j.compbiomed.2024.107927

Osunkoya, A. O. (2018). Mucinous and secondary tumors of the prostate. *Modern Pathology*, *31*, 80-95.

Paissoni, C., Spiliotopoulos, D., Musco, G., & Spitaleri, A. (2014). GMXPBSA 2.0: A GROMACS tool to perform MM/PBSA and computational alanine scanning. *Computer Physics Communications*, *185*(11), 2920-2929.

Parimi, V., Goyal, R., Poropatich, K., & Yang, X. J. (2014). Neuroendocrine differentiation of prostate cancer: a review. *American journal of clinical and experimental urology*, *2*(4), 273.
Podder, T. K., Fredman, E. T., & Ellis, R. J. (2018). Advances in Radiotherapy for Prostate Cancer Treatment. *Advances in experimental medicine and biology*, *1096*, 31–47. https://doi.org/10.1007/978-3-319-99286-0_2

Quinn, D. I., Sandler, H. M., Horvath, L. G., Goldkorn, A., & Eastham, J. A. (2017). The evolution of chemotherapy for the treatment of prostate cancer. *Annals of oncology*, *28*(11), 2658-2669.

Ratnacaram, C. K., Teletin, M., Jiang, M., Meng, X., Chambon, P., & Metzger, D. (2008). Temporally controlled ablation of PTEN in adult mouse prostate epithelium generates a model of invasive prostatic adenocarcinoma. *Proceedings of the National Academy of Sciences*, *105*(7), 2521-2526.

Rawla, P. (2019). Epidemiology of prostate cancer. *World journal of oncology, 10*(2), 63.

Ribelles, N., Pascual, J., Galvez-Carvajal, L., Ruiz-Medina, S., Garcia-Corbacho, J., Benitez, J. C., . . . Zalabardo, M. (2024). Increasing annual cancer incidence in patients age 20-49 years: A real-data study. *JCO Global Oncology, 10*, e2300363.

Roy, K. (Ed.). (2015). *Quantitative structure-activity relationships in drug design, predictive toxicology, and risk assessment*. IGI Global.

Sahputra, I. H., & Echtermeyer, A. (2021). The effects of the van der Waals potential energy on the Young's modulus of a polymer: comparison between molecular dynamics simulation and experiment. *Journal of Polymer Research*, *28*, 1-7.

Saikia, S., & Bordoloi, M. (2019). Molecular Docking: Challenges, Advances and its Use in Drug Discovery Perspective. *Current drug targets*, *20*(5), 501–521. https://doi.org/10.2174/1389450119666181022153016

Sanguedolce, F., Russo, D., Mancini, V., Selvaggio, O., Calò, B., Carrieri, G., & Cormio, L. (2019). Morphological and immunohistochemical biomarkers in distinguishing prostate carcinoma and urothelial carcinoma: a comprehensive review. *International Journal of Surgical Pathology*, *27*(2), 120-133.

Schaeffer, E. M., Srinivas, S., Adra, N., An, Y., Bitting, R., Chapin, B., . . . Dorff, T. (2024). NCCN guidelines® insights: prostate cancer, version 3.2024: featured updates to the NCCN guidelines. *Journal of the National Comprehensive Cancer Network, 22*(3), 140-150.
Schaeffer, E., Srinivas, S., Antonarakis, E. S., Armstrong, A. J., Bekelman, J. E., Cheng, H., ... & Freedman-Cass, D. A. (2021). NCCN guidelines insights: Prostate cancer, version 1.2021: Featured updates to the NCCN guidelines. *Journal of the National Comprehensive Cancer Network*, *19*(2), 134-143.

Sekhoacha, M., Riet, K., Motloung, P., Gumenku, L., Adegoke, A., & Mashele, S. (2022). Prostate cancer review: genetics, diagnosis, treatment options, and alternative approaches. *Molecules, 27*(17), 5730.

Sharifi, N., Gulley, J. L., & Dahut, W. L. (2005). Androgen deprivation therapy for prostate cancer. *JAMA*, *294*(2), 238–244. https://doi.org/10.1001/jama.294.2.238

Siddiqui, M. M., Rais-Bahrami, S., Turkbey, B., George, A. K., Rothwax, J., Shakir, N., . . . Linehan, W. M. (2015). Comparison of MR/ultrasound fusion–guided biopsy with ultrasound-guided biopsy for the diagnosis of prostate cancer. *JAMA, 313*(4), 390-397.

Silakari, O., & Singh, P. K. (2020). *Concepts and experimental protocols of modelling and informatics in drug design*. Academic Press. doi: 10.1016/C2019-0-00785-6

Sunay, M. (2010). Selenyum ve vitamin E'nin prostat kanseri riski üzerine etkileri. *Turk Urol Sem, 1*, 164-167.

Tagai, E. K., Miller, S. M., Kutikov, A., Diefenbach, M. A., Gor, R. A., Al-Saleem, T., ... & Roy, G. (2019). Prostate cancer patients' understanding of the Gleason Scoring System: implications for shared decision-making. *Journal of Cancer Education*, *34*, 441-445.

Tan, M. H., Li, J., Xu, H. E., Melcher, K., & Yong, E. L. (2015). Androgen receptor: structure, role in prostate cancer and drug discovery. *Acta pharmacologica Sinica*, *36*(1), 3–23. https://doi.org/10.1038/aps.2014.18

Tanner, D. E., Phillips, J. C., & Schulten, K. (2012). GPU/CPU Algorithm for

Generalized Born/Solvent-Accessible Surface Area Implicit Solvent Calculations. *Journal of chemical theory and computation*, *8*(7), 2521–2530. https://doi.org/10.1021/ct3003089

Tatlı, A., Uysal, M., Başsongur, C., Arslan, D., & Coşkun, H. (2016). Küçük hücreli prostat kanseri: Olgu sunumu. *Kocatepe Tıp Dergisi, 17*(1).

Terefe, E. M., & Ghosh, A. (2022). Molecular Docking, Validation, Dynamics Simulations, and Pharmacokinetic Prediction of Phytochemicals Isolated From *Croton dichogamus* Against the HIV-1 Reverse Transcriptase. *Bioinformatics and biology insights*, *16*, 11779322221125605. https://doi.org/10.1177/11779322221125605

Thibaut U. (2002). Bioinformatics and rational drug design: tools for discovery and better understanding of biological targets and mode of action of drugs. *Scandinavian journal of gastroenterology. Supplement*, (236), 95–99. doi: 10.1080/003655202320621544

Tosun Yildirim, H., & Şen Türk, N. (2012). Analysis of IMP3 expression in prostate adenocarcinomas. *Turkish Journal of Pathology*, *28*(2).

Toukmaji, A. Y., & Board Jr, J. A. (1996). Ewald summation techniques in perspective: a survey. *Computer physics communications*, *95*(2-3), 73-92.

Tripathi, M. K., Ahmad, S., Tyagi, R., Dahiya, V., & Yadav, M. K. (2022). Fundamentals of molecular modeling in drug design. In *Computer Aided Drug Design (CADD): From ligand-based methods to structure-based approaches* (pp. 125-155). Elsevier. doi:10.1016/B978-0-323-90608-1.00001-0

Trock, B. J., Han, M., Freedland, S. J., Humphreys, E. B., DeWeese, T. L., Partin, A. W., & Walsh, P. C. (2008). Prostate cancer-specific survival following salvage radiotherapy vs observation in men with biochemical recurrence after radical prostatectomy. *JAMA*, *299*(23), 2760–2769. https://doi.org/10.1001/jama.299.23.2760

Turkbey, B., Pinto, P. A., & Choyke, P. L. (2009). Imaging techniques for prostate cancer: implications for focal therapy. *Nature reviews. Urology*, *6*(4), 191–203. https://doi.org/10.1038/nrurol.2009.27

Tuffaha, H., Edmunds, K., Fairbairn, D., Roberts, M. J., Chambers, S., Smith, D. P., . . . Scuffham, P. (2024). Guidelines for genetic testing in prostate cancer: a scoping review. *Prostate Cancer and Prostatic Diseases, 27*(4), 594-603.

van Brandwijk, E. A., Aalbersberg, E. A., Hosseini, A. S., Huitema, A. D., & Hendrikx, J. J. (2024). Automated radiolabelling of [68Ga] Ga-PSMA-11 (gallium (68Ga)-gozetotide) using the Locametz® kit and two generators. *EJNMMI Radiopharmacy and Chemistry, 9*(1), 31.

Van Nieuwenhove, S., Van Damme, J., Padhani, A. R., Vandecaveye, V., Tombal, B., Wuts, J., . . . Lecouvet, F. E. (2022). Whole-body magnetic resonance imaging for prostate cancer assessment: Current status and future directions. *Journal of Magnetic*

Resonance Imaging, 55(3), 653-680.
Vlasiou, M. C., Nikolaou, G., Spanoudes, K., & Mavrides, D. E. (2024). β-Tocotrienol and δ-Tocotrienol as Additional Inhibitors of the Main Protease of Feline Infectious Peritonitis Virus: An In Silico Analysis. *Veterinary Sciences*, *11*(9), 424.

Voter, A. F., Werner, R. A., Pienta, K. J., Gorin, M. A., Pomper, M. G., Solnes, L. B., & Rowe, S. P. (2022). Piflufolastat F-18 (^{18}F-DCFPyL) for PSMA PET imaging in prostate cancer . *Expert review of* anticancer therapy, 22(7), 681–694.

Wang, H., Zhu, H., Li, G., Dai, J., Huang, H., & Jia, Q. (2024). Effect of 18F-DCFPyL PET on changes in management of patients with prostate cancer: a systematic review and meta-analysis. Frontiers in Medicine, 11, 1355236.
Wang, I. E., Morrissette, L. J., Wong, K. K., Brooks, A. F., Dakanali, M., & Scott, P. J. (2024). A comparison of routine [68Ga] Ga-PSMA-11 preparation using Locametz and Illuccix kits. EJNMMI Radiopharmacy and Chemistry, 9(1), 87.

Wang, L., & O'Mara, M. L. (2021). Effect of the Force Field on Molecular Dynamics Simulations of the Multidrug Efflux Protein P-Glycoprotein. *Journal of chemical theory and computation*, *17*(10), 6491–6508. https://doi.org/10.1021/acs.jctc.1c00414

Wokołorczyk, D., Kluźniak, W., Stempa, K., Rusak, B., Huzarski, T., Gronwald, J., ... & Cybulski, C. (2021). PALB2 mutations and prostate cancer risk and survival. *British Journal of Cancer*, *125*(4), 569-575.

Xiong, G., Wu, Z., Yi, J., Fu, L., Yang, Z., Hsieh, C., Yin, M., Zeng, X., Wu, C., Lu, A., Chen, X., Hou, T., & Cao, D. (2021). ADMETlab 2.0: an integrated online platform for accurate and comprehensive predictions of ADMET properties. *Nucleic acids research*, *49*(W1), W5–W14. https://doi.org/10.1093/nar/gkab255

Yan, X., & Chaudhuri, S. (2022). An interactive polymer building toolkit for molecular dynamics simulations: PolyMAPS. *arXiv preprint arXiv:2204.14218*.

Yu, X.-d., Yan, S.-s., Liu, R.-j., & Zhang, Y.-s. (2024). Apparent differences in prostate zones: susceptibility to prostate cancer, benign prostatic hyperplasia and prostatitis. *International Urology and Nephrology*, 1-8.

Zaorsky, N. G., Harrison, A. S., Trabulsi, E. J., Gomella, L. G., Showalter, T. N., Hurwitz, M. D., Dicker, A. P., & Den, R. B. (2013). Evolution of advanced technologies in prostate cancer radiotherapy. *Nature reviews. Urology*, *10*(10), 565–579. https://doi.org/10.1038/nrurol.2013.185

Zhang, J., & Chadha, J. S. (2024). Developmental Therapeutics in Metastatic Prostate Cancer: New Targets and New Strategies. *Cancers, 16*(17), 3098.

APPENDICES

APPENDIX A

MOLEKÜLER YERLEŞTIRME FORMATI		ChEMBL AKTİVİTELERİ			RESEPTÖRLER Yerleştirme Sonuçları (kcal/mol)	
PDBQT biçimi	**SDF biçimi**	**Order**	**CHEMBL KODU**	**Standart Değer (nM)**	**1E3G(AR)**	**8E1A(AR)**
Liga	Lig	1	CHEMBL302870 (Preclinical)	0.0	-7.7	-7.0
Liga	Lig	2	CHEMBL184313 (Preclinical)	0.009	-8.4	-7.7
Liga	Lig	3	CHEMBL256769 (Preclinical)	0.2	-8.3	-8.8
Liga	Lig	4	CHEMBL391548 (Preclinical)	0.2	-9.5	-10.2
Liga	Lig	5	CHEMBL427898 (Preclinical)	0.2	-9.4	-9.5
Liga	Lig	6	CHEMBL4060271 (Preclinical)	0.2	-8.7	-8.9
Liga	Lig	7	CHEMBL4092535 (Preclinical)	0.29	-8.5	-8.9
Liga	Lig	8	CHEMBL2112312	0.3	-8.9	-9.5
Liga	Lig	9	CHEMBL257151 (Preclinical)	0.3	-10.3	-9.5
Liga	Lig	10	CHEMBL182412 (Preclinical)	0.4	-11.0	-8.9
Liga	Lig	11	CHEMBL398431 (Preclinical)	0.8	-8.0	-7.5
Liga	Lig	12	CHEMBL235159 (Preclinical)	0.8	-7.6	-9.1
Liga	Lig	13	CHEMBL3402221 (Preclinical)	0.84	-9.1	-7.0
Liga	Lig	14	CHEMBL5192412 (Preclinical)	0.9	-7.5	-8.2

Liga	Lig	15	CHEMBL1957613 (Preclinical)	0.95	-8.4	-8.7
Liga	Lig	16	CHEMBL27769 (Phase 2)	1.0	-8.2	-7.5
Liga	Lig	17	CHEMBL3402227 (Preclinical)	1.0	-8.8	-10.0
Liga	Lig	18	CHEMBL3410856 (Preclinical)	1.0	-6.5	-7.2
Liga	Lig	19	CHEMBL391798 (Preclinical)	1.0	-9.3	-8.9
Liga	Lig	20	CHEMBL1276308 (Approved)	1.0	-7.7	-8.0
Liga	Lig	21	CHEMBL4226259 (Preclinical)	1.4	-7.8	-8.2
Liga	Lig	22	CHEMBL4227715 (Preclinical)	1.4	-8.0	-8.6
Liga	Lig	23	CHEMBL1934442 (Preclinical)	1.4	-8.3	-7.9
Liga	Lig	24	CHEMBL4095364 (Preclinical)	1.6	-9.2	-8.5
Liga	Lig	25	CHEMBL401711 (Preclinical)	1.9	-8.5	-8.3
Liga	Lig	26	CHEMBL267270 (Preclinical)	2.0	-9.6	-11.3
Liga	Lig	27	CHEMBL246006 (Preclinical)	2.0	-7.8	-8.5
Liga	Lig	28	CHEMBL3238280 (Preclinical)	2.4	-7.2	-8.2
Liga	Lig	29	CHEMBL1163630 (Preclinical)	2.9	-8.1	-8.3
Liga	Lig	30	CHEMBL4065842 (Preclinical)	2.9	-8.4	-8.5
Liga	Lig	31	CHEMBL1738889 (Phase 3)	3.0	-7.2	-8.0
Liga	Lig	32	CHEMBL4067691 (Preclinical)	3.4	-8.6	-8.2

Liga	Lig	33	CHEMBL1934443 (Preclinical)	3.4	-8.2	-8.2
Liga	Lig	34	CHEMBL4088914 (Preclinical)	3.6	-9.2	-9.0
Liga	Lig	35	CHEMBL1934434 (Preclinical)	3.8	-8.1	-7.3
Liga	Lig	36	CHEMBL3706929 (Preclinical)	4.1	-9.4	-9.8
Liga	Lig	37	CHEMBL3623122 (Preclinical)	6.0	-8.4	-8.0
Liga	Lig	38	CHEMBL3221237 (Preclinical)	6.6	-9.1	-9.7
Liga	Lig	39	CHEMBL2337509 (Preclinical)	8.0	-8.1	-8.2
Liga	Lig	40	CHEMBL2337511 (Preclinical)	8.6	-7.5	-7.7
Liga	Lig	41	CHEMBL1274 (Approved)	9.0	-9.5	-9.5
Liga	Lig	42	CHEMBL4447539 (Preclinical)	9.0	-7.3	-10.1
Liga	Lig	43	CHEMBL3920715	9.0	-8.3	-8.9
Liga	Lig	44	CHEMBL1934444 (Preclinical)	9.0	-8.1	-8.2
Liga	Lig	45	CHEMBL2337510 (Preclinical)	9.0	-8.3	-8.6
Liga	Lig	46	CHEMBL3233071 (Preclinical)	9.1	-7.5	-8.5
Liga	Lig	47	CHEMBL238365 (Preclinical)	9.8	-9.5	-10.4
Liga	Lig	48	CHEMBL409 (Approved)	10.0	-7.8	-8.4
Liga	Lig	49	CHEMBL1099086 (Preclinical)	10.0	-6.4	-6.6
Liga	Lig	50	CHEMBL5204114 (Preclinical)	10.0	-7.0	-6.8
Liga	Lig	51	CHEMB188297	10.0	-	-

			(Preclinical)		7.8	9.3
Liga	Lig	52	CHEMBL2337516 (Preclinical)	11.0	-8.1	-8.4
Liga	Lig	53	CHEMBL462664 (Preclinical)	11.0	-7.3	-7.6
Liga	Lig	54	CHEMBL1288323 (Preclinical)	13.0	-8.1	-8.6
Liga	Lig	55	CHEMBL1082407 (Approved)	14.0	-7.6	-7.7
Liga	Lig	56	CHEMBL393280 (Preclinical)	15.0	-7.8	-6.9
Liga	Lig	57	CHEMBL1288959 (Preclinical)	15.0	-8.5	-8.7
Liga	Lig	58	CHEMBL1099140 (Preclinical)	15.0	-8.4	-7.3
Liga	Lig	59	CHEMBL2112349 (Preclinical)	15.0	-8.1	-8.3
Liga	Lig	60	CHEMBL491 (Phase 2)	15.0	-8.6	-8.5
Liga	Lig	61	CHEMBL4105484 (Preclinical)	15.41	-8.6	-8.4
Liga	Lig	62	CHEMBL9337 (Preclinical)	15.9	-6.8	-7.1
Liga	Lig	63	CHEMBL1916247 (Preclinical)	16.0	-8.1	-7.8
Liga	Lig	64	CHEMBL3183409 (Approved)	16.0	-8.4	-8.1
Liga	Lig	65	CHEMBL3238293 (Preclinical)	16.1	-8.4	-7.5
Liga	Lig	66	CHEMBL272509 (Preclinical)	19.0	-7.2	-9.3
Liga	Lig	67	CHEMBL5186213 (Preclinical)	19.0	-8.3	-7.8
Liga	Lig	68	CHEMBL504179 (Preclinical)	22.0	-8.3	-8.7
Liga	Lig	69	CHEMBL139835	23.0	-	-

			(Approved)		7.3	6.9
Liga	Lig	70	CHEMBL255918 (Preclinical)	25.0	-7.3	-8.4
Liga	Lig	71	CHEMBL4797715	2400.0	-8.6	-9.2
Liga	Lig	72	CHEMBL446790	3200.0	-8,9	-8,6

Figure A.1. 1E3G and 8E1A receptors (AR) molecular docking with ChEMBL codes and Autodock Vina moleküler docking results.

MOLEKÜLER YERLEŞTIRME FORMATI		**ChEMBL AKTİVİTELERİ**			**RESEPTÖRLER Yerleştirme Sonuçları (kcal/mol)**	
PDBQT biçimi	**SDF biçimi**	**Order**	**CHEMBL KODU**	**Standart Değer (nM)**	**2ZCH(KLK3)**	**2ZCL(KLK3)**
Liga	Lig	1	CHEMBL257151	0.3	-7.8	-8.5
Liga	Lig	2	CHEMBL182412	0.4	-8.8	-8.6
Liga	Lig	3	CHEMBL267270	2	-8.7	-8.2
Liga	Lig	4	CHEMBL3706929	4.1	-8.8	-8.4
Liga	Lig	5	CHEMBL4447539	9	-7.9	-8.2
Liga	Lig	6	CHEMBL238365	9.8	-7.6	-8.0
Liga	Lig	7	CHEMBL10	14	-8.9	-9.0

			82407			
Liga	Lig	8	CHEMBL4760141	150	-8.1	-8.6
Liga	Lig	9	CHEMBL2011751	226	-8.5	-8.2
Liga	Lig	10	CHEMBL4797715	1400	-9.0	-9.0
Liga	Lig	11	CHEMBL446790	3200	-10.4	-9.6

Figure A.2. 2ZCH and 2ZCL receptors (KLK3) molecular docking with ChEMBL codes and Autodock Vina moleküler docking results.

MOLECULAR DOCKING FORMAT		**ChEMBL ACTIVITIES**			**RECEPTORS Docking Results (kcal/mol)**			
pdbqt	**sdf**	**Order**	**ChEMBL Code**	**Drug Name**	**1E3G**	**8E1A**	**2ZCH**	**2ZCL**
curcumin	curcumin	1	CHEMBL116438	Curcumin	-7.7	-7.1	-7.1	-8.1
matrine	matrine	2	CHEMBL204860	Matrine	-8.7	-6.7	-6.8	-7.2
quercetin	quercetin	3	CHEMBL50	Quercetin	-9.1	-9.9	-8.7	-8.3
triptolide	triptolide	4	CHEMBL463763	Triptolide	-8.2	-8.0	-8.3	-9.2
astragalosi de	astragalosi de	5	CHEMBL498853	Astragaloside	-7.3	-7.6	-9.0	-10.2
shikonin	shikonin	6	CHEMBL9470	Shikonin	-8.0	-8.9	-7.9	-8.0
artesunate	artesunate	7	CHEMBL361497	Artesunate	-6.9	-7.4	-8.0	-8.1
baicalin	baicalin	8	CHEMBL485818	Baicalin	-8.7	-10	-8.8	-9.3
brucine	brucine	9	CHEMBL501756	Brucine	-8.0	-8.9	-8.2	-8.4
oroxindin	oroxindin	10	CHEMBL397591	Oroxindin	-8.1	-8.5	-9.0	-9.4
dyphylline	dyphylline	11	CHEMBL1752	Dyphylline	-7.0	-6.7	-6.3	-6.7
patchouli alcohol	patchouli alcohol	12	CHEMBL4588682	Patchouli Alcohol	-6.3	-5.4	-6.1	-6.7
lycopene	lycopene	13	CHEMBL501174	Lycopene	-7.0	-7.7	-7.1	-7.3
apigenin	apigenin	14	CHEMBL2	Apigenin	-10.0	-9.3	-8.0	-8.0

			8					
tangeretin	tangeretin	15	CHEMBL73930	Tangeretin	-7.1	-7.5	-7.3	-7.4
acacetin	acacetin	16	CHEMBL243664	Acacetin	-7.8	-9.1	-8.0	-8.2
resveratrol	resveratrol	17	CHEMBL165	Resveratrol	-9.0	-8.4	-7.2	-7.3
fisetin	fisetin	18	CHEMBL31574	Fisetin	-9.3	-9.7	-8.2	-7.9
luteolin	luteolin	19	CHEMBL151	Luteolin	-9.4	-9.7	-8.6	-8.4
genistein	genistein	20	CHEMBL44	Genistein	-8.9	-9.7	-7.6	-7.9
silybin	silybin	21	CHEMBL9509	Silybin	-9.1	-9.3	-8.3	-9.7
kaempferol	kaempferol	22	CHEMBL150	Kaempferol	-9.8	-9.7	-7.9	-7.9
(EGCG)	(EGCG)	23	ChEMBL297453	Epigallocatechin-3-gallate (EGCG)	-7.2	-8.9	-9.3	-9.6
tocotrienol	tocotrienol	24	CHEMBL4297330	Tocotrienol	-6.6	-9.0	-8.3	-8.3
ginsenosides	ginsenosides	25	CHEMBL1773987	Ginsenosides	-8.1	-7.7	-7.3	-7.9
ursolic acid	ursolic acid	26	CHEMBL169	Ursolic acid	-7.6	-8.1	-8.8	-8.4
berberine	berberine	27	CHEMBL295124	Berberine	-7.8	-8.1	-7.9	-8.1
honokiol	Honokiol	28	CHEMBL16901	Honokiol	-8.0	-9.2	-7.4	-7.3
xanthohumol	xanthohumol	29	CHEMBL253896	Xanthohumol	-7.3	-8.4	-7.6	-8.2
oridonin	oridonin	30	CHEMBL4639672	Oridonin	-7.4	-7.1	-7.6	-7.8

Figure A.3. 1E3G (AR), 8E1A (AR), 2ZCH (KLK3) and 2ZCL (KLK3) receptors molecular docking natural drugs and Autodock Vina docking results.

MOLECULAR DOCKING FORMAT		**CHEMICAL ID**		**RECEPTORS Docking Results (kcal/mol)**			
pdbqt	**sdf**	**Order**	**PubChem CID**	**1E3G**	**8E1A**	**2ZCH**	**2ZCL**
druq	Dru	1	1085	-6.1	-7.6	-8.3	-8.4
druq	Dru	2	1697733	-5.4	-4.9	-5.2	-5.2
druq	Dru	3	409	-	-7.5	-	-9.0

				7.3		9.1	
druq	Dru	4	125236	-7.2	-8.7	-8.1	-8.5
druq	Dru	5	209073	-8.0	-7.4	-7.6	-8.4
druq	Dru	6	2106059	-5.5	-7.2	-6.1	-6.8
druq	Dru	7	1201748	-7.1	-7.6	-7.8	-8.5
druq	Dru	8	3590187	-7.2	-6.8	-7.8	-7.3
druq	Dru	9	139835	-7.3	-7.1	-7.7	-7.5
druq	Dru	10	1479	-7.7	-7.6	-8.8	-8.4
druq	Dru	11	1201864	-9.0	-6.9	-7.5	-8.3
druq	Dru	12	411	-8.2	-8.7	-7.1	-7.0
druq	Dru	13	3545252	-7.4	-7.2	-9.1	-9.8
druq	Dru	14	128748	-7.0	-7.7	-7.3	-7.8
druq	Dru	15	1509	-8.7	-8.4	-9.2	-8.7
druq	Dru	16	1582	-7.1	-7.7	-7.3	-7.6
druq	Dru	17	2104261	-7.8	-6.9	-7.2	-8.0
druq	Dru	18	482581	-7.7	-8.3	-8.0	-8.7
druq	Dru	19	1405	-12.0	-9.9	-7.6	-8.3
druq	Dru	20	42710	-6.5	-6.2	-5.6	-6.2
druq	Dru	21	23588	-9.2	-8.9	-8.0	-7.8
druq	Dru	22	806	-8.1	-8.5	-6.8	-7.0
druq	Dru	23	1445	-7.7	-7	-7.5	-8.4
druq	Dru	24	726	-7.7	-7.8	-8.7	-8.3
druq	Dru	25	1868702	-9.8	-7.8	-8.0	-9.1
druq	Dru	26	1377575	-8.6	-8.2	-8.3	-7.7
druq	Dru	27	157101	-7.4	-7.8	-8.7	-9.2
druq	Dru	28	4297185	-7.1	-8.2	-8.7	-9.4
druq	Dru	29	1389	-9.6	-8.0	-7.7	-8.8
druq	Dru	30	5170587	-	-7.8	-8.0	-

				8.3			7.9
druq	Dru	31	2218923	-7.1	-7.8	-6.5	-7.6
druq	Dru	32	1395	-7.5	-6.9	-7.4	-8.3
druq	Dru	33	166444	-10.8	-10.1	-7.5	-9.0
druq	Dru	34	425863	-11.3	-10.8	-7.6	-8.6
druq	Dru	35	1670	-7.3	-7.4	-6.9	-6.5
druq	Dru	36	1200946	-7.1	-7.4	-6.3	-7.3
druq	Dru	37	1200412	-7.3	-9.3	-8.0	-8.4
druq	Dru	38	1274	-9.3	-7.8	-8.0	-7.5
druq	Dru	39	1200807	-7.0	-7.1	-7.5	-8.2
druq	Dru	40	1162	-7.5	-7.1	-7.7	-8.1
druq	Dru	41	1387	-10.9	-9.6	-8.1	-8.5
druq	Dru	42	4303574	-6.9	-7.5	-7.4	-7.3
druq	Dru	43	2107797	-9.6	-8.0	-7.7	-8.7
druq	Dru	44	1200436	-8.3	-7.0	-7.8	-8.2
druq	Dru	45	1625	-7.3	-8.5	-7.0	-6.8
druq	Dru	46	1200585	-8.1	-7.3	-8.0	-7.7
druq	Dru	47	428647	-7.7	-7.9	-9.8	-9.7
druq	Dru	48	251940	-7.2	-8.0	-8.3	-8.1
druq	Dru	49	828	-7.9	-7.9	-6.4	-6.1
druq	Dru	51	90593	-7.9	-7.8	-7.5	-7.9
druq	Dru	52	103	-7.2	-7.5	-7.4	-8.0
druq	Dru	53	4650276	-7.1	-7.6	-7.7	-8.1
druq	Dru	54	3707377	-7.4	-7.5	-7.3	-8.4
druq	Dru	55	1393	-7.1	-7.3	-8.7	-8.3
druq	Dru	56	27769	-7.7	-7.2	-7.3	-7.9
druq	Dru	57	3275971	-7.2	-7.5	-7.6	-8.0
druq	Dru	58	2079587	-	-7.4	-	-

				7.2		8.3	8.4
druq	Dru	59	83	-7.1	-7.3	-7.8	-7.8
druq	Dru	60	386630	-8.2	-7.6	-7.1	-8.4
druq	Dru	61	1201101	-7.2	-8.8	-7.8	-7.7
druq	Dru	62	1200335	-6.9	-7.6	-6.5	-7.5
druq	Dru	63	1170	-7.5	-7.5	-7.4	-7.8
druq	Dru	64	2107067	-7.1	-7.7	-6.4	-6.6
druq	Dru	65	1229684	-11	-8.2	-7.4	-9.1
druq	Dru	66	849	-7.1	-7.5	-7.0	-6.7
druq	Dru	67	2103846	-7.4	-7.3	-7.7	-8.4

Figure A.4. 1E3G (AR), 8E1A (AR), 2ZCH (KLK3) and 2ZCL (KLK3) receptors molecular docking conventional drugs and Autodock Vina docking results.

MOLEKÜLER YERLEŞTIRME FORMATI				**RESEPTÖRLER Yerleştirme Sonuçları (kcal/mol)**			
PDBQT biçimi	**SDF biçimi**	**Order**	**DRUG NAME**	**1E3G (AR)**	**8E1A (AR)**	**2ZCH**	**2ZCL**
New_Drug	New_Drug	1	ABİRATERONE (2018)	8.4	7.9	8.7	8.6
New_Drug	New_Drug	2	APALUTAMİDE (2018)	8.2	8.0	8.6	8.7
New_Drug	New_Drug	3	TALAZOPARİB (TALZENNA) (2018)	8.1	8.7	9.4	9.4
New_Drug	New_Drug	4	DAROLUTFAMİDE (2019)	7.4	8.4	8.0	9.4
New_Drug	New_Drug	5	ENZALUTAMİDE (2019)	7.6	7.5	8.9	9.0
New_Drug	New_Drug	6	OLAPARİB (2020)	8.5	11.2	10.1	9.5
New_Drug	New_Drug	7	RUCAPARİB CAMSYLATE (2020)	8.8	8.7	8.6	8.6
New_Drug	New_Drug	8	ORGOVYX (2020)	8.3	7.6	9.2	10.5
New_Drug	New_Drug	9	PYLARIFY (2021)	6.4	5.7	6.3	6.7
New_Drug	New_Drug	10	LOCAMETZ				

			(GALLIUM GA 68 GOZETOTİDE) (2022)	6.5	6.9	6.7	6.5
New_Drug	New_Drug	11	NİRAPARİB (2023)	8.1	8.5	8.3	8.5

Figure A.5. 1E3G (AR), 8E1A (AR), 2ZCH (KLK3) and 2ZCL (KLK3) receptors molecular docking FDA approved new drugs and Autodock Vina docking results

APPENDIX B

GROMACS Tutorial/ Protein-Ligand Complex

source /usr/local/gromacs/bin/GMXRC

tar -zxvf charmm36_ljpme-jul2022.ff.tgz

gmx_mpi pdb2gmx -f REC.pdb -ignh

8 (CHARMM27)

1 (TIP3P)

gmx_mpi editconf -f LIG.pdb -o LIG.gro

gedit conf.gro LIG.gro

*(Copy content from 3rd line of lig.gro to the conf.gro file up to the 2nd last line)

*(Check the column number from where the lig.gro data ends (x) in conf.gro and replace the value in 2nd line by x-3)

*(Open file in chimera to check ligand and receptor)

-----EDIT THE FOLLOWING in topol.top -----

gedit topol.top

(add

; Include ligand topology

#include "LIG.itp"

below- Include forcefield parameters

#include "amberGS.ff/forcefield.itp")

AT THE BOTTOM OF THE SAME FILE PERFORM FOLLOWING CHANGES

(add LIG 1

align exactly below-

Protein_chain_E 1)

-----EDIT THE FOLLOWING in lig.itp -----

gedit lig.itp

[moleculetype]

; Name nrexcl

lig_gmx2 3

TO

[moleculetype]

; Name nrexcl

LIG 3

(in certain cases this will already be LIG 3 so for such case no change is needed)

gmx_mpi editconf -f conf.gro -d 2.0 -bt triclinic -o box.gro

gmx_mpi solvate -cp box.gro -cs spc216.gro -p topol.top -o box_sol.gro

gmx grompp -f ions.mdp -c box_sol.gro -p topol.top -o ION.tpr

(OR)

gmx_mpi grompp -f ions.mdp -c box_sol.gro -maxwarn 2 -p topol.top -o ION.tpr

gmx_mpi genion -s ION.tpr -p topol.top -conc 0.1 -neutral -o box_sol_ion.gro

15

gmx grompp -f EM.mdp -c box_sol_ion.gro -p topol.top -o EM.tpr (OR)

gmx_mpi grompp -f EM.mdp -c box_sol_ion.gro -maxwarn 2 -p topol.top -o EM.tpr

gmx mdrun -v -deffnm EM

```
; LINES STARTING WITH ';' ARE COMMENTS
title           = Minimization  ; Title of run

; Parameters describing what to do, when to stop and what to save
integrator      = steep     ; Algorithm (steep = steepest descent minimization)
emtol           = 1000.0    ; Stop minimization when the maximum force < 10.0 kJ/mol
emstep          = 0.01      ; Energy step size
nsteps          = 50000     ; Maximum number of (minimization) steps to perform

; Parameters describing how to find the neighbors of each atom and how to calculate the interactions
nstlist         = 1             ; Frequency to update the neighbor list and long range forces
cutoff-scheme   = Verlet
ns_type         = grid          ; Method to determine neighbor list (simple, grid)
rlist           = 1.2           ; Cut-off for making neighbor list (short range forces)
coulombtype     = PME           ; Treatment of long range electrostatic interactions
rcoulomb        = 1.2           ; long range electrostatic cut-off
vdwtype         = cutoff
vdw-modifier    = force-switch
rvdw-switch     = 1.0
rvdw            = 1.2           ; long range Van der Waals cut-off
pbc             = xyz           ; Periodic Boundary Conditions
DispCorr        = no
```

gedit nvt.mdp (This file is already modified)

Now make index files

gmx_mpi make_ndx -f LIG.gro -o index_LIG.ndx

> 0 & ! a H*

> q

gmx_mpi genrestr -f LIG.gro -n index_LIG.ndx -o posre_LIG.itp -fc 1000 1000 1000

> select group "3"

Now, open topol.top file

at the end of the document

after

"; Include Position restraint file

#ifdef POSRES

#include "posre.itp"

#endif

"Here"

add this

; Ligand position restraints

#ifdef POSRES

#include "posre_LIG.itp"

#endif

Again, Make other Index file for System

gmx_mpi make_ndx -f EM.gro -o index.ndx

> 1 | 13

> q

-----[NVT]-----

gedit NVT.mdp (This file is already modified)

gmx_mpi grompp -f NVT.mdp -c EM.gro -r EM.gro -p topol.top -n index.ndx -maxwarn 2 -o NVT.tpr

gmx mdrun -deffnm NVT

```
title                    = Protein-ligand complex NVT equilibration
define                   = -DPOSRES  ; position restrain the protein and ligand
; Run parameters
integrator               = md        ; leap-frog integrator
nsteps                   = 50000     ; 2 * 50000 = 100 ps
dt                       = 0.002     ; 2 fs
; Output control
nstenergy                = 500   ; save energies every 1.0 ps
nstlog                   = 500   ; update log file every 1.0 ps
nstxout-compressed       = 500   ; save coordinates every 1.0 ps
; Bond parameters
continuation             = no        ; first dynamics run
constraint_algorithm     = lincs     ; holonomic constraints
constraints              = h-bonds   ; bonds to H are constrained
lincs_iter               = 1         ; accuracy of LINCS
lincs_order              = 4         ; also related to accuracy
; Neighbor searching and vdW
cutoff-scheme            = Verlet
ns_type                  = grid      ; search neighboring grid cells
nstlist                  = 20        ; largely irrelevant with Verlet
rlist                    = 1.2
vdwtype                  = cutoff
vdw-modifier             = force-switch
rvdw-switch              = 1.0
rvdw                     = 1.2       ; short-range van der Waals cutoff (in nm)
; Electrostatics
coulombtype              = PME       ; Particle Mesh Ewald for long-range electrostatics
rcoulomb                 = 1.2       ; short-range electrostatic cutoff (in nm)
pme_order                = 4         ; cubic interpolation
fourierspacing           = 0.16      ; grid spacing for FFT
; Temperature coupling
tcoupl                   = V-rescale                     ; modified Berendsen thermostat
tc-grps                  = Protein_LIG Water_and_ions    ; two coupling groups - more accurate
tau_t                    = 0.1   0.1                     ; time constant, in ps
ref_t                    = 300   300                     ; reference temperature, one for each group, in K
; Pressure coupling
pcoupl                   = no        ; no pressure coupling in NVT
; Periodic boundary conditions
pbc                      = xyz       ; 3-D PBC
; Dispersion correction is not used for proteins with the C36 additive FF
DispCorr                 = no
; Velocity generation
gen_vel                  = yes       ; assign velocities from Maxwell distribution
gen_temp                 = 300       ; temperature for Maxwell distribution
gen_seed                 = -1        ; generate a random seed
```

-----[NPT]-----

gedit NPT.mdp (This file is already modified)

gmx_mpi grompp -f NPT.mdp -c NVT.gro -r NVT.gro -p topol.top -n index.ndx -maxwarn 2 -o NPT.tpr

gmx mdrun -deffnm NPT

```
title                    = Protein-ligand complex NPT equilibration
define                   = -DPOSRES  ; position restrain the protein and ligand
; Run parameters
integrator               = md        ; leap-frog integrator
nsteps                   = 50000     ; 2 * 50000 = 100 ps
dt                       = 0.002     ; 2 fs
; Output control
nstenergy                = 500       ; save energies every 1.0 ps
nstlog                   = 500       ; update log file every 1.0 ps
nstxout-compressed       = 500       ; save coordinates every 1.0 ps
; Bond parameters
continuation             = yes       ; continuing from NVT
constraint_algorithm     = lincs     ; holonomic constraints
constraints              = h-bonds   ; bonds to H are constrained
lincs_iter               = 1         ; accuracy of LINCS
lincs_order              = 4         ; also related to accuracy
; Neighbor searching and vdW
cutoff-scheme            = Verlet
ns_type                  = grid      ; search neighboring grid cells
nstlist                  = 20        ; largely irrelevant with Verlet
rlist                    = 1.2
vdwtype                  = cutoff
vdw-modifier             = force-switch
rvdw-switch              = 1.0
rvdw                     = 1.2       ; short-range van der Waals cutoff (in nm)
; Electrostatics
coulombtype              = PME       ; Particle Mesh Ewald for long-range electrostatics
rcoulomb                 = 1.2
pme_order                = 4         ; cubic interpolation
fourierspacing           = 0.16      ; grid spacing for FFT
; Temperature coupling
tcoupl                   = V-rescale                     ; modified Berendsen thermostat
tc-grps                  = Protein_LIG Water_and_ions    ; two coupling groups - more accurate
tau_t                    = 0.1   0.1                     ; time constant, in ps
ref_t                    = 300   300                     ; reference temperature, one for each group, in K
; Pressure coupling
pcoupl                   = Berendsen                     ; pressure coupling is on for NPT
pcoupltype               = isotropic                     ; uniform scaling of box vectors
tau_p                    = 2.0                           ; time constant, in ps
ref_p                    = 1.0                           ; reference pressure, in bar
compressibility          = 4.5e-5                        ; isothermal compressibility of water, bar^-1
refcoord_scaling         = com
; Periodic boundary conditions
pbc                      = xyz       ; 3-D PBC
; Dispersion correction is not used for proteins with the C36 additive FF
DispCorr                 = no
; Velocity generation
gen_vel                  = no        ; velocity generation off after NVT
```

-----[FINAL MD RUN/PRODUCTION]-----

gedit NPT.mdp (Change MD RUN TIME as per your need)

gmx_mpi grompp -f MD.mdp -c NPT.gro -t NPT.cpt -p topol.top -n index.ndx -maxwarn 2 -o MD.tpr

gmx mdrun -deffnm MD

```
title                    = Protein-ligand complex MD simulation
; Run parameters
integrator               = md        ; leap-frog integrator
nsteps                   = 25000000  ; 2 * 25000000 = 50000 ps (50 ns)
dt                       = 0.002     ; 2 fs
; Output control
nstenergy                = 5000      ; save energies every 10.0 ps
nstlog                   = 5000      ; update log file every 10.0 ps
nstxout-compressed       = 5000      ; save coordinates every 10.0 ps
; Bond parameters
continuation             = yes       ; continuing from NPT
constraint_algorithm     = lincs     ; holonomic constraints
constraints              = h-bonds   ; bonds to H are constrained
lincs_iter               = 1         ; accuracy of LINCS
lincs_order              = 4         ; also related to accuracy
; Neighbor searching and vdW
cutoff-scheme            = Verlet
ns_type                  = grid      ; search neighboring grid cells
nstlist                  = 20        ; largely irrelevant with Verlet
rlist                    = 1.2
vdwtype                  = cutoff
vdw-modifier             = force-switch
rvdw-switch              = 1.0
rvdw                     = 1.2       ; short-range van der Waals cutoff (in nm)
; Electrostatics
coulombtype              = PME       ; Particle Mesh Ewald for long-range electrostatics
rcoulomb                 = 1.2
pme_order                = 4         ; cubic interpolation
fourierspacing           = 0.16      ; grid spacing for FFT
; Temperature coupling
tcoupl                   = V-rescale                     ; modified Berendsen thermostat
tc-grps                  = Protein_LIG Water_and_ions    ; two coupling groups - more accurate
tau_t                    = 0.1   0.1                     ; time constant, in ps
ref_t                    = 300   300                     ; reference temperature, one for each group, in K
; Pressure coupling
pcoupl                   = Parrinello-Rahman             ; pressure coupling is on for NPT
pcoupltype               = isotropic                     ; uniform scaling of box vectors
tau_p                    = 2.0                           ; time constant, in ps
ref_p                    = 1.0                           ; reference pressure, in bar
compressibility          = 4.5e-5                        ; isothermal compressibility of water, bar^-1
; Periodic boundary conditions
pbc                      = xyz       ; 3-D PBC
; Dispersion correction is not used for proteins with the C36 additive FF
DispCorr                 = no
; Velocity generation
gen_vel                  = no        ; continuing from NPT equilibration
```